The maintenance of mitochondrial DNA after oxidative stress

Doctoral thesis

to obtain a PhD

from the Faculty of Medicine

of the University of Bonn

Genevieve Trombly

from Lansing, Michigan, United States of America

2024

Written with authorization of

the Faculty of Medicine of the University of Bonn

First reviewer: Prof. Dr. Wolfram S. Kunz

Second reviewer: Prof. Dr. Rudolf J. Wiesner

Day of oral examination: September 19th, 2024

From the Institute of Experimental Epileptology and Cognition Research

Director: Prof. Dr. Heinz Beck

Table of Contents

List of abbreviations

5’-dRP	5’-deoxyribose-phosphate
ADP	adenosine diphosphate
aH_2O	autoclaved sterile Millipore water
APEX1	apurinic/apyrimidinic endonuclease 1
AP-site	apurinic/apyrimidinic site or abasic site
ATP	adenosine triphosphate
BER	base excision repair
BrdU	5’-Bromo-2’-Deoxyuridine
BSA	bovine serum albumin
CRISPR	clustered regularly interspaced short palindromic repeats
CSPD	Disodium3-(4-methoxyspiro{1,2-dioxetane-3,2′-(5′-chloro)tricyclo[3.3.1.13,7] decan}-4-yl)phenyl phosphate
Ct	cycle threshold
D-loop	displacement
DIG	digoxigenin
DMEM	Dulbecco’s Modified Eagle Medium
DMSO	dimethyl sulfoxide
DNA	deoxyribonucleic acid
DNA2	DNA replication helicase/nuclease 2
dNTP	deoxyribonucleotide triphosphate
DSB	double-strand break
dsDNA	double-stranded deoxyribonucleic acid
dUTP	deoxyuridinetriphosphate
ECL	enhanced chemiluminescence
EDTA	Ethylenediaminetetraacetic acid
ENDOG	endonuclease G
EtBr	ethidium bromide
ETC	electron transport chain
EXOG	exo/endonuclease G
FBS	fetal bovine serum

FADH	flavin adenine dinucleotide
FEN1	flap structure-specific endonuclease 1
gRNA	guide ribonucleic acid
GPX	glutathione peroxidase
HAP1	human near-haploid cell line
H_2O_2	hydrogen peroxide
HCl	hydrochloric acid
HDR	homologous directed repair
HEK293	human embryonic kidney cell line
HEPES	4-(2-hydroxyethyl)-1-piperazineethanesulfonic acid
HR	homologous recombination
HRP	horseradish peroxidase
H-strand	heavy strand of mitochondrial DNA
HSP	heavy-strand RNA transcription promoter
IB	isolation buffer
KCNJ10	Kir4.1, ATP-sensitive potassium inward rectifying channel 10
KOH	potassium hydroxide
LB	Luria broth (Miller) medium
LIG3	DNA ligase 3
LP-BER	long-patch base excision repair
L-strand	light strand of mitochondrial DNA
LSP	light-strand RNA transcription promotor
MGME1	mitochondria genome maintenance endonuclease 1
$MgCl_2$	magnesium chloride
MMR	mismatch repair
mTER	mitochondrial transcription termination site
mtDNA	mitochondrial deoxyribonucleic acid
mtSSB	mitochondrial single-stranded DNA binding protein
MTS	mitochondrial targeting sequence
NaCl	sodium chloride
NADH	nicotinamide adenine dinucleotide
NADPH	nicotinamide adenine dinucleotide

NaOH	sodium hydroxide
NCR	non-coding region
NGS	next-generation sequencing
NER	nucleotide excision repair
NHEJ	non-homologous end joining
NLS	nuclear localization signal
OFP	orange fluorescent protein
OriH	heavy strand origin of replication
OriL	light strand origin of replication
OXPHOS	oxidative phosphorylation
qPCR	quantitative polymerase chain reaction
ρ^0	cells depleted for mitochondrial DNA
PAM	protospacer adjacent motif
PBS	phosphate buffered saline
PBST	phosphate buffered saline solution with tween20
PCR	polymerase chain reaction
POLG	DNA polymerase gamma
POLGexo	3’-5’ exonuclease function of DNA polymerase gamma
RNA	ribonucleic acid
RITOL	RNA incorporation throughout the lagging strand
rRNA	ribosomal ribonucleic acid
RT	room temperature
SOD1	superoxide dismutase 1
SOD2	superoxide dismutase 2
SSB	single-strand break
SSC	saline-sodium citrate
ssDNA	single-stranded deoxyribonucleic acid
TAS	termination-associated sequence
TBS	Tris-buffered saline
TE	Tris-EDTA
Tris	Trizma base
tRNA	transfer ribonucleic acid

1. Introduction

1.1 Mitochondria

Mitochondria are cytoplasmic organelles within eukaryotic cells. They are composed of an outer membrane and a highly folded inner membrane, which segregates the mitochondria into the intermembrane space and the mitochondrial matrix (Figure 1). A major function of mitochondria is the synthesis of adenosine triphosphate (ATP), the hydrolysis of which provides energy for many essential processes within cells. Mitochondria are also involved in the synthesis of heme and steroids, the regulation of calcium, adaptive thermogenesis, apoptosis, and they are a signal hub for innate immunity (Scheibye-Knudsen et al., 2015; Mills et al., 2017). Mitochondria play a central role in cellular iron metabolism with the biosynthesis of iron-sulfur clusters and heme groups localized in the mitochondrial matrix space (Levi and Rovida, 2009). Mitochondria are dynamic organelles that form a network within cells and undergo constant fission divisions and fusion combining of mitochondria within the mitochondrial network (Kasahara and Scorrano, 2014), thereby allowing for the transfer of mtDNA and vital resources required by mitochondria such as proteins, RNA, and lipids.

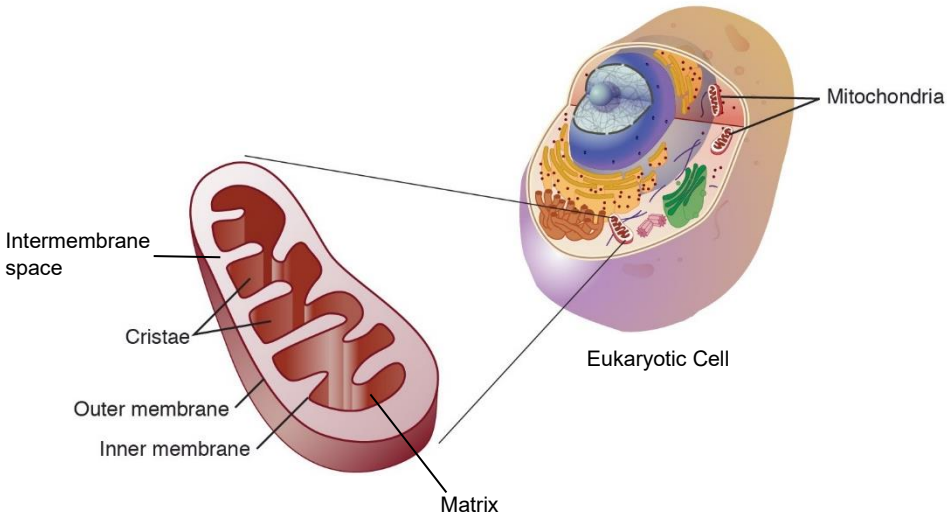

Fig. 1: Diagram of mitochondria. Mitochondria consist of an outer membrane and an inner membrane, which form the inner mitochondrial matrix and the intermembrane space. The cristae folds of the inner membrane serve to increase the surface area for ATP energy production. Adapted from National Institute of Health (2023).

1.1.1 OXPHOS

Within the inner membrane of mitochondria, the complexes of the electron transport chain (ETC) along with ATP synthase produce ATP via oxidative phosphorylation (OXPHOS) (Figure 2). The cristae folds of the inner membrane increase the surface area and maximize ATP production. In normal conditions, OXPHOS produces over 80% of the ATP energy in mammalian cells, while the remaining energy is generated through chemical processes such as glycolysis (Papa et al., 2012). The ETC consists of four complexes that transfer protons from the matrix across the inner membrane into the intermembrane space through a series of redox reactions where NADPH and oxygen are reduced. This results in an electro-chemical proton gradient that flows through ATP synthase back into the matrix and generates ATP from ADP and phosphate (Papa et al., 2012). In the production of ATP for cellular energy, OXPHOS consumes roughly 85% of the oxygen used by mammalian cells (Tann et al., 2011).

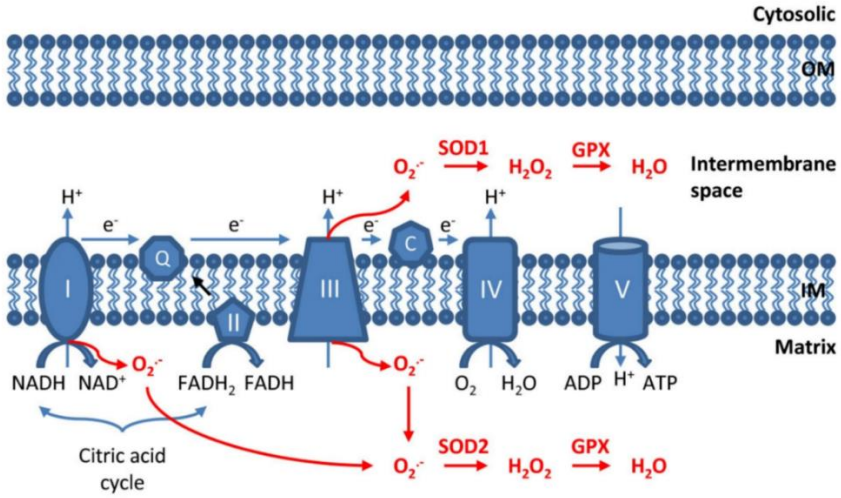

Fig. 2: Mitochondrial OXPHOS and ROS production. NADH and $FADH_2$ produced in the citric acid cycle donate electrons (e^-) to complex I and II of the electron transport chain, which then reduce O_2 into H_2O in complex IV in the inner membrane (IM; outer membrane OM). Complexes I, II, and IV facilitate the transport of protons (H^+) to the inter-membrane space, which flow back into the matrix through complex V (ATP synthase) generating ATP from ADP and phosphate. Superoxide, $O_2^{\bullet -}$, is formed from electron leakage at complexes I and III. Superoxide is dismutated to H_2O_2 by superoxide dismutases SOD1 or SOD2. H_2O_2 is fully reduced to water by glutathione peroxidase (GPX). Both H_2O_2 and $O_2^{\bullet -}$ are considered to be mitochondrial ROS. Scheme from Li et al. (2013).

1.2 Mitochondrial DNA

Separate from nuclear DNA, mitochondria have their own multicopy circular genome that is self-autonomously maintained and maternally inherited. mtDNA is composed of a heavy

strand and a light strand based on the nucleotide bases that are present: the heavy strand contains a larger amount of guanine and thymine. Human mtDNA is 16,569 bases in size and encodes for 13 proteins essential for OXPHOS, 22 tRNAs, and 2 rRNAs specific to mitochondria (Figure 3). The OXPHOS proteins encoded in the mitochondrial genome are 7 subunits for complex I, cytochrome b of complex III, 3 subunits of complex IV, and 2 subunits of complex V (Anderson et al., 1981). mtDNA also contains a non-coding region (NCR) which encodes many conserved elements involved in the regulation of replication and transcription: the heavy strand origin of replication (OriH), the RNA transcription promoters LSP and HSP, and the termination-associated sequence TAS. The triple-stranded D-loop is often generated in the NCR by the stable incorporation of third short 7S DNA strand of approximately 650 bp (Nicholls and Minczuk, 2014). The light strand origin of replication (OriL) is located within a cluster of tRNAs 11 kb downstream from the OriH, and the two origins of replication segregate mtDNA in what is known as the major and minor arcs (Falkenberg and Gustafsson, 2020). mtDNA is extensively covered with proteins (Zhao, 2019) and packed into DNA-protein complexes called nucleoids that are dispersed along the mitochondrial network and are associated with the inner mitochondrial membrane (Fu et al., 2020). The circular structure of mtDNA along with the function of topoisomerases results in supercoiling, where the native conformation of mtDNA is to compact around itself (Menger et al., 2021). The approximately 1,100 other proteins that are required by mitochondria (Rath et al., 2021), including those involved in mtDNA replication and repair, are encoded in the nuclear genome, translated in the cytoplasm, and imported into the mitochondria.

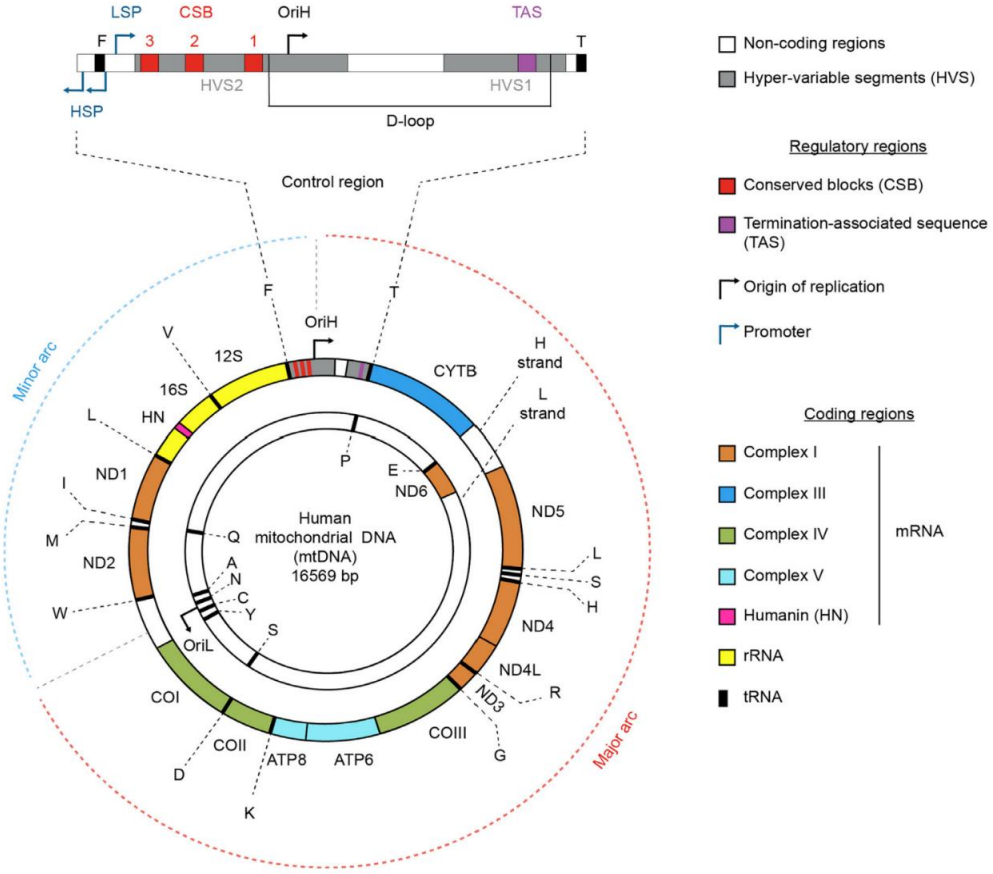

Fig. 3: Human mitochondrial DNA. MtDNA contains a heavy strand (H-strand, outer circle) and a light strand (L-strand, inner circle), each with their own origins of replication (OriH and OriL, respectively). mtDNA contains a non-coding region (upper linear segment) where both replication and transcription (HSP and LSP) are initiated, and additionally contains the termination-associated sequence (TAS, purple), and 3 conserved elements (red). mtDNA can be segmented into a major arc and a minor arc based on the origins of replication. mtDNA codes for mitochondrial proteins: 7 subunits of complex I (orange), cytochrome B of complex III (blue), cytochrome c oxidase of complex IV (green), and 2 ATP synthase subunits of complex V (teal). Additionally, 2 ribosomal RNAs (yellow) and 22 tRNAs (black boxes) are encoded within mtDNA. Diagram from Fontana and Gahlon (2020).

1.2.1 mtDNA replication

Replication of mtDNA occurs independently from the cell cycle. The basic mitochondrial replisome consists of the mitochondrial polymerase POLG, the mitochondrial single-stranded DNA-binding protein (mtSSB), and the mtDNA helicase TWINKLE (Falkenberg and Gustafsson, 2020). Three models of mtDNA replication have been proposed, and the exact mode of mtDNA replication is still under investigation. The first is the asynchronous strand-displacement model, where replication is initiated at the OriH and replication of the H-strand proceeds along 70% of the mtDNA until the OriL is exposed and replication of

the L-strand is initiated and proceeds in the opposite direction (Brown et al., 2005). A second replication model is based on RNA incorporation throughout the lagging strand (RITOL) (Yasukawa et al., 2006), which proceeds as the strand-displacement model but with the H-strand as a DNA/RNA hybrid to stabilize single-stranded DNA until made into dsDNA by POLG. The third model is the strand-coupled or synchronous model, where there is a single origin of replication and both strands of mtDNA are synthesized bi-directionally: the leading strand is continuously synthesized while Okazaki fragments are discontinuously synthesized on the lagging strand which must be continuously ligated (Holt et al., 2000). However, the generation of Okazaki fragments in the strand-coupled model of mtDNA replication is unlikely because a reduction of LIG3, the enzyme required to join the fragments, did not affect mtDNA replication or copy number (Shokolenko et al., 2013). The strand-displacement model has the most evidence, such as the finding of the highest presence of mtSSB near the OriH and D-loop region of mtDNA (Miralles Fusté et al., 2014). After the full mtDNA strand is replicated, the RNA primers at the 5'-ends are displaced by POLG and the generated flaps are removed before the strands are ligated to complete synthesis (Uhler and Falkenberg, 2015; Karlowicz et al., 2022), resulting in two double-stranded daughter mtDNA molecules.

1.2.2 mtDNA copy number and heteroplasmy

Most eukaryotic cells have a single nucleus with two copies of nuclear DNA, while there are 100–1000 mitochondria per cell (Fu et al., 2020) with approximately 8–10 copies of mtDNA per mitochondria (Allkanjari and Baldock, 2021). The mtDNA copy number per cell varies and is tissue-specific, and the mechanisms involved in the regulation of mtDNA copy number have yet to be determined (Shokolenko and Alexeyev, 2022). The term homoplasmy is used to describe when all copies of mtDNA within a cell are identical, as opposed to heteroplasmy when there are both wild-type and mutant species of mtDNA (Gorman et al., 2015). Due to the multiple copies of mtDNA that exist within a cell, there is a 'threshold' effect where pathogenic mutations within mtDNA generally only have a physiological consequence when they reach a certain percentage of the total amount of mtDNA (Stewart and Chinnery, 2015). Low levels of heteroplasmy can be maternally inherited, and heteroplasmy levels are shown to increase with age with the type of mutation tolerated within a cell being tissue specific (Stewart and Chinnery, 2021).

1.2.3 mtDNA maintenance and disease

Mitochondrial function is vital for cells, and therefore maintaining the integrity of mtDNA is crucial. Mitochondria-associated diseases affect many tissue types, manifesting most frequently in cells with high energy requirements. These diseases involve problems with ROS regulation, mtDNA maintenance, or mitophagy and are generally characterized by the fact that they impact multiple organ systems, which leads to progressive degeneration and eventually death (Scheibye-Knudsen et al., 2015). Mutations within mtDNA as well as mutations within nuclear genes that are involved in mtDNA maintenance have been shown to result in pathological phenotypes. The threshold at which a mtDNA mutation becomes pathogenic varies between cell and tissue types and primarily manifests in neurons and muscle cells (Fu et al., 2020). The clinical severity of mtDNA diseases is dictated by the type of mutation or deletion and the percentage of heteroplasmy (Nissanka et al., 2019). mtDNA point mutations generally exceed 85-90% heteroplasmy before they become pathogenic, while mtDNA deletions already begin to have a functional effect at 60% heteroplasmy (Wallace, 1992). Deletions in mtDNA have been correlated with aging (Fontana and Gahlon, 2020) and changes in mtDNA copy number have been observed in disease due to its correlation with mitochondrial function (Malik and Czajka, 2013).

1.3 Mitochondrial ROS

Due to the chemical nature and abundance of oxygen, reactive oxygen species (ROS) are the most abundant free radicals (Goffart et al., 2021). The ETC is a major ROS generator within the cell (Alencar et al., 2019) with mitochondria being the main source for production and detoxification of ROS. Cytoplasmic enzymes such as monoamine oxidases also play a role in ROS generation (Nicholls and Ferguson, 2013); while peroxisomes produce ROS and are involved in redox regulation within cells (Fransen et al., 2012). The exact amount of ROS produced by mitochondria is difficult to quantify experimentally, but studies have found that approximately 1–5% of the oxygen consumed by OXPHOS is partially reduced to ROS (Nicholls and Ferguson, 2013; Turrens, 2003), with superoxide ($O_2^{\bullet -}$) being the major species (Kudin et al., 2004, Kudin et al., 2008). An electron is transferred from either the flavin moiety in complex I or the semiquinone radical in complex III to molecular oxygen to produce superoxide, which is rapidly converted by superoxide dismutase into H_2O_2 (Figure 2; Nicholls and Ferguson, 2013). This H_2O_2 is then fully reduced to water or partially reduced which generates the highly reactive hydroxyl radical ($^{\bullet}OH$). ROS are

known to be a damaging agent as well as a vital signaling molecule within the cell that indicate mtDNA integrity and mitochondrial function. ROS can signal fragmentation of the mitochondrial network, activation of antioxidant defenses, the recruitment of DNA repair enzymes, and the induction of mitophagy (Scheibye-Knudsen et al., 2015). In addition, H_2O_2 in the cytosol can act in multiple signaling networks involved in “cell cycle, stress response, energy metabolism, and redox balance” (Kowaltowski et al., 2009).

1.3.1 Mitochondrial ROS defenses

Many antioxidant pathways exist in mitochondria to help to regulate the presence of ROS and circumvent potential molecular damage. Uncoupling proteins lower the membrane potential of mitochondria to allow the electrons to flow more freely in the electron transport chain, which decreases the likelihood of oxygen being reduced to superoxide (Scheibye-Knudsen et al., 2015). Superoxide dismutases SOD1 in the cytoplasm of the cell and the intermembrane space and SOD2 in the matrix convert superoxide to H_2O_2 (Li et al., 2013; Figure 2). H_2O_2 is then further reduced by glutathione peroxidase and catalase to water, or thioredoxins neutralize H_2O_2 by the formation of a disulfide bond (Kudin et al., 2012). Glutathione, vitamin C, and vitamin E also function as scavengers of oxidants (Pigeolet et al., 1990; Fu et al., 2020).

1.3.2 Oxidative mtDNA damage

It has been known for some time that mtDNA is more prone to oxidative damage than nuclear DNA (Yakes and Van Houten, 1997) due to its proximity to the ROS produced during OXPHOS, which is exacerbated by the fact that the TFAM associated nucleoids are not very protective and mtDNA repair is limited (Alencar et al., 2019). H_2O_2, generated by superoxide dismutase to resolve the formation of superoxide radical anion, is by itself a non-reactive species. However, in the presence of free iron, the Fenton reaction with H_2O_2 produces the highly reactive hydroxyl radical ($^{\bullet}OH$) which is responsible for oxidative damage to mtDNA (Dizdaroglu and Jaruga, 2012; Henle et al., 1999). The iron within the mitochondria matrix is primarily sequestered within ferritin which can serve as a protective measure against oxidative stress (Levi and Arosio, 2004), but even low concentrations of free iron are enough to result in the generation of the hydroxyl radical (Petrat et al., 2002). In addition, the H_2O_2 splitting activity within mitochondria is insufficient to cope with the rate of production from OXPHOS and varies upon tissue type (Kudin et al., 2008, Kudin et al., 2012). The localization of mtDNA nucleoids associated with the inner mitochondria

membrane in matrix combined with the presence of free iron results in mtDNA being more prone to this ˙OH oxidative damage. Hydrogen peroxide is membrane permeable through aquaporin channels (Henzler and Steudle, 2000), so cytoplasmic and extracellular H_2O_2 can also impact mtDNA. ROS associated mtDNA damage from the hydroxyl radical causes the formation of thymine glycol from pyrimidine bases and 8-oxoG from guanine (Bohr, 2002; Wang et al., 1998), as well as the formation of single- and double-strand breaks (Trombly et al., 2023). Oxidative base modifications are expected to result in frequent G>T / C>A transversions due to the mispairing of 8-oxoG with adenine rather than cytosine (Freudenthal et al., 2015), however G>A / C>T mutations have been more frequently observed in aging tissues (Itsara et al., 2014). The absence of the expected transversions due to oxidative stress can be explained by the nucleotide specificity of POLG, which allows the pairing of 8-oxoG with cytosine (Hanes et al., 2006). POLG replication errors have been found to be the main source of mtDNA mutations (Kennedy et al., 2013), which also explains the presence of somatic mutations that differ from those generated by oxidative damage (Szczepanowska and Trifunovic, 2017). Nevertheless, oxidative mtDNA damage has been implicated in degenerative diseases, aging, and cancer (Alexeyev, 2009; Fu et al., 2020). Oxidative lesions can stall the mitochondrial replisome, with thymine glycol known to be a strong replicative block (Alencar et al., 2019). Neuronal cells with the highest levels of free iron, and therefore the most hydroxyl radical production, have been found to have the highest levels oxidative damage leading to mtDNA deletions (Xu et al., 2013; Genoud et al., 2017; Bender et al., 2006), demonstrating the damaging role that ROS can play.

1.4 Elimination of mtDNA damage

The maintenance of functional mtDNA and sufficient copy number is vital for cells. mtDNA damage can occur via reaction with intra- or extracellular chemical species and results in base modifications, the loss of a base or AP-site, a strand-break in the phosphodiester backbone, multiple strand breaks leading to a DSB, or intra- or inter-strand crosslinks (Scheibye-Knudsen et al., 2015). There are five main DNA repair pathways present in the nucleus: direct reversal of base modifications, mismatch repair (MMR), base excision repair (BER), nucleotide excision repair (NER), and DSB repair by homologous recombination (HR) or non-homologous end joining (NHEJ) (Scheibye-Knudsen et al., 2015; Fu et al., 2020). Of the DNA repair pathways, there has only been significant evidence that

BER exists within mitochondria (Alencar et al., 2019; Shokolenko and Alexeyev, 2022). There is no evidence for NER or any DSB repair (Alencar et al., 2019), likely because these repair pathways are error prone. Rather, these damaged genomes are degraded in mitochondria (Peeva et al., 2018; Nissanka et al., 2018) to prevent the accumulation of mutant mtDNA.

1.4.1 Base excision repair

BER exists to prevent the accumulation of mutations that can result from small chemical or structural modifications to DNA (Alencar et al., 2019). ROS generated lesions include oxidized bases, AP-sites, oxidized AP-sites that lead to DNA strand breaks, or direct SSBs (Szczesny et al., 2008), all of which can be remedied by BER. Mitochondrial BER proteins are associated with nucleoids to facilitate this repair (Stuart et al., 2005). BER consists of three steps: 1) recognition and removal of the damaged base, 2) end processing, and 3) gap filling and ligation (Figure 4; Alencar et al., 2019). Modified or damaged bases are first recognized by a DNA glycosylase, and hydrolytic cleavage of the N-glycosyl bond releases the base generating an AP-site. If the glycosylase is mono-functional, the AP-site is cleaved by APEX1 to form a single-strand break with 3’-OH and 5’-dRP ends. If the glycosylase is bi-functional with an additional β-lyase or β/δ-lyase activity, β-elimination results in a 3’-end that is an unsaturated hydroxyaldehyde or a 3’-phoshate, respectively, and a 5’-phosphate end. In both cases of bi-functional glycosylase, APEX1 processes the 3’-end into 3’-OH. Then either short-patch BER proceeds where a single nucleotide is incorporated by POLG which also processes the 5’-end and the nick is sealed by LIG3, or long-patch BER occurs where POLG incorporates an additional 6–9 nucleotides which generates a flap structure from strand displacement that is removed before ligation of the nick by LIG3 (Alencar et al., 2019; Fu et al., 2020). The type of BER likely depends on the type of damage that is present.

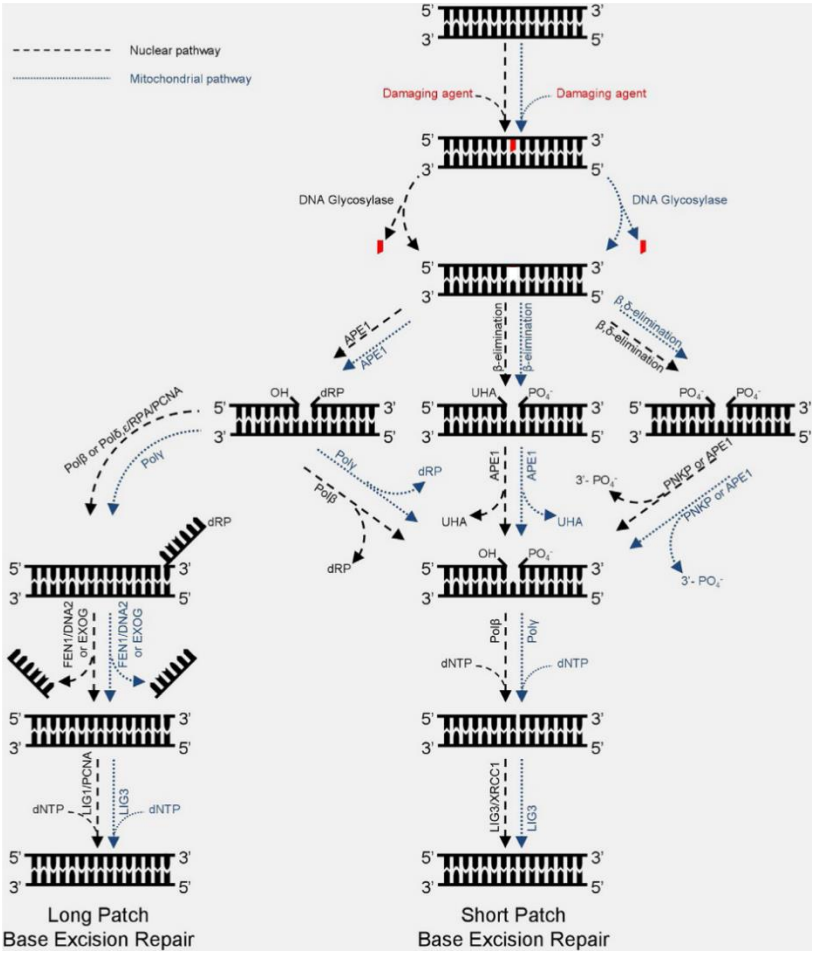

Fig. 4: Base-excision repair (BER) scheme. Nuclear pathway (black) and mitochondrial pathway (blue). After DNA is damaged, DNA glycosylases remove the damaged base leaving an abasic site that is then cleaved by APEX1 or removed via elimination. In long-patch BER, POLG fills in the gap and generates a strand displacement flap that is then removed by EXOG before ligation by LIG3. In short-patch BER, APEX1 must perform end processing before the single nucleotide is filled by POLG and LIG3 closes the nick. Adapted from Alencar et al. (2019).

1.4.1.1 APEX1

Apurinic/apyrimidinic endonuclease I (APEX1) is the main AP-site endonuclease within eukaryotic cells and plays an essential role in BER. APEX1 is a multifunctional protein that is involved in transcription regulation and in the cellular response to oxidative stress in addition to DNA repair (Tell et al., 2009; Li et al., 2010). APEX1 is primarily a nuclear protein with an NLS located in the first 13 residues in the N-terminus of the gene, but is conditionally targeting to mitochondria upon oxidative stress via a MTS in residues 289-319 of the C-terminus (Li et al., 2010), which also contains the enzymatic activity for the processing and removal of abasic sites (residues 161-318, Tell et al., 2009). APEX1 is an

abundant enzyme that is essential for cell viability and knock-out was found to be lethal in cultured fibroblasts (Izumi et al., 2005), embryonic lethal in mice, and haploinsufficent mice showed increased mtDNA depletion due to an accumulation of abasic sites (Ballista-Hernández et al., 2017). Upregulation of APEX1 has been shown to increase cellular resistance to oxidative stress (Tell et al., 2009).

1.4.1.2 POLG

DNA polymerase gamma (POLG) is localized exclusively to mitochondria and is the sole polymerase responsible for the replication of mtDNA. The functional polymerase consists of one catalytic subunit and two accessory subunits that help stimulate the catalytic activity and stabilize the interactions of the polymerase with mtDNA. In addition to the polymerase activity, the catalytic subunit of POLG contains a 5'-deoxyribose phosphate lyase activity and a 3'-5' exonuclease activity that primarily serves as a proof-reading function and cleaves single-stranded DNA (Graziewicz et al., 2006) and has also been shown to be involved in mtDNA degradation (Peeva et al., 2018). POLG is an efficient polymerase and can bypass several types of damage including 8-oxoG, but this bypass is prone to errors (Copeland et al., 2016). Because POLG is the major polymerase present in mitochondria, it plays a role in BER in addition to replication of mtDNA (Karlowicz et al., 2022).

1.4.1.3 EXOG

Exo/endonuclease G (EXOG) is a dimeric protein that contains a 5'-3' exonuclease activity as well as an endonuclease function and is exclusively localized to mitochondria via a specific leader sequence (Cymerman et al., 2008). The exonuclease removes bases by hydrolyzing ester linkages with a preference for the 5'-phosphate in ssDNA but contains a wing-domain that increases its affinity to dsDNA (Szymanski et al., 2017). EXOG has been proposed to be crucial for the repair of oxidative lesions in mtDNA. Specifically, EXOG is involved in LP-BER, where it degrades 5'-flap incorporated by POLG before nick ligation by LIG3 (Alencar et al., 2019). FEN1 and DNA2, two other proposed exonucleases to be involved in this step, were found to have no effect on mtDNA (Tann et al., 2011). EXOG has also been found to be associated in a mtDNA SSB repair complex along with POLG, APEX1, and LIG3 (Tann et al., 2011). The overexpression of EXOG was found to improve the cellular response to oxidative stress (Szymanski et al., 2017; Karlowicz et al., 2022). EXOG has also been implicated in the removal of RNA primers during mtDNA replication (Wu et al., 2019), specifically EXOG cleaves strand-displacement intermediate

flaps that contain RNA, which are generated by POLG and could impair mtDNA integrity if not removed (Karlowicz et al., 2022).

1.4.1.4 LIG3

DNA ligase III (LIG3) is an ATP-dependent ligase (Simsek et al., 2011) that is involved in most mtDNA reactions, including replication, repair, and recombination (Simsek and Jasin, 2011) by catalyzing the formation of phosphodiester bonds to seal breaks in the DNA backbone. LIG3 contains a conserved catalytic core with the DNA binding domain, a nucleotidyltransferase domain, and an oligonucleotide binding domain (Ellenberger and Tomkinson, 2008). LIG3 is vital for the maintenance of mitochondrial DNA (Lakshmipathy and Campbell, 2001) as it seals mtDNA ends during replication and facilitates the final step in the repair of mtDNA damage (Simsek and Jansin, 2011), and may be the only DNA ligase that acts within the mitochondria. LIG3 is the rate limiting step in BER (Akbari et al., 2014). LIG3 contains an in-frame upstream start codon that when used to initiate translation includes the mitochondrial targeting sequence in the form of an N-terminal helix with positive charges (Lakshmipathy and Campbell, 1999). The catalytic domain of mitochondrial LIG3, but not nuclear LIG3, has been found to be vital for cell survival (Simsek et al., 2011). Early research indicated that a LIG3 knock-out is not possible due to embryonic lethality in mice and cultured cells only survived when complemented with another ligase targeted to mitochondria because of the resulting mtDNA loss (Puebla-Osorio et al., 2006; Simsek et al., 2011), although later publications asserted that the generation of a LIG3 knock-out is possible in cells with uridine and pyruvate supported medium (Shokolenko et al., 2013).

1.4.2 mtDNA degradation

Due to the redundant nature and multiple copies of mtDNA, it is likely that degradation of damaged mtDNA is the most efficient pathway to cope with DSBs or an overwhelming number of mutagenic lesions (Furda et al., 2012). mtDNA has been shown to be rapidly degraded after oxidative stress (Shokolenko et al., 2009). mtDNA replication proteins were found to be involved in the degradation of linear mtDNA, specifically the 5’-3’ exonuclease MGME1 and the 3’-5’ exonuclease function of POLG (Peeva et al., 2018). Degradation of mtDNA after DSBs, as opposed to end joining repair pathways, avoids the formation of deletions or error prone repair (Nissanka et al., 2018). Intact mtDNA is then replicated to repopulate wild-type mtDNA species (Fu et al., 2020). This has led to the idea of mtDNA

being a “disposable” genome due to the multiple copies and the ability to repopulate (Shokolenko and Alexeyev, 2015), because degradation is more efficient to maintain intact mtDNA rather than to invest in repair (Torregosa-Muñumer et al., 2019). Degradation of mtDNA occurs rapidly with linear species, and mtDNA molecules with excessive DNA damage or difficult to repair lesions will also be degraded, the rate of which varies based on the type of damage and cell type (Shokolenko et al., 2016), with DSBs being most available to the linear degradation machinery.

1.4.2.1 POLG exonuclease function

In a mouse model with a mutation that eliminated the POLG exonuclease function, mice exhibited accelerated aging that was attributed to an increased somatic mtDNA point mutation profile (Trifunovic et al., 2004). Our lab discovered in a HEK293 cell model that the exonuclease function of POLG is involved in the degradation of linear mtDNA (Peeva et al., 2018). The absence of functional POLG exonuclease activity leads to a persistence of linear mtDNA as evident by the accumulation of mtDNA DSBs (Trifunovic et al., 2004; Hämäläinen et al., 2019), which could lead to an increase in the formation of deletions (Nissanka et al., 2018). POLG can form short 5’-flaps during replication due to its intrinsic ability to displace downstream DNA or RNA, and the loss of the POLG exonuclease function also leads to increased flap generation which are unable to be ligated (Macao et al., 2015). The mutant POLG has been shown to exhibit excessive mtDNA replication that depletes dNTP pools within the cells and can result in nuclear DNA replication stress (Hämäläinen et al., 2019).

1.4.2.2 MGME1

Mitochondrial maintenance exonuclease 1 (MGME1) is a 5’-3’ exonuclease that acts upon linear ssDNA (Kornblum et al., 2013), is specific to mitochondria, and is crucial for mtDNA maintenance. MGME1 is part of the replication machinery and interacts with all three components (POLG, mtSSB, and TWINKLE), and has been shown to be involved in the turnover of 7S DNA and maintenance of the D-loop region of mtDNA (NCR in Figure 3) (Nicholls et al., 2014; Urrutia et al., 2022). MGME1 binds preferentially to a 5’-phosphate, processes dT sequences most efficiently, and dC sequences the least efficiently (Urrutia et al., 2022). MGME1 has been proposed to work in conjunction with the exonuclease activity of POLG to remove 5’-flaps to yield nicks that can be ligated by LIG3 (Uhler et al., 2016; Zhao, 2019), and may be able to process certain RNA-DNA flaps (Falkenberg and

Gustaffson, 2020). In addition to its role in replication, the 5'-3' exonuclease activity of MGME1 has been shown to be involved in degradation of linear mtDNA (Peeva et al., 2018). MGME1 deficiencies have been associated with the accumulation of a linear 11 kb fragment spanning from OriH to OriL (Nicholls et al., 2014).

1.4.2.3 ENDOG

Endonuclease G, ENDOG, belongs to a nonspecific nuclease family and is a paralog of the endonuclease function of EXOG (Cymerman et al., 2008). In the nucleus, ENDOG is involved in DNA cleavage during replication stress and degradation during apoptosis (Wiehe et al., 2018), and while targeted to mitochondria the role that ENDOG plays on mtDNA is not well known. The activity of ENDOG is nonspecific and it degrades single- and double-stranded DNA as well as RNA during apoptosis (Szymanski et al., 2017). ENDOG in mitochondria may stimulate replication and transcription, as well as mtDNA depletion, and the binding and nuclease activity of ENDOG has been thought to be essential for the regulation of these processes (Wiehe et al., 2018). ENDOG differs from EXOG in substrate specificity, and the activity of ENDOG is not specific enough to process 5'-ends in mtDNA BER. ENDOG is not involved in the degradation of linear mtDNA (Peeva et al., 2018), however ENDOG has been shown to be involved in the removal of mtDNA during spermatogenesis, thus contributing to the maternal inheritance of mtDNA (DeLuca and O'Farrell, 2012) in a process that also involves POLG (Yu et al., 2017).

1.5 Aims

The aim of this thesis is to investigate the maintenance of mtDNA after H_2O_2 induced oxidative stress. Specifically, to determine 1) the type of damage occurs to mtDNA after a transient H_2O_2 pulse, 2) which type of damage is repaired and the rate of this repair, concurrently with the conditions in which damaged molecules are degraded and mtDNA is repopulated by replication with intact species, and 3) the proteins that are involved in this process. H_2O_2 is applied to HEK293 cells to induce oxidative stress and establish the paradigm for the resulting mtDNA oxidative damage and the subsequent recovery of intact mtDNA after this damage. CRISPR/Cas9 technology is used to generate knock-out cell lines of proteins known to be involved in the maintenance of mtDNA. MGME1 and POLGexo are vital for mtDNA degradation, while APEX1, EXOG, and LIG3 are known to be involved in base excision repair. The relevance of these pathways for the recovery of mtDNA after oxidative damage can then be elucidated. The results in this thesis will

provide valuable insight for how mtDNA is affected by H_2O_2 induced oxidative stress and have the potential for helping to understand the effects of chronic oxidative stress, which is known to be associated with inflammatory disease.

2. Material and methods

2.1 Cell culturing

2.1.1 HEK293 cells

HEK293 cells are an immortal cell line that was developed from human embryonic kidney cells that were transfected with sheared adenovirus 5 DNA (Graham et al., 1977). HEK293 cells were commercially obtained from ATCC (Nr. CRL-1573). The cells have developed hypotriploid chromosome duplications with 64 chromosomes in total and are tumorigenic. They show no tissue specific gene expression, but do show markers from renal progenitor cells, neuronal cells, and adrenal cells (Stepanenko and Dmitrenko, 2015). They are ideal for our experimental conditions because they are very resilient and can be genetically modified by CRISPR/Cas9.

2.1.2 Medium

Cells were cultured in DMEM with high glucose (4.5 g/L), 1 mM sodium pyruvate, sodium bicarbonate, and GlutaMAX™ (Gibco) or stable Glutamine (PAN Biotech). This medium was supplemented with 10 % heat-inactivated tetracycline-free FBS (PAN Biotech), 10 U/ml penicillin and streptomycin (Gibco), and 50 µg/ml uridine (Sigma-Aldrich).

2.1.3 Incubation conditions

Cells were maintained in an HERAcell 150 (Thermo Fisher Scientific) incubator at 37 °C with a humidified atmosphere with 10 % CO_2. All cell culture work is performed in a sterile HERAsafe hood (Thermo Fisher Scientific).

2.1.4 Passaging and trypsinization

Cells were observed at a minimum of every 2 days using an Axiovert 40 C microscope (Zeiss) for growth. Cells were grown to a level of approximately 90 % confluence where they were then split to prevent overgrowth. The medium was removed, cells were washed gently with 1× PBS (Gibco), then incubated for 5 minutes with trypsin (Gibco). After cells began to detach, medium was added to inactivate the trypsin and the cells were resuspended and split as needed.

2.1.5 Mycoplasma testing

Cell lines were routinely tested for the presence of mycoplasma, a frequent contaminant of cell culture. A 1 ml sample of medium is collected when the cells were above 80 % confluence then heated at 95 °C for 5 minutes. The cell line was tested using the Lookout® Mycoplasma PCR Detection Kit (Sigma-Aldrich) according to the manufacturer's protocol.

2.1.6 Cell counting and viability

A volume of cell culture suspension is diluted in 1× PBS and 0.1 % erythosin B (Sigma-Aldrich) to visualize and count alive and dead cells. For instance, a 1:10 dilution contains 10 µl sample, 10 µl erythrosine B dye, and 80 µl 1× PBS. 10 µl of this dilution is applied to one side of a Neubauer hemocytometer slide (Marienfeld) and 4 squares are counted using the Axiovert 40 C microscope.

2.2 CRISPR/Cas9-based genome editing

gRNA targeted to the gene of interest is inserted into the CRISPR/Cas9 plasmid vector which contains the necessary machinery to cut the DNA, and upon repair can introduce a loss of function mutation or correct insertion of the HDR sequence within that gene. The MGME1 knock-out cell line was produced by Dr. Daniel Blei using plasmids purchased from Origene. All other altered cell lines have been produced by the author for the purpose of this PhD thesis.

2.2.1 Design of gRNA

The gRNA and plasmid vector for POLG, EXOG, and ENDOG were designed according to the method described in Schmidt et al. (2015) and produced in partnership with Daniel Blei as part of the author's master's thesis. For LIG3, gRNA and primers sequences were gathered from published data from Horizon Discovery Ltd of their successful HAP1 knock-out cell line in the third exon of the gene. Genomic sequences of genes of interest were obtained from NCBI.gov. A protospacer adjacent motif (PAM) sequence containing the nucleotides 5'-NGG-3' was identified in the coding region of the protein of interest, most often within the first exon to ensure elimination of all protein function. The sequence 20 base pairs upstream from the PAM site is the gRNA sequence that directs the CRISPR gene editing plasmid to this gene (Table 1). These chosen gRNA sequences were ran in the NCBI blast tool (https://blast.ncbi.nlm.nih.gov/Blast.cgi) to confirm the absence of off-target effects. To anneal the gRNA into the CRISPR vector, overhangs were added: 5'-GTTTT-3' to the forward single-strand oligo and, 5'-CGGTG-3' to the reverse (see 2.2.2). gRNA ssDNA oligonucleotides were ordered from Biomers.net.

gene	targeted region	gRNA	HDR oligo
APEX1	Exon 5 (C terminus)	TGACAGCAAGATCCGTTCCA	TCCAAGAATGTTGGTTGGCGCC TTGATTACTTTTTGTTGTCCCAC TCTCTGTTACCTGCATTGTGTGA CAGC**GC**GATC**GC**TTCCAAG**A**CC CTCGGCAGTG**T**TCACTGTCCTAT CACCCTATACCTAGCACTGTGAC ACCACCCCTAAATCACT
ENDOG	Exon 1	GGGCGAGCTGGCCAAGTAC	
EXOG	Exon 1	AGTATCGCTTCCCGCCTCCG	
LIG3	Exon 3	CAGTGGTTGTCAACTTAGCC	
POLG	Exon 3	CCTTTGACCGAGCTCATATC	GTCCCTACTGGTGCCAGCAGC CCCACCCAGAGAGACTGGCAG GAGCAGTTAGTGGTGGGGCAC AATGTTTCCTTTG**C**CCGAGCTC ATATCAG**A**GAGCAGTACCTGAT CCAGGTAAGGTTCCTGGGGCC AACTGC**C**GGTTCTGGCATGG

Tab. 1: CRISPR/Cas9 gRNA and HDR oligo sequences. The gene, the targeted region of the gene, the respective gRNA, and HDR oligos where needed are listed. All sequences are written in the 5' to 3' direction. In the HDR oligo, bold bases indicate those that are altered from the normal sequence: the desired mutation to change protein function (blue), the PAM site alteration (red), and the digestion site alteration (green) to aid in screening.

2.2.1.1 Homology-directed repair oligonucleotides

For POLG and APEX1, a HDR oligonucleotide was designed to be incorporated into the genome and result in a specific missense mutation, rather than a general loss-of-function knock-out (Table 1). The HDR oligos contain the desired mutation as well as an alteration to the PAM site so that once the HDR oligo is incorporated it will no longer be targeted to be cut by CRISPR/Cas9. In addition, there is an alteration to a restriction digest site to aid in the screening of potential mutant cell lines, because the efficiency of generating the specific missense mutation is less than that of a functional knock-out. For POLG, the HDR oligo is designed to eliminate the 3'-5' exonuclease function while the polymerase activity remains intact. An accelerated aging phenotype in mice was previously described by Trifunovic et al. (2004) that resulted from a mutation at position 257 in the mouse POLG sequence, which corresponds to position 274 within the human sequence of POLG. A missense mutation eliminates the exonuclease activity by the single nucleotide change of GAC (aspartic acid) to GCC (alanine). The HDR oligo contains three single nucleotide changes to be incorporated: the GAC to GCC change to eliminate exonuclease function, an alteration of the PAM site, and a change in the *Pst*I digestion sequence for clone screening (Peeva et al., 2018). To minimize nuclear effects by a loss of APEX1, a HDR

oligo that edits only the mitochondria targeting sequence was produced for positive residues in 289–318 of the C-terminus of the gene (Li et al., 2010). Two positively charged amino acid residues of lysine (AAG) and arginine (CGT) were altered to non-polar and hydrophobic alanine (GCG or GCT) in the HDR oligo. The APEX1 HDR oligo also has the *Bcl*I digestion site alteration to aid in the screening of clones, as well as the change in the PAM sequence. These HDR oligonucleotides were ordered from Biomers.net.

2.2.2 Generation of CRISPR plasmid vectors

Plasmid vectors were produced using the GeneArt® CRISPR Nuclease Vector with OFP Reporter Kit (Thermo Fisher Scientific) according to the manufacturer's protocol. Two ssDNA gRNA oligonucleotides were annealed together generating a double-stranded oligonucleotide with the appropriate overhangs that is then ligated into the linearized GeneArt® Nuclease Vector. Complete plasmid vectors containing the gene of interest were transformed into One Shot® TOP10 Chemically Competent *E. coli* bacteria (Thermo Fisher Scientific) and selected using ampicillin resistance. 100 µg/ml ampicillin agar plates are made from 7.5 g agarose (Sigma-Aldrich) in 500 ml of LB medium (Sigma-Aldrich) with 500 µl ampicillin (Sigma-Aldrich), and 20-25 ml is poured into 94x16 petri dishes without vents (Roth). The transformed bacteria were spread onto the ampicillin agar plates and incubated at 37 °C overnight. Five colonies were picked and grown in 5 µl LB medium with 100 µg/ml ampicillin in sterile 14 ml pp-tubes (Sigma-Aldrich) overnight at 37 °C with shaking. The next day, CRISPR plasmid vectors were isolated using PeqGOLD plasmid miniprep kit (Peqlab) and a sample was sent for Sanger sequencing (Eurofins Genomics) with the U6 forward primer (Table 1) to confirm correct insertion of the gRNA.

2.2.3 Genome edited single-cell clones

2.2.3.1 Transfection

Wild-type HEK293 cells with a low passage number were seeded 10,000 cells/well in a 96-well plate (Falcon). The next day, the medium was removed and replaced with 100 µl fresh medium. In a sterile 1.5 ml microtube (Axygen), 200 ng of plasmid vector is mixed with Opti-MEM™ Reduced-Serum Medium (Gibco) in a total volume of 25 µl for each well to be transfected. For knock-in cell lines, 200 ng of the HDR oligonucleotide was included in addition to the gRNA. In separate 1.5 ml tubes, 24.5 µl of Opti-MEM™ was mixed with 0.5 µl Genejuice (Millipore). Both solutions were incubated 5 minutes at RT. The Gene-juice solution is gently added to the vector DNA solution and mixed by slowly pipetting up

and down, then incubated 20 minutes at RT. The 50 µl final transfection mixture is added dropwise to the 100 µl of fresh medium in the 96-well plate, and gently rocked back and forth to ensure even distribution, then left to incubate for 48–72 hours. Transfection efficiency is observed using an Axiovert 40 CFL fluorescent microscope via the OFP reporter in the GeneArt vector which causes cells to fluoresce red under green light when the plasmid has been transfected. Cells were checked daily during transfection incubation and a minimum efficiency of 60 % was used to perform a single-cell dilution.

2.2.3.2 Single-cell dilution

The transfection medium was removed from the efficiently transfected cells, detached with 20 µl of trypsin for 5 minutes, then inactivated with 80 µl of medium and resuspended. 50 µl of the cell suspension was taken for counting, while the other 50 µl was added to 5 ml medium in a 15 ml falcon. The cells were counted (2.1.6) and the concentration of cells/ml was then calculated. 0.5 cells/well in 150 µl was pipetted into each well of ten 96-well plates using a 200 µl multi-pipette (Brand) and incubated for two weeks. After two weeks of incubation, the 96-well plates were checked for cell growth, which becomes apparent due to a pH change in the medium from cell respiration which causes the phenol red to shift from red to yellow. Wells were observed under the microscope to confirm growth of a single cell colony. Once the colony grew to cover roughly 30 % of the well, it was re-suspended physically in 150 µl medium, 50 µl of which was put into a fresh 96-well for further growth, and the remaining 100 µl put in a separate well for lysis and sequencing.

2.2.4 Screening of cells for mutations

2.2.4.1 Lysis

Lysis buffer contains 1 mM $CaCl_2$ (1 M stock, Sigma-Aldrich), 3 mM $MgCl_2$ (25 mM stock, Sigma-Aldrich), 1 mM EDTA (0.5 M stock, Sigma-Aldrich), 1 % Triton X-100 (Sigma-Aldrich), and 10 mM Tris (1 M pH 7.5 stock, Sigma-Aldrich), with 0.2 mg/ml proteinase K (Qiagen) added fresh on the day of lysis. Once cells to be lysed (2.2.3.2) had grown to at least 70 % confluency, the medium was removed, 50 µl lysis buffer was applied for 5 minutes, then resuspended and transferred to a PCR microtube strip (Axygen). The cells lysis buffer suspension is then cycled at 65 °C for 10 minutes followed by 95 °C for 15 minutes in a thermocycler then stored at 4 °C for use in further screening.

PCR application	primer	sequence	annealing temp (°C)	product size (bp)
CRISPR screening	APEX1 forward	TGCTGTGTGGAGACCTCAAT	58	479
	APEX1 reverse	CTATCACAGGAGCCTGGTTG		
	ENDOG forward	GCGACGCGGCTCCTTTA	60	424
	ENDOG reverse	GTGCACCGAGTCGTCCTC		
	EXOG forward	ATCATATTCCCCATCCATCG	60	506
	EXOG reverse	TCTGACCTTTATTCTCCCGG		
	LIG3 forward	AGTGCTAGGGTAGTGACTTAACAAG	56	354
	LIG3 reverse	AGCACAGAATTTTCACTCTTTAGCC		
	POLG forward	CAGTGGTTGTTGTGGAGTGG	66	509
	POLG reverse	AAATGCCACAGAGACGAAGG		
	U6 forward	GGACTATCATATGCTTACCG		
southern probe	*18S rRNA* forward	GTTGGTGGAGCGATTTGTCT	55.5	390
	18S rRNA reverse	GGCCTCACTAAACCATCCAA		
	MT-ND5 forward	TCATCCCTGTAGCATTGTTCG	55.5	88
	MT-ND5 reverse	GAAGAACTGATTAATGTTTGGGTCT		
	MT-CO1 forward	CCCACTTCCACTATGTCCTATCAAT	56	114
	MT-CO1 reverse	TGGATTTTGGCGTAGGTTTGGTCT		
qPCR	minor arc forward	ACACCGCTGCTAACCCCATAC	66.2	5104
	minor arc reverse	TTGCGTTCAGTTGATGCAGAGTGG		
	MT-ND1 forward	GAACTAGTCTCAGGCTTCAACATCG	62.5/66.2	115
	MT-ND1 reverse	CTAGGAAGATTGTAGTGGTGAGGGTG		
	KCNJ10 forward	GCGCAAAAGCCTCCTCATT	62.5	69
	KCNJ10 reverse	CCTTCCTTGGTTTGGTGGG		
linker PCR	LMP25	GCGGTGACCCGGGAGATCTGTATTC		
	LMP11	GAATACAGATC		

Tab. 2: PCR primer sequences. Annealing temperatures used and resulting product size for forward and reverse primer pairs are identified. All sequences are written in the 5' to 3' direction.

2.2.4.2 Gradient PCR

PCR Primers were designed for each gene to have an amplicon 500 bp in size with the CRISPR/Cas9 target site centrally located (Table 2). For each primer pair, the annealing temperature was determined using gradient PCR: a master mix contaiing 1 µl of wild-type HEK293 DNA standard, 18.35 µl water, 2.5 µl Accutaq Buffer (Sigma-Aldrich), 2.5 µl of 2.5 mM dNTPs (TaKaRa), 0.4 µl of 25 pmol mix of both forward and reverse primers, and 0.25 µl Jumpstart Accutaq polymerase (Sigma-Aldrich) was made for each 25 µl reaction across 12 microtubes. The gradient program in a MJ Research PTC-200 Peltier Thermal Cycler is performed where each column employs a different annealing temperature from

low (56 °C) to high (68 °C), and thus each microtube is subject to a different annealing temperature. Samples were cycled at 95 °C 5 minutes, 35 cycles of 95 °C 30 seconds, the annealing temp 25 seconds, 72 °C 30 seconds, held for 72 °C for 5 minutes, then to 15 °C. The annealing temperature that resulted in the most defined single band after agarose gel electrophoresis (2.2.4.4) was used for PCRs in clone screening (Table 2).

2.2.4.3 Clone lysate PCR

All PCRs to screen cells for CRISPR/Cas9 generated mutations use same protocol with the annealing temperature based on the corresponding primers (Table 2). The master mix has 18.35 µl water, 2.5 µl Accutaq Buffer, 2.5 µl 2.5 mM dNTPs, 0.4 µl of 25 pmol primers mix, and 0.25 µl Jumpstart Accutaq polymerase each. 24 µl master mix was pipetted into a microtube strip, 1 µl of lysis sample from each clone or wild-type HEK293 cell positive control or water negative control is added to each tube and mixed by pipetting. In a GeneAmp® PCR System 9700 thermocycler, samples underwent a program of 96 °C 5 minutes, 42 cycles of 94 °C 30 seconds, annealing temperature 30 seconds, and 68 °C 1 minute, held at 68 °C for 5 minutes then down to 15 °C. PCR products were visualized in an agarose gel (2.2.4.4). If a band was present, the remaining 20 µl of PCR product was purified using the QIAquick PCR purification kit (Qiagen) according to the manufacturers protocol and the concentration measured using a Simplinano nanodrop (Biochrom).

2.2.4.4 Agarose gel electrophoresis

A 2 % agarose gel was made from 3 g agarose in 150 ml 1× TBE buffer (Sigma-Aldrich), with 6 µl peqGreen DNA/RNA dye (Peqlab) in a 15×25 cm Sub-Cell GT UV-Transparent Gel Tray (Bio-Rad) with a 20-well comb (fixed height, 1.5 mm thickness, Bio-rad), placed in a Bio-Rad sub-cell GT chamber and submerged in 1× TBE buffer. 5 µl of PCR product was mixed with 5 µl loading buffer (New England Biolabs) and loaded into individual wells with 5 µl 1 kb Plus DNA ladder (New England Biolabs) molecular weight marker and ran 45 minutes at 180 V using a Bio-Rad PowerPac Basic power supply. Gels were visualized in an Intas GelStick Imager.

2.2.4.5 Digestion screening

Restriction endonuclease digestion was utilized for knock-in mutation detection due to lower efficiency of HDR oligo incorporation and was designed so that cells that incorporate the oligo are undigested. PCR was performed as in 2.2.4.3. 12.5 µl of lysis PCR product was combined with 7.5 µl of digestion master mix to a total volume of 20 µl. A digestion

master mix contains 2 µl NEB r3.1 buffer (New England Biolabs), 0.4 µl enzyme, and 5.1 µl water per digestion reaction. For POLG the enzyme is *Pst*I (New England Biolabs), incubated at 37 °C for 1 hour followed by 80 °C 20-minute heat inactivation. For APEX1 the enzyme is *Bcl*I (New England Biolabs), incubated at 50 °C for 1 hour. The entire 20 µl digest reaction was mixed with 5 µl loading dye, separated by agarose gel electrophoresis and visualized (2.2.4.4). Undigested clones were then sequenced. The remaining 12.5 µl of lysis PCR product was purified with the QIAquick PCR purification kit according to the manufacturer's protocol and the concentration measured using a Simplinano nanodrop.

2.2.4.6 Sanger sequencing

Purified products from lysate PCR amplification were sent for Sanger sequencing at Eurofins Genomics according to the company guidelines (10 ng/µl) and sequenced with the corresponding forward and reverse primers for that gene (10 pmol). The sequencing results were viewed and compared to the corresponding reference sequence using the *scftk* sequencing program developed by Dr. Gábor Zsurka.

2.2.4.7 HEK293 knock-out cell line expansion and freezing

Once a desired mutation was identified, the cell lines were expanded (2.1.4) for future experimentation. Stock aliquots were frozen by resuspending a cell pellet in Bambanker® freezing medium (Nippon Genetics Europe and GC Lymphotec Inc.), and aliquoting the cell suspension in 2 ml cryogenic tubes (Cryo.s™, Roth). Samples were frozen at -80 °C, followed by transfer to liquid nitrogen for long-term storage.

2.3 Transient oxidative damage

2.3.1 H_2O_2 decay in medium

H_2O_2 decay experiments were performed by Dr. Alexei P. Kudin according to the protocol outlined in Malinska et al. (2012). The H_2O_2 decay was determined in cell culture medium without the phenol red pH-indicator by the fluorometric Amplex red/peroxidase-coupled method using 1 µM Amplex red (Sigma-Aldrich) and 20 U/ml horseradish peroxidase (Sigma-Aldrich) at λ_{ex}=560 nm and λ_{em}=590 nm. H_2O_2 was added to medium or medium with cells and the fluorescence was measured at 0, 10, 30, 60, 180, and 300 seconds. The half-life of the H_2O_2 in either medium alone or in medium with cells was calculated using the equation: half-life = (time × log2) / log (beginning amount/ending amount) for the 10 second time point.

2.3.2 Oxidative damage by H_2O_2

Cells were seeded in 6-well plates (Falcon) either 1 million per well two days before or 1.5 million per well the day before the time course. Six wells were seeded for the different experimental time points: 0 hour (non-treated), 30 minute, 2, 4, 6, and 24 hours. The day of the experiment, a 1 mM H_2O_2 medium master mix was prepared from stock hydrogen peroxide solution (9.8 M, Honeywell) 2 ml per treated well + 1 mL extra. The cell medium was replaced with either 2 ml of fresh medium (0 hour) or 2 ml 1 mM H_2O_2 medium. At each time point cells are collected by gentle resuspension in the 2 ml of medium within the well using a 1000 µl pipette (Eppendorf) with a snipped 1000 µl pipette tip (Axygen). The cell resuspension was transferred directly to a 2 ml microtube (Axygen), and 10 µl of this suspension was taken for cell survival (2.1.6). Cells were centrifuged at 3000 *g* for 10 min, the medium is removed, and the pellets were immediately frozen at -20 °C.

2.3.3 Deferiprone

Deferiprone is an iron chelator that can mediate the effects of H_2O_2 oxidative stress in mitochondria (Kaklon et al., 2008). 50 mg deferiprone powder (Sigma-Aldrich) in 50 ml aH_2O was heated at 37 °C to dissolve, then sterile filtered to make a 7186 µM stock. 50 µM deferiprone medium was applied to the cells for 24 hours before the application of the H_2O_2 (2.3.1), as well as 50 µM deferiprone was included in the H_2O_2 medium.

2.3.4 BrdU

BrdU is a synthetically produced nucleoside analog that is incorporated into the genome in the place of thymidine, and therefore mtDNA replication and repair kinetics can be visualized (Hussain et al., 2021; Kai et al., 2006; Magnusson et al., 2003). 10 mg of 5'-bromo-2'-deoxyuridine powder (Roche) in 10 ml aH_2O is sterile filtered to make 3256 µM stock. 1 ml aliquots were frozen at -20 °C for long-term storage. To visualize the BrdU incorporation into mtDNA and to minimize the nuclear DNA background signal, the nuclear DNA replication inhibitor aphidicolin was used. 1 mg of aphidicolin powder (Sigma-Aldrich) was dissolved in 1 ml sterile DMSO (Sigma-Aldrich) and stored at -20 °C. The 2878 µM stock was used at a 20 µM concentration over cells and applied for 1 hour before the BrdU (Davis and Clayton, 2005). Cells were seeded as in the oxidative stress experiments (2.3.1) with 10 µM BrdU applied to the HEK293 cells in medium or 1 mM H_2O_2 medium. To observe how BrdU is eliminated from cells in different experimental conditions, BrdU is allowed to incorporate into the mtDNA (pulse) and followed (chase) to visualize mtDNA

turnover (Kai et al. 2006). Cells were seeded at a density of 1 million/well in 14 wells of 6-well plates, the next day BrdU is “pulsed” for 24 hours by applying aphidicolin and BrdU. On the day of the experiment, the aphidicolin + BrdU medium was removed from all wells besides the 0-hour time points, and 2 ml medium or medium with 1 mM H_2O_2 is applied as in 2.3.1 with a 48-hour time point included.

2.3.5 DNA isolation

DNA from frozen cell pellets is isolated with the QIAamp DNA mini kit (Qiagen) according to the manufacturers tissue isolation protocol. The initial 56 °C lysis step in ATL buffer and proteinase K was performed for a minimum of 4 hours to ensure that the cell pellet was completely dissolved. DNA samples were eluted twice in 200 µL buffer AE with 5-minute incubations then stored at 4 °C. DNA concentration was measured using a Qubit™ 4 fluorometer (Invitrogen). Qubit™ 1× dsDNA HS Assay Kit (Invitrogen) was used according to the manufacturer’s protocol using the Qubit™ assay tubes (Invitrogen). Standards were calibrated for every set of measurements by mixing 10 µl standard DNA + 190 µl Qubit™ 1× dsDNA HS Working Solution. For each sample, 2 µl of DNA was mixed with 198 µl fluorescent working solution. All tubes were vortexed and incubated for 2 minutes at RT and then measured in ng/µl.

2.4 qPCR

Quantitative PCR (qPCR) can be used to determine the relative amount of DNA present in a sample. SYBR green fluorescent dye intercalates with dsDNA and the amount of light signal emitted directly correlates to the abundance of the corresponding DNA within that sample as measured by the amplification dynamics cycle by cycle.

2.4.1 mtDNA copy number

qPCR was used to determine the number of mtDNA copies per cell and enrichment when isolating mitochondria from whole cells (2.6.1). 20 ng and 10 ng of DNA samples were pipetted in triplicate in a 0.2 ml semi-skirted 96-well PCR plate (Thermo Fisher Scientific) in a volume of 12.5 µl using a 200 µl Research pro multipipette (Eppendorf), including a triplicate of water negative control. A master mix is made with 11.9 µl 2× SYBR Green qPCR master mix (Bimake™) and 0.6 µl of 12.5 pmol forward and reverse primer mix per reaction. Primers for a single-copy gene *KCNJ10* quantify the amount of nuclear DNA and primers for the *MT-ND1* quantify mtDNA (Table 2). 12.5 µl of Master mix was pipetted in the 96-well plate on top of the DNA dilutions (6 reactions per primer pair: 2 DNA concen-

trations in triplicate). The plate was then sealed with an adhesive sealing sheet (Peqlab), vortexed, and spun down in a PerfectSpin plate centrifuge (Peqlab) to collect the reaction then ran in a C1000 Touch™ Thermal Cycler CFX96™ Real-Time System (Bio-Rad). The qPCR program employs an initial denaturation step to make all the supercoiled mtDNA available at 95 °C for 15 minutes (Zsurka et al., 2023), followed by 45 cycles of 95 °C for 15 seconds and 62.5 °C for 1 minute, where the fluorescence intensity is measured after each cycle. A melting curve follows to verify the amplification efficiency of a single product: the temperature is increased from 55 °C to 95 °C by 0.5 of a degree every 10 seconds and the denaturing of dsDNA releases the bound SYBR green and leads to a decrease in fluorescence. A DNA specific qPCR reaction results in one singular fluorescent peak and a singular band of the correct size after gel electrophoresis (Svec et al., 2015).

2.4.2 qPCR data analysis

The results from the Bio-Rad CFX Manager program, without background subtraction or curve fit, were fit to a sigmoidal regression or Chapman curve (Zhao and Fernald, 2005) in SigmaPlot. The inflection point in this sigmoid curve for sample fluorescence determines the Ct value and likewise the relative amount of DNA present. From the Ct values for the nuclear and mitochondrial primers, the mtDNA copy number per cell can be calculated, with the Ct of the nuclear gene used as the reference:

mtDNA copy number = (2^(nuclear Ct – mitochondria Ct))x2.

2.4.3 mtDNA damage quantification

By comparing a short mtDNA qPCR product to a product over a larger region of mtDNA, the relative amount of damage in different samples can be quantified. The small fragment should be easily amplified, and damage present in the large fragment will cause the polymerase to fall off and that fragment to not be amplified. DNA was diluted and the mix prepared as in 2.4.1. The *MT-ND1* primers were used for the short 115 bp product, and primers that cover 5104 bps of the minor arc were the long product (Table 2). The cycling conditions were 95 °C for 15 minutes, 45 cycles of 95 °C for 15 seconds and 69.1 °C for 6 minutes. The Ct values were determined as in 2.4.2. The short product Ct is subtracted from the long product Ct for a numerical representation of the amount of damage present within the mtDNA of that sample. The Ct difference of the 0-hour control sample was taken as baseline and subtracted from every sample. The relative frequency of mtDNA strand breaks in the sample was calculated as: $\ln(2^{((Ct_{long} - Ct_{short}) - \Delta Ct_{non\text{-}treated\ control})}$.

2.5 Southern blotting

2.5.1 Gel electrophoresis

Agarose gel electrophoresis was used to separate 1 µg of total DNA per sample. 1 µg of total DNA was brought to 26.5 µl by the addition of Millipore water, or by evaporation at 45 °C in a Concentrator 5301 (Eppendorf). *Mlu*I-HF (New England Biolabs) digests the nuclear encoded 18S ribosomal RNA genes as a loading control while leaving mtDNA undigested. The 18S gene is repeated five times in the nuclear genome and *Mlu*I digests twice in the sequence of the *18S rRNA* genes generating a fragment 5856 bp in size. A master mix of 0.5 µl *Mlu*I and 3 µl rCutsmart™ buffer (New England Biolabs) per sample was made and 3.5 µL was added to each then incubated at 37 °C for 1 hour. 0.5 µl *SnaB*I (New England Biolabs) was added if it was desired to linearize the mtDNA in addition to the 18S loading control. A 0.6 % agarose gel was made from 1.8 g agarose in 300 ml 1× TBE buffer, heated to dissolve, and allowed to cool for 10 minutes before the addition of 15 µl EtBr (1 % solution, 10 mg/mL, Biochemica). After DNA digestion, 5 µl of 6× Purple loading dye (New England Biolabs) was added to each sample. A 3× ladder master mix has 15 µl 1 kb extend ladder (New England Biolabs), 6 µl DIG marker II (Roche) and 15 µl 6× Purple loading dye. The total 35 µl of digested DNA and loading dye was loaded in the gel and 12 µl of the ladder master mix was loaded on either side of the samples, which were separated at 40 V overnight.

2.5.2 Transfer to membrane

The 250 mM HCl solution is 125 ml 2 M stock (Bernd Kraft) with aH_2O to 1 liter. Denaturing solution is 100 ml 10 M NaOH (Merck), 175.3 g NaCl (Sigma-Aldrich), and aH_2O to 2 liters. Neutralizing solution is 175.2 g NaCl, 121.1 g Tris (Sigma-Aldrich), 80 ml of 37 % HCl (VWR) to adjust the pH to 7, and aH_2O to 2 liters. 2× SSC solution is 200 ml of 20× SSC buffer (VWR) with aH_2O to 2 liters. After the DNA has been separated, the gel undergoes depurination by washing in 1 liter 250 mM HCl for 30 minutes with shaking. The gel was then rinsed twice in aH_2O. The gel is denatured by washing 2× in 1 liter denaturing solution for 20 minutes with shaking. The gel was again rinsed twice in aH_2O. Finally, the gel is neutralized by washing 2× in 1 liter neutralizing solution for 20 minutes with shaking. The DNA from the washed gel is transferred to a Zeta-Probe® blotting membrane (Bio-Rad) via a stack. The membrane and filter papers are cut to size (14 cm by 23 cm for a full comb), and then the membrane is soaked in aH_2O for at least 5 minutes. The bottom

chamber is filled with approximately 1.6 liters of 2× SSC (400 ml 2× SSC for the next day). A plastic gel tray is then placed upside-down in the chamber, and thin 3 mm CHR Whatman® filter paper (25x23 cm, GE) soaked in 2× SSC is placed on top with the sides dipping into the SSC in the chamber. Between each layer bubbles are removed by rolling a pipette over the layers of the stack. The gel is placed on the tray and thin filter paper in the chamber. The membrane is soaked in 2× SSC before being placed on top of the gel. Two layers of Thick Blot Filter Paper (Bio-Rad) soaked in 2× SSC are added to the stack. Parafilm® (Amcor) is used along the sides of the membrane to avoid contact with the next layer. Finally, an 8 cm tall stack of paper towels is added to facilitate flow of the buffer and transfer of the DNA. The stack is left to transfer overnight at RT. The next day, all the papers are removed, and the membrane is washed in 2× SSC for 3 minutes to remove gel traces. The excess 2× SSC is then allowed to drip from the membrane before it is laid flat to dry for 30 minutes at RT then baked for 30 minutes at 80 °C between two Whatman® paper sheets. After baking the membrane can be stored long term at 4 °C.

2.5.3 DIG probe hybridization and imaging

The DIG hybridization system from Roche works by employing an alkali-labile DIG-11dUTP construct. When incorporated into a DIG probe labeling a DNA region of interest, it allows for non-radioactive visualization of DNA on a Southern blot.

2.5.3.1 DIG probe production

A mitochondrial probe labels the *MT-ND5* region of the mitochondrial genome, and an *18S rRNA* nuclear DNA probe labels the loading control (Table 2). Probes are made using the DIG Probe PCR Kit (Roche). A reaction mix containing 28.25 µl water, 5 µl 10x PCR Buffer with $MgCl_2$, 5 µl 10× PCR DIG Probe Synthesis Mix, 10 µl 25 pmol of both forward and reverse primers, 0.75 µl Expand High Fidelity 3.5 U/µl Enzyme Mix, and 1 µl HEK293 control DNA (50–150 ng/µl) was made. The mix was aliquoted into 25 µl reactions in PCR strips and ran in the thermocycler: 95 °C for 5 minutes, 30 cycles of 95 °C for 30 seconds, 55.5 °C for 45 seconds, and 72 °C for 45 seconds, followed by 72 °C for 10 minutes then lowered to 4 °C. Gel electrophoresis was performed as in 2.2.4.4. The resulting band of PCR generated hybridization probe was excised from the gel and purified using QIAquick® Gel Extraction Kit (Qiagen) according to the manufacturers protocol, eluting 2× in 50 µl elution buffer, and the concentration was measured using a Simplinano nanodrop.

2.5.3.2 Hybridization

The Southern blot membrane was cut to size to prevent overlapping (10.5 cm maximum for tube circumference) and placed in the glass hybridization tube (30 cm, UVP) with the DNA facing inside. 40 ml DIG Easy Hyb (Roche) hybridization buffer was added into the tube and rolled for 3 hours at 48 °C in a UVP Hybridizer Oven (AnalytikJena). 10 ml DIG Easy Hyb was preheated to 48 °C in a falcon-tube 30 minutes before 200 ng of the desired DIG probe was denatured at 95 °C for 15 minutes. The buffer from the hybridization tube was discarded, the denatured probe was spun down and then immediately added to the preheated 10 ml buffer for a final concentration of 20 ng/ml, poured over the membrane and rolled at 48 °C overnight.

2.5.3.3 Imaging

Southern blots were imaged using the DIG Wash and Block Buffer Set (Roche). Washing buffer is 15 ml 10× washing buffer in aH_2O to 150 ml. Blocking buffer is 10 ml 10× blocking solution with 90 ml 1× maleic acid buffer in aH_2O to 100 ml. All wash steps were performed at RT with rolling. The hybridization buffer was discarded, the membrane was rinsed in aH_2O, washed for 3 minutes in aH_2O, then for 5 minutes in 50 ml washing buffer. The membrane was blocked in 50 ml blocking buffer for 1 hour. 5 µl of alkaline phosphatase conjugate antibody (Anti-Digoxigenin-AP, Fab fragments; Roche) was added to the remaining 50 ml of blocking buffer, spread over the membrane, and rolled for 45 minutes. The membrane was washed 2× in 50 ml washing buffer for 15 minutes, rinsed in aH_2O, and 20 ml of fresh detection buffer from 2 ml of 10× detection buffer in aH_2O was spread over the membrane and rolled for 5 minutes. The membrane was then removed from the hybridization tube and placed in a nylon bag cut from 3 sides. CSPD (Roche), an alkaline phosphatase substrate which emits chemiluminescence, was added dropwise to cover the membrane and the nylon bag was closed removing all bubbles. The membrane was incubated at RT for 10 minutes, the excess CSPD was removed, then baked at 37 °C for 15 minutes. Visualization was done in a ChemiDoc Imaging System (Bio-Rad) selected for single-channel chemi-blots.

2.5.3.4 Stripping

The membrane must be stripped before a new probe can be hybridized to observe another region of DNA. Stripping buffer contains 0.2 M NaOH (8 ml 10M NaOH stock), 0.1 % SDS (4 ml 10% SDS stock, Sigma-Aldrich), and aH_2O to 400 ml. The membrane was inserted

in the hybridization tube with the DNA facing inside, rinsed in aH_2O, and washed 2× at 37 °C for 15 minutes in the stripping buffer, then washed for 5 minutes in 2× SSC, after which hybridization and imaging can be completed as before (2.5.3.2 and 2.5.3.3).

2.5.4 BrdU detection

A Southwestern imaging technique was used to visualize BrdU incorporation into mtDNA (2.3.4). DNA was separated in a gel and transferred to a nylon membrane as outlined in 2.5.1 and 2.5.2, and a BrdU antibody was used to image the BrdU incorporated DNA.

2.5.4.1 BrdU antibody imaging

Southwestern imaging was based on the protocol described in Magnusson et al. (2003). 1 liter of 1× PBS is 100 ml 10× PBS stock in 900 ml aH_2O. PBST was made from 598 ml 1× PBS and 2 ml TWEEN®20 (Sigma-Aldrich). 50 ml of 1× PBS with 5 g nonfat dry milk powder (ROTH) creates a 10 % w/v solution, and 50 ml of PBST with 1 g nonfat dry milk powder creates a 2 % w/v solution. All steps were carried out at RT with rolling. The membrane was inserted into the hybridization tube with the DNA facing inside and washed in aH_2O for 3 minutes, followed by 5 minutes in PBST. The membrane was blocked in the 10 % w/v solution for 1 hour and then washed with PBST. The primary antibody Anti-bromodeoxyuridine (mouse IgG, Sigma-Aldrich) was diluted 1:600 in 25 ml 2 % w/v solution and the membrane was incubated for 2 hours. The membrane was washed 3× for 10 minutes in PBST. The secondary antibody goat anti-mouse HRP conjugate (Bio-Rad) was diluted 1:3000 in 25 ml 2 % w/v solution and the membrane was incubated for 1 hour. The membrane was washed 3× for 10 minutes in PBST, followed by a wash in 1× PBS. Clarity Western ECL Substrate Chemiluminescent Development (Bio-Rad) solutions were used to image the membrane by mixing the Clarity Western Peroxide Reagent and the Clarity Western Luminol/Enhancer Reagent in a 1:1 ratio (20 ml, 10 ml of each buffer) and then incubating for 5 minutes. The membrane was removed from the hybridization tube and placed in a nylon bag cut from 3 sides ensuring no bubbles are present. The blot was imaged using the ChemiDoc Imaging System selected for single-channel chemi-blots.

2.5.4.2 BrdU antibody stripping

BrdU blot membranes can be additionally probed with DIG labeled DNA probes (2.5.3) to image the nuclear loading control, ladder, and total mtDNA. BrdU antibody labeling was stripped using a glycine solution to dissociate the bound antibodies and low pH to alter the protein structure so that binding sites are altered and rendered inactive. Western blot

stripping buffer is 15 g glycine (1.5 % w/v, Merck), 0.1–1 % SDS (10 ml 10 % stock), 10 ml Tween20 (1% v/v), and aH_2O to 800 ml. The pH was adjusted to 2.2 with 37 % HCl, and the final volume was brought to 1 liter with aH_2O. All steps in stripping were carried out at RT with rolling. The membrane was inserted into a hybridization tube, rinsed in aH_2O, then incubated twice in stripping buffer for 10 minutes. The membrane was washed twice in 1× PBS for 10 minutes, followed by two washings in 2× SSC for 5 minutes (PBST is used if imaging by western blotting after stripping). The blot can then be DIG probe hybridized and imaged as outlined in 2.5.3.2 and 2.5.3.3.

2.5.5 Southern blot quantification

ImageJ was used to quantify the bands in the southern. Mean intensity of the selected region including the band and the area were measured, as well as a mean intensity background measurement directly proximal to the band. The background was subtracted from each band intensity and multiplied by the area of the region including the band to determine total band intensity. The 18S band intensity was used to normalize as a loading control. Bands were then further normalized to the non-treated sample for that cell line, where the sum of the major mtDNA species is treated as 100 % of mtDNA. In BrdU blots, samples were normalized to the 18S and to the 24-hour control sample on the blot.

2.6 Western blotting

Western blotting was performed by Dr. Alexei P. Kudin according to the protocol outlined in Peeva et al. (2018): Cells were sonicated (2 × 15 s at 8 % amplitude) in cell lysis buffer containing 20 mM Tris-HCl (pH 7.4), 150 mM NaCl, 1mM EDTA, 1mM EGTA, 1 % Triton and protease inhibitor cocktail (Roche). Protein amount was determined using the BCA assay. Protein (15–40 µg) in Laemmli buffer were resolved on a 10% polyacrylamide gel and transferred to a HybondTM P 0.45 PVDF-membrane (Amersham). Membranes were incubated overnight at 4 °C with the primary antibodies: β-actin (Gene Tex, 1:10,000), LIG3 (Sigma-Aldrich, 1:500). Detection was performed with a HRP-conjugated secondary antibody (goat anti-rabbit IgG–Peroxidase, Sigma-Aldrich, 1:20,000) and SuperSignal West Pico Plus chemiluminescent substrate (Thermo Scientific) on a ChemiDoc Imaging System.

2.7 Next-generation deep sequencing

To determine the nature and location of mtDNA DSBs and ends of linear fragments in the different treatment conditions, next-generation massively parallel deep-sequencing was

employed. The non-treated, acute oxidative stress 30 minutes after H_2O_2, and long-term recovery from oxidative stress of 24 hours after H_2O_2 were chosen to observe the mtDNA in more detail. Isolated mtDNA samples for deep sequencing were collected by the author, Dr. Viktoria Peeva, and Afaf M. Said.

2.7.1 Mitochondrial DNA isolation

Mitochondria were isolated from whole cells via differential centrifugation as outlined in Trounce et al. (1996).

2.7.1.1 Cell collection

Cells were expanded (2.1.4) to 16 TC Dish 150 plates (Sarstedt) per isolation condition to have 300-900 million cells, and treated accordingly if H_2O_2 stress was desired (2.3.1). The medium was removed, the cells were washed with 5 ml 1× PBS, detached with 2 ml of trypsin for 5 minutes which is then inactivated with 7 ml medium, and the resuspended cells were moved to 50 ml falcons. The cells were pelleted at 500 *g* for 10 minutes, the supernatant was removed, the cell pellets were resuspended in 50 ml 1× PBS and combined in one falcon. The 50 µl cell suspension was spun at 3000 *g* for 10 minutes for a total DNA pellet. Another 50 µl of cell suspension was taken for counting and cell survival (1:20, 2.1.1.6). The remaining 50 ml cell suspension is then pelleted at 500 *g* 10 minutes, the supernatant is removed, and the pellet is placed on ice.

2.7.1.2 Buffer preparation

A 0.5 M HEPES-KOH buffer solution is 11.915 g HEPES-KOH (Sigma-Aldrich) in 100 ml of aH_2O with pH=7.2 by KOH (Sigma-Aldrich). IB is 210 mM mannitol (19.1 g, Sigma-Aldrich), 70 mM sucrose (11.98 g, Sigma-Aldrich), and 5 mM HEPES-KOH (5 ml buffer solution) to 500 ml in aH_2O, which is stored at 4 °C. Digitonin solution is 40 mg digitonin powder (Serva) in 800 µl aH_2O, heated at 95 °C for 5 min or until dissolved. On the day of isolation, the Multifuge 1 centrifuge (Thermo Fisher Scientific) is cooled to 4 °C and 50 ml falcons and the 15 ml glass homogenizer with pestle “A” (Kontes glass co.) are put on ice.

2.7.1.3 Homogenization

Before mitochondria isolation, cold IB was bubbled with argon gas (Linde) for a minimum of 30 minutes to remove any oxygen in the solution that would result in additional oxidative mtDNA damage. After bubbling, 1 ml per sample of IB + argon was reserved for later use, and the working IB+BSA solution was made by adding 250 mg of BSA (PAN Biotech) per 100 ml bubbled IB. All steps were performed on ice. Cell pellets were weighed and

resuspended in 4 ml of IB+BSA per 1 g of pellet. 2× the grams of cell pellet in µl of digitonin was added to the IB+BSA cell suspension and incubated for 1 minute. Cells were checked for membrane permeability by mixing 10 µl of suspension with 10 µl erythrosin B dye and visualized under the microscope in a Neubauer hemocytometer slide. Digitonin was added in this manner until 80–90 % of the cells were permeable, after which the falcon was filled to 50 ml with IB+BSA to dilute the digitonin. The falcon was spun at 3000 *g* for 5 minutes at 4 °C. The supernatant was discarded, the cell pellet was resuspended in 15 ml IB+BSA and transferred to the 15 ml homogenizer. Cells were homogenized by two down and up strokes of the pestle, and the amount of disruption was checked under the microscope using erythorsin B dye until there was no more than 10 % of undisrupted cells; if additional homogenization was required the amount of cell disruption was checked again after each additional down and up stroke. The homogenate was moved to a cold 50 ml falcon tube and the homogenizer was then washed with 11 ml additional IB+BSA which was added to the falcon and filled to 50 ml with IB+BSA.

2.7.1.4 Differential centrifugation

All centrifugation steps were carried out at 4 °C. The 50 ml of cell homogenate IB+BSA was spun 2× at 1000 *g* for 5 minutes to remove the nuclei, transferring the supernatant to a new cold falcon tube after each spin. The cell homogenate supernatant was then spun at 10,000 *g* for 30 minutes. The supernatant and white membranes were discarded, and the brown mitochondria pellet was resuspended in 5 ml IB+BSA and centrifuged at 10,000 *g* for 30 minutes. At this step the Centrifuge 5415 R (Eppendorf) is cooled to 4 °C. The supernatant and the remaining white pellet were discarded, and the mitochondria were resuspended in 700 µl of IB+BSA and moved to a cold 1.5 ml microtube. The falcon was washed with an additional 700 µl of IB+BSA which was added to the microtube. The suspension is centrifuged at 10,000 *rpm* for 15 minutes, the supernatant and any white pellet was removed, the mitochondria were dissolved in 1 ml of IB+BSA and spun again at 10,000 *rpm* for 15 minutes. The mitochondria were then proteinase K digested by re-suspension in 900 µl cold IB+argon with 15 µl of proteinase K (Qiagen) at 26 °C for 1 hour. The mitochondria were pelleted at 10,000 *rpm* for 15 minutes, the supernatant was removed, and washed twice more by resuspension in 1 ml IB+BSA and spinning at 10,000 *rpm* for 15 minutes. mtDNA isolation was proceeded with directly by following the QIAamp DNA mini kit tissue isolation protocol with minor alterations. The mitochondria pellet was

dissolved in 180 µl of ATL buffer with 20 µl proteinase K at 56 °C for 10 minutes. After ethanol is added, the pellet was split into 2 or 3 isolation columns depending on the size of the mitochondria pellet. mtDNA was eluted 4× in 200 µl AE buffer per column, with a 10-minute incubation before each elution. Samples were evaporated at 45 °C for at least 2 hours until approximately 200 µl volume remained, after which the multiple aliquots were combined. mtDNA concentration was measured by the Qubit (see 2.3.5) and the volume was estimated to determine the amount of mtDNA isolated.

2.7.2 Sample preparation

Before isolated mtDNA samples were sent for deep sequencing, mtDNA copy number qPCR (2.4.1) was performed on the isolated mtDNA and compared to the total DNA from the same sample to observe mtDNA enrichment, as well as visualized using southern blotting (2.5) where 20 ng of isolated mtDNA was loaded into the gel.

2.7.2.1 S1 treatment

S1 nuclease cleaves dsDNA at nicks, gaps, mismatches, or loops, and it also degrades ssDNA (Chaudhry and Weinfeld, 1995; Shishido and Ando, 1975; Tullman et al., 2011), and was utilized to observe the amount of SSBs present in our mtDNA samples. Due to DNA loss during purification processes, the ideal starting amount of mtDNA is a minimum of 6 µg. 1 µl S1 nuclease (Thermo Fisher Scientific) digests 350 ng of mtDNA with 5× S1 nuclease buffer (Thermo Fisher Scientific) and aH_2O to the appropriate volume. Samples were digested at 37 °C for 15 minutes, then inactivated with 2 µl 0.5 M EDTA per 30 µl digestion mix at 70 °C for 10 minutes. S1-nuclease digested mtDNA was purified with the QIAamp DNA mini kit using the blood protocol, scaling up the digestion buffers as necessary, using two columns, and eluting 4× in 200 µl of elution buffer. Samples were evaporated and aliquots were combined for a final S1 treated mtDNA sample. Volumes were estimated and the concentration was measured with the Qubit (2.3.5).

2.7.2.2 Enzymatic blunting of DNA ends

To convert potential overhangs at DSBs to ligatable blunt-ends and increase the efficiency of linker ligation, mtDNA samples were treated with the Quick Blunting™ Kit (New England Biolabs) according to the manufacturer's protocol. The kit contains T4 DNA polymerase which blunts any DNA overhangs with its 3'-5 exonuclease activity and 5'-3' polymerase activity, and T4 polynucleotide kinase that phosphorylates the blunt ends to increase ligation efficiency. 3 µg mtDNA was treated with 1 µl of enzyme mix for 30 minutes at RT.

2.7.3 Illumina sequencing

2.7.3.1 Linker generation

The linker construct is annealed from two single-stranded oligos into a double-stranded oligo that is ligated to blunt ends in the mtDNA. A master mix of 20 µl of LMP25, 20 µl of LMP11 (Table 2, both 100 pmol/µl), and 60 µl of TE buffer (Sigma-Aldrich) was mixed and pipetted into 50 µl aliquots in PCR microtubes. The oligos were annealed by a program of 95 °C for 3 minutes, 95 °C for 1 minute, and 181 cycles with a temperature decrease of 0.5 °C each cycle before being brought to 4 °C.

2.7.3.2 Linker ligation

5 µl of linker (2.7.3.1), 1 µl T4-DNA ligase (New England Biolabs), and 10× T4-ligase buffer (New England Biolabs) was used to ligate 200 ng of DNA and scaled according to the amount of mtDNA. Ideally, 3000 ng of mtDNA underwent linker ligation due to DNA loss during purification. Samples were incubated overnight at RT and inactivated the next day at 65 °C for 10 minutes. Ligated mtDNA samples were purified with the QIAamp DNA mini kit using the blood protocol, eluting 4× in 200 µl of elution buffer, then evaporated to approximately 200 µl and the concentration was measured with the Qubit (2.3.5).

2.7.3.3 Illumina short-read sequencing

1 µg of each linker ligated mtDNA sample was sent to the Cologne Center for Genomics (CCG) as part of the West German Genome Center (WGGC) in Cologne, Germany, for sequencing (https://ccg.uni-koeln.de/). Methods taken from Trombly et al. (2023): “The Illumina TruSeq nano DNA Sample Preparation Kit and Agencourt AMPure XP beads were used for library preparation and size selection. One cycle of PCR followed to complete library adaptor structure. Libraries were validated with the Agilent 2200 TapeStation and quantified by qPCR. 150-bp paired-end reads were generated using an Illumina NovaSeq 6000 instrument (Illumina, San Diego, CA, USA). For each sample, $0.7–1.4 \times 10^7$ paired mitochondrial reads were obtained representing 50–95% of all reads and resulting in $1.2–2.3 \times 10^5$ average coverage.”

2.7.4 PacBio sequencing

2.7.4.1 mtDNA linearization

6 µg mtDNA (ideally, due to loss in purification) was digested with *Eag*I (New England Biolabs): 1 µl of *Eag*I per 1 µg of mtDNA and 10× rCutsmart™ buffer was combined with aH_2O to the appropriate volume, incubated at 37 °C for 1 hour, and inactivated at 65 °C

for 20 minutes. The digested mtDNA samples were purified with the QIAamp DNA mini kit using the blood protocol, eluted 4× 200 µl elution buffer, evaporated to approximately 200 µl, and the concentration was measured with the Qubit (2.3.5).

2.7.4.2 PacBio single-molecule long-read sequencing

1 µg of each linearized mtDNA sample was sent to the Genomics & Transcriptomics Laboratory (GTL) as part of the West German Genome Center (WGGC) in Düsseldorf, Germany, for sequencing (https://www.gtl.hhu.de/). Methods taken from Trombly et al. (2023): “Samples were RNase digested and purified on 0.8X AMPure PB beads prior to library preparation with the Express Template 2.0 kit (Pacific Biosciences) according to the protocol “Procedure & Checklist - Preparing Multiplexed Microbial Libraries Using SMRTbell Express Template Prep Kit 2.0” (Version 04, November 2019) without additional DNA shearing, starting with removal of single-strand overhangs, and using the Barcoded Overhang Adapter Kit 8A or B (Pacific Biosciences) for adapter ligation. After library preparation six libraries were pooled equimolarly and the pools size selected with diluted AMPure PB beads to remove fragments < 3kb. Library pools were quantified (Qubit) and analyzed for final fragment size distribution (Fragment Analyzer). Sequencing primers and polymerase were successively annealed and bound to the libraries and each pool was sequenced on one 8M SMRT cell on a Sequel II Instrument (Pacific Biosciences) with 30 h movie time and 2 h pre-extension. Circular consensus sequence reads were generated and demultiplexed with SMRT Link v9 (Pacific Biosciences). $5–22\times10^4$ reads were obtained per sample.”

2.7.5 Deep sequencing analysis

Analysis of all deep sequencing samples for the purpose of this thesis was generously performed by Dr. Gábor Zsurka, as described in Trombly et al. (2023). For Illumina sequencing, reads were aligned to sample-specific reference mitochondrial sequences and screened for the linker sequence using an in-house Perl script. In PacBio sequencing, alignment of long-reads was performed using an in-house R script based on the pairwise Alignment function of the Biostrings package (version 2.64.1). Only ends with a relative frequency of $> 3 \times 10^{-5}$ were used for further analysis.

3. Results

3.1 H_2O_2 decays rapidly in cell culture medium

To determine how the application of H_2O_2 oxidative stress would act on the HEK293 cells in our experiments, it was necessary to first determine the rate of decay of the hydrogen peroxide when it is added to the cell culture medium. 1 mM H_2O_2 was added to cell culture medium without phenol red and measured using Amplex™ red – horseradish peroxidase coupling (Figure 5). As soon as the H_2O_2 is added to the cell culture medium, it begins to undergo chemical reactions and the amount of hydrogen peroxide rapidly decays, which is potentially exacerbated by the pyruvate in our medium added to support the metabolism of the HEK293 cells (Guarino et al., 2019). The half-life of H_2O_2 in medium was measured to be 9.75 seconds, while in medium containing cells H_2O_2 decays at a faster rate with a half-life of 7.8 seconds, with there being significantly less H_2O_2 present in the medium with cells from the 10 second measurement and onward. This faster rate of decay is due to additional metabolism of the H_2O_2 when cells are present. Because of the rapid decay that occurs once the H_2O_2 is added, the application of H_2O_2 represents a short pulse and we observe the effects of transient oxidative stress on our cell lines.

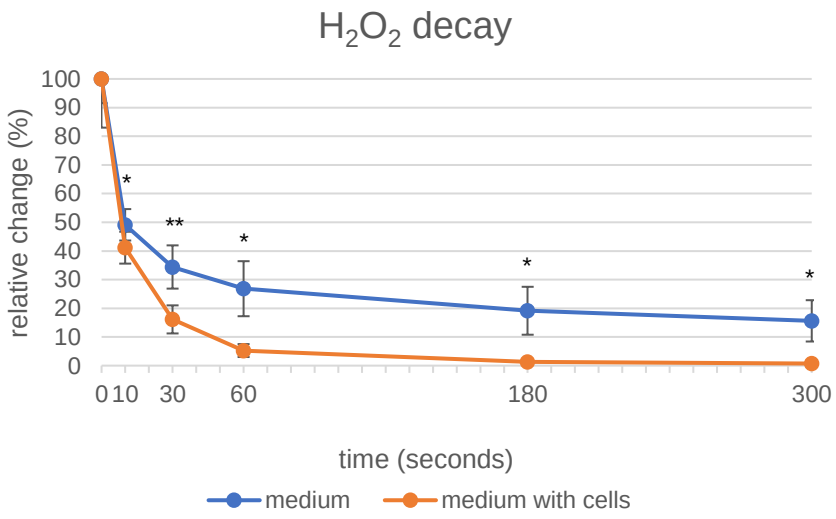

Fig. 5: The decay of hydrogen peroxide in cell culture medium. The amount of hydrogen peroxide measured in cell-free medium is represented by the blue curve, while the orange curve represents hydrogen peroxide added to medium containing HEK293 cells. Samples were taken at the starting point, 10, 30, 60, 180, and 300 seconds, and the percentage of the original amount of hydrogen peroxide in the medium is shown. n=4. error bars, ±SD. *, $p<0.05$, **, $p<0.01$ by a Student's unpaired t-test at each time point. The half-life of hydrogen peroxide was determined to be 9.75 seconds in medium alone and 7.8 seconds in medium with cells.

3.2 H_2O_2 induced oxidative stress on control HEK293 cells

Control, wild-type, HEK293 cells were used to establish how exposure to H_2O_2 affects mtDNA. Oxidative stress was induced on the HEK293 cell lines by applying 1 mM H_2O_2 and the resulting effect on mtDNA was followed in a time course to observe the mtDNA damage after this applied oxidative stress and the subsequent repair or degradation as well as *de novo* synthesis of the mtDNA.

3.2.1 Control cells survive H_2O_2 application

Viability was determined during the application of 1 mM H_2O_2 to ensure that observed effects are not a result of an increase in cell death (Figure 6). The average viability before H_2O_2 application, at the 0-hour time point, is 76.7 %. The viability remains constant throughout the initial time course but does decrease significantly to an average of 62.2 % living cells 24-hours after H_2O_2 application. However, because the major fraction of cells survive the applied H_2O_2 pulse, it was concluded that cell death is not a major contributor to the later observed effects on mtDNA.

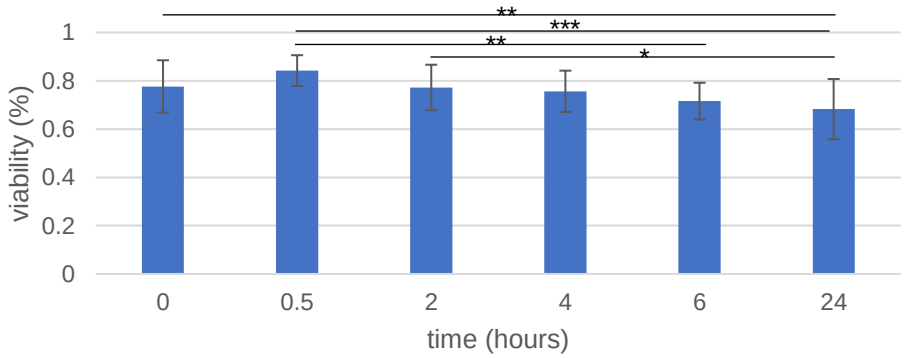

Fig. 6: Cell survival data for control cells lines during the H_2O_2 time course. At each time point (0 hour, 30 minute, 2, 4, 6, and 24 hour) viability is determined by calculating the percentage of alive cells out of the total number of cells. n=15. error bars, ±SD. *, $p<0.05$, **, $p<0.01$, ***, $p<0.001$ by one-way ANOVA with Bonferroni comparison of means. The viability of cells remains consistent throughout the experiment and remains above 60 % 24-hours after H_2O_2 application.

3.2.2 Control cells eliminate damaged mtDNA after H_2O_2 induced oxidative stress

Southern blotting without in vitro linearization was used to observe the conformation of mtDNA from the time course experiment of 1 mM H_2O_2 induced oxidative stress (Figure 7). Four major species of mtDNA can been seen: the native supercoiled, the relaxed or open circle form, the full-length double-stranded linear, as well as a smear of linear mtDNA

fragments of different sizes. Due to the intercalation of EtBr into the DNA the supercoiled species becomes even more compact and migrates faster through the agarose gel, which allows for more separation and better observation of the mtDNA conformations (Aaij and Borst, 1972; Kolesar et al., 2013). Before the application of H_2O_2, at the 0-hour point, the major species of mtDNA is the native supercoiled form. After the transient H_2O_2 pulse the supercoiled species decreases which corresponds with an increase in the level of open circle and linear forms. Because of the large amount of damage that results from the strong 1 mM H_2O_2 treatment, DSBs are frequent and the amount of linear mtDNA species increases significantly. Over the time course of the experiment the level of supercoiled is seen to recover, and the amount of linear mtDNA decreases significantly. Therefore, we were able to observe the damage that occurs after the application of H_2O_2 oxidative stress, and the partial recovery of the native supercoiled species.

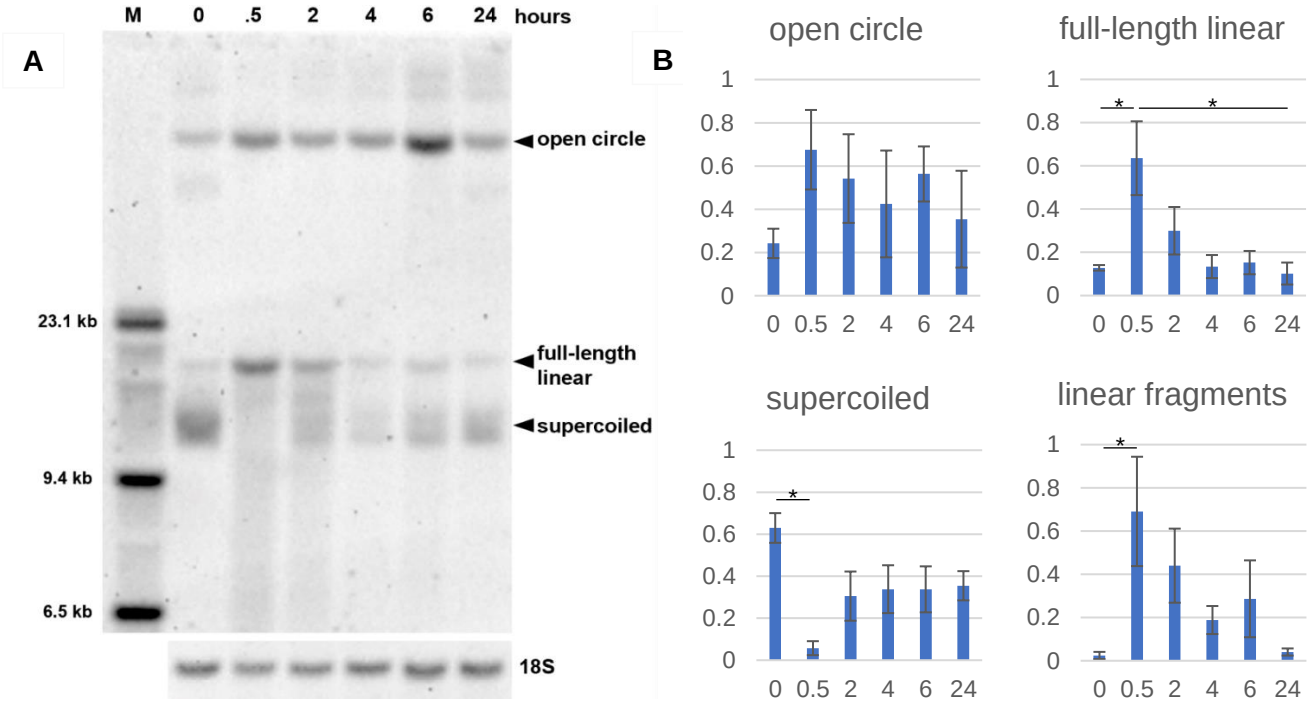

Fig. 7: Southern blot of a 1 mM H_2O_2 experiment on control HEK293 cells. **A)** Southern blot depicting the time course of a H_2O_2 pulse on control HEK293 cells. The top label is time after H_2O_2 application in hours with "M" molecular weight marker. The blot is labeled for the *MT-ND5* region of the mitochondrial genome with the 18S nuclear band as a loading control. Four main conformations of mtDNA can be seen: the open circle, the full-length linear, the supercoiled circular genome, and a smear of linear fragments of different sizes. **B)** Quantification of the intensity of the major mtDNA species mtDNA at each time point. Time after H_2O_2 application in hours is on the x-axis and relative intensity is on the

y-axis. n=7. error bars, ±SEM. *, p<0.05 by a one-way ANOVA with Bonferroni comparison of means. At the 0-hour time point, the major species is in the native supercoiled form. After H_2O_2 is applied, the mtDNA is damaged and the open circle and linear species become the most prominent, with little to no supercoiled mtDNA remaining. During the time course of the experiment, the supercoiled species is recovered, and the level of linear species decreases.

To confirm the Southern blot results by an independent method, qPCR was used to determine the relative frequency of breaks in mtDNA after the application of H_2O_2 by comparing the relative amplification of a long minor arc product to a short product in the *MT-ND1* gene. Upon H_2O_2 application, the number of breaks in the mtDNA increases with the measured peak at the 30-minute time point with a frequency of 3.44 breaks per mtDNA molecule. After which the frequency of mtDNA breaks decreases until it returns to near baseline level 24 hours (Figure 8). This further emphasizes the physical mtDNA damage that occurs with the H_2O_2 induced oxidative stress, and that this damage is resolved in control cells through repair or degradation.

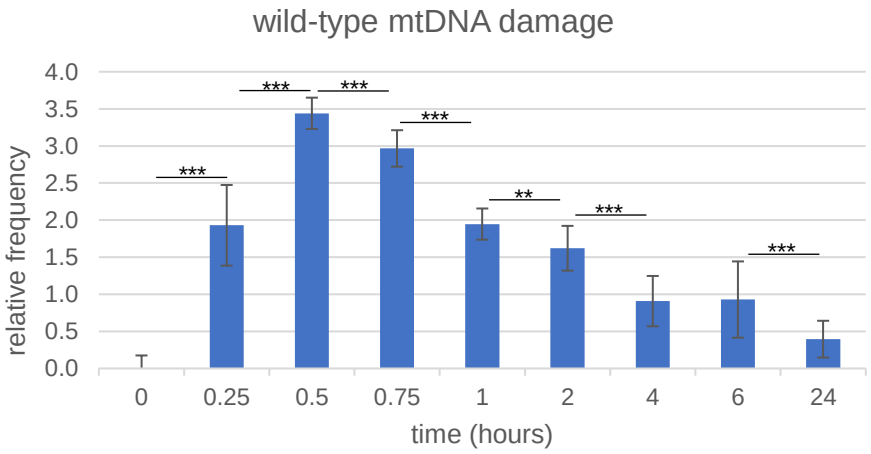

Fig. 8: The relative frequency of breaks in mtDNA in wild-type cells. Determined by qPCR Ct-value differences between a long mtDNA minor arc product and a short *MT-ND1* product for the H_2O_2 time course on control cells. The starting Ct difference at the 0-hour time point before oxidative stress considered baseline. n=18 technical replicates. error bars, ±SD. **, p<0.01, ***, p<0.001 by Student's unpaired t-test between each subsequent time point. The relative frequency of breaks and the mtDNA damage it represents increases with the addition of H_2O_2 to a maximum measured value of 3.44, before decreasing throughout the time course to a final measured value of 0.395 24-hours after H_2O_2 application.

3.2.3 H_2O_2 oxidative damage delays BrdU incorporation

BrdU is a synthetically produced nucleoside analog that is incorporated into the genome in the place of thymidine, which allows for unique labeling of its incorporation into mtDNA and therefore the visualization of replication and repair kinetics in our oxidative stress experiments (Hussain et al., 2021; Kai et al., 2006; Magnusson et al., 2003). To better observe the BrdU incorporation into mtDNA and to minimize the nuclear DNA background signal, aphidicolin is added to impair nuclear replication by blocking the function of DNA polymerase alpha and delta, causing the cells to remain in the S phase of the cell cycle (Baumstark-Khan, 1991). BrdU that is incorporated into mtDNA results from *de novo* replication, thus the amount of newly generated mtDNA after the pulse of H_2O_2 can be observed by comparing the amount of BrdU that is incorporated in cells where no H_2O_2 is applied. There was no effect on cell viability with the addition of aphidicolin and BrdU (Figure 9D). BrdU incorporation into three major mtDNA species was confirmed by hybridizing the same membrane with the *MT-ND5* probe (Figure 9C). In the early time points no mtDNA BrdU incorporation is observed due to the short time scale, but after 2 hours mtDNA BrdU incorporation begins to be visible in conditions without H_2O_2 which reaches a maximum after 24 hours (Figure 9A and B). A nuclear DNA smear is visible that starts at approximately 25 kb, particularly at the 24-hour time point, due to incomplete inhibition of nuclear DNA replication. When H_2O_2 is applied, BrdU incorporation is delayed and appears preferentially in the open circle conformation with the supercoiled species showing the most dramatic decrease when compared to 24 hours in normal medium (Figure 9A). Total BrdU incorporation after 24 hours is 60.4 % of that which is incorporated without the application of oxidative stress (Figure 9B). The decreased BrdU incorporation in the presence of H_2O_2 is due to the presence of damaged mtDNA molecules which need to be returned to the intact state via either repair or degradation before replication can occur. Because of the observed delayed BrdU incorporation with H_2O_2, the fast recovery of supercoiled mtDNA in the period of 2–6 hours seen in the Southern blot (Figure 7 and 9C) can be determined to be the result of repair rather than *de novo* replication.

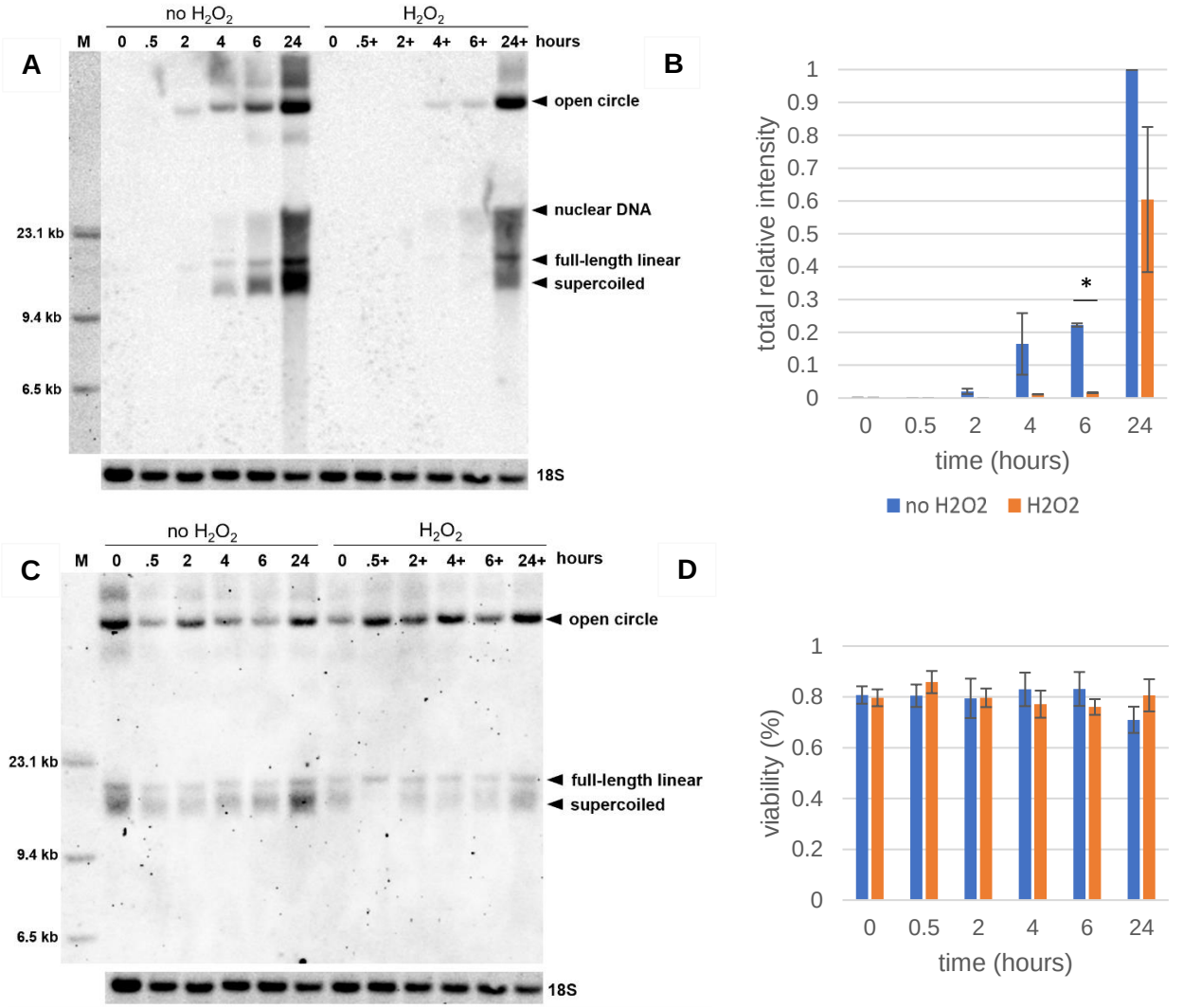

Fig. 9: BrdU incorporation into control HEK293 cells. **A**) Southern blot of the time course of BrdU incorporation in control HEK293 cells under normal conditions and conditions with 1 mM H_2O_2. The experiment was performed in parallel so that the only difference in the incorporation of BrdU is the addition of H_2O_2. "M" molecular weight marker with time in hours after BrdU was applied to the cells, "+" have H_2O_2 applied. The blot has been labeled with a BrdU antibody to visualize the BrdU incorporated DNA. The 18S nuclear band is a loading control. Three main conformations of mtDNA can be seen: the open circle, the full length linear, and the supercoiled. The dark cloud smear that begins at approximately 25 kb in size and can be seen at later time points is due to nuclear DNA incorporation of BrdU from incomplete inhibition. **B**) Quantification of all BrdU incorporated mtDNA bands. BrdU intensity has been quantified and summed for the three major mtDNA species and normalized for the 18S loading control and to the 24-hour normal medium signal. n=2. error bars, ±SEM. *, $p<0.05$ by a Student's unpaired t-test. BrdU begins to be visibly incorporated into cells in normal medium starting at 2 hours and reaches maximum corporation after 24 hours. The BrdU incorporation in the cells with H_2O_2 is delayed and after 24 hours reaches 60.4 % of the BrdU incorporation in normal medium. **C**) DIG *MT-ND5* labeled membrane from part A. The *MT-ND5* probe shows 3 main species: open circle, full-length linear, and supercoiled, which can be confirmed to be in the same positions as the identified mtDNA labeled with the BrdU antibody. **D**) Cell survival for n=4

BrdU experiments in normal medium and in medium with H_2O_2. There is no significant difference in cell survival with the application of BrdU and aphidicolin.

3.2.4 mtDNA shows increased turnover in the presence of H_2O_2

In parallel to the BrdU incorporation experiments, cells "pulsed" with BrdU (Kai et al., 2006) to incorporate it into the mitochondrial genome are then "chased" to reveal the rate of BrdU depletion which can help distinguish the relevance mtDNA repair and elimination by degradation after H_2O_2 (Figure 10). After 24 hours of the BrdU pulse, BrdU can be seen to be incorporated into all three major species of mtDNA. In medium without H_2O_2 after the BrdU pulse, the BrdU gradually is diluted from mtDNA as the mtDNA replicates and the cells divide. When H_2O_2 is applied after the BrdU pulse, the amount of BrdU in mtDNA decreases at a significantly faster rate during the time course of the experiment, indicating that mtDNA degradation results from the applied H_2O_2. Interestingly, because aphidicolin is also removed from the medium when BrdU is no longer applied, at the later time points the nuclear cloud of BrdU incorporation has increased in intensity. Nucleosides, including the BrdU, from degraded mtDNA species are likely released back into the cytoplasm in the cell and can be reused in the nucleotide pool for nuclear DNA (Hämäläinen et al., 2019).

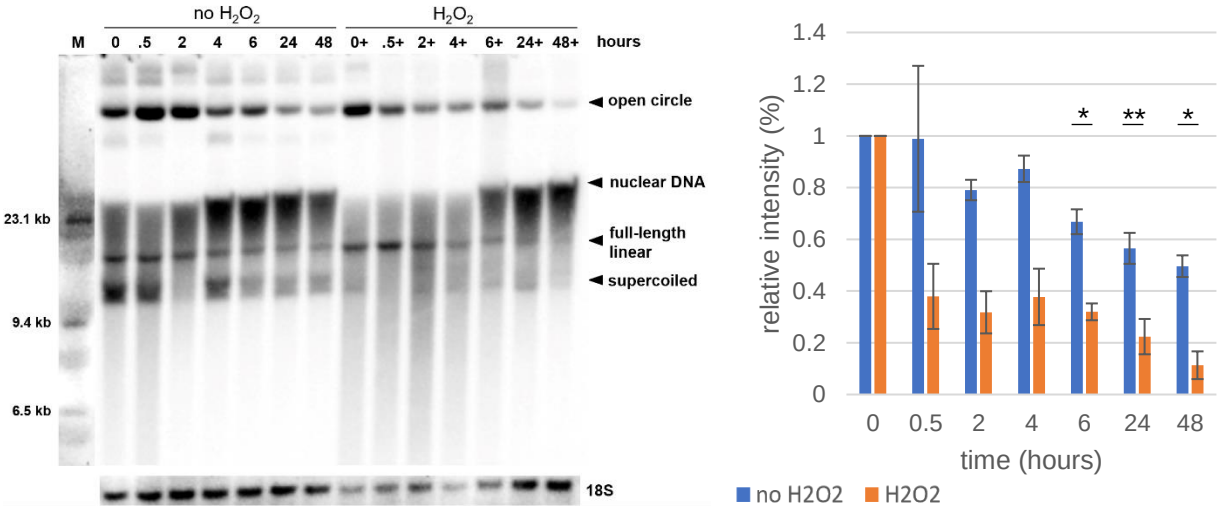

Fig. 10: BrdU pulse/chase in control HEK293 cells. The label at the top is "M" molecular weight marker and time in hours after BrdU was removed from the medium, "+" have H_2O_2 applied in the medium. The blot is labeled with a BrdU antibody to visualize the BrdU incorporated DNA. The 18S nuclear band is a loading control. Three main conformations of BrdU mtDNA can be seen: the open or relaxed circle, the full-length double stranded linear, and the supercoiled circular genome. The dark cloud smear that can be seen at 25 kb in most lanes is due to nuclear DNA incorporation of BrdU. The sum of the intensity of the 3 main species of mtDNA is quantified and normalized to the 18S and the 0-hour

sample. n=2. error bars, ±SEM. *, p<0.05, **, p<0.01 by a Student's unpaired t-test between medium and H_2O_2 medium samples at each time point. The amount of BrdU incorporated mtDNA is depleted at a faster rate in the cells treated with H_2O_2.

3.2.5 Ultra-deep sequencing

To determine the exact positions and nature of the mtDNA damage after H_2O_2 application, ultra-deep sequencing techniques on isolated mtDNA were utilized. In short-read Illumina sequencing, samples are ligated with a blunt-end linker before fragmentation to aid in the determination of in vivo ends in the sequencing library. In PacBio long-read sequencing the entire 16.5 kb mtDNA species as well as fragmentation products can be sequenced in one read after linearization with an appropriate restriction enzyme.

3.2.5.1 H_2O_2 damages mtDNA but leaves nuclear DNA intact

mtDNA isolation via differential centrifugation in whole cells is a robust technique for mitochondrial enrichment, but it is not able to completely remove all nuclear DNA and roughly 3-20% of sequences did not align to mtDNA in samples investigated using PacBio long-read deep sequencing (Trombly et al., 2023). This allowed for the comparison of mtDNA and nuclear DNA damage after the applied H_2O_2. The size of fragments that align to the corresponding genome is an indicator of the amount of damage present: an increase in the abundance of the smaller DNA fragments can be attributed to more DNA damage. After the pulse of H_2O_2, the amount of full length mtDNA drastically decreases and the amount of mtDNA fragments smaller than 8 kb increases. The level of full length mtDNA recovers after 24 hours (Figure 11A). This increase in fragmentation after H_2O_2 application is not observed in nuclear DNA fragments in this size range (Figure 11B). With S1 nuclease to convert SSBs into DSBs there is a further increase in DNA fragmentation in both mitochondrial and nuclear DNA (Figure 11C and D), but still no transient increase in nuclear fragments as a result of the H_2O_2 treatment. This confirms that our applied H_2O_2 specifically affects mitochondrial DNA but not the nuclear genome, at least in the range of fragment sizes available from the PacBio sequencing.

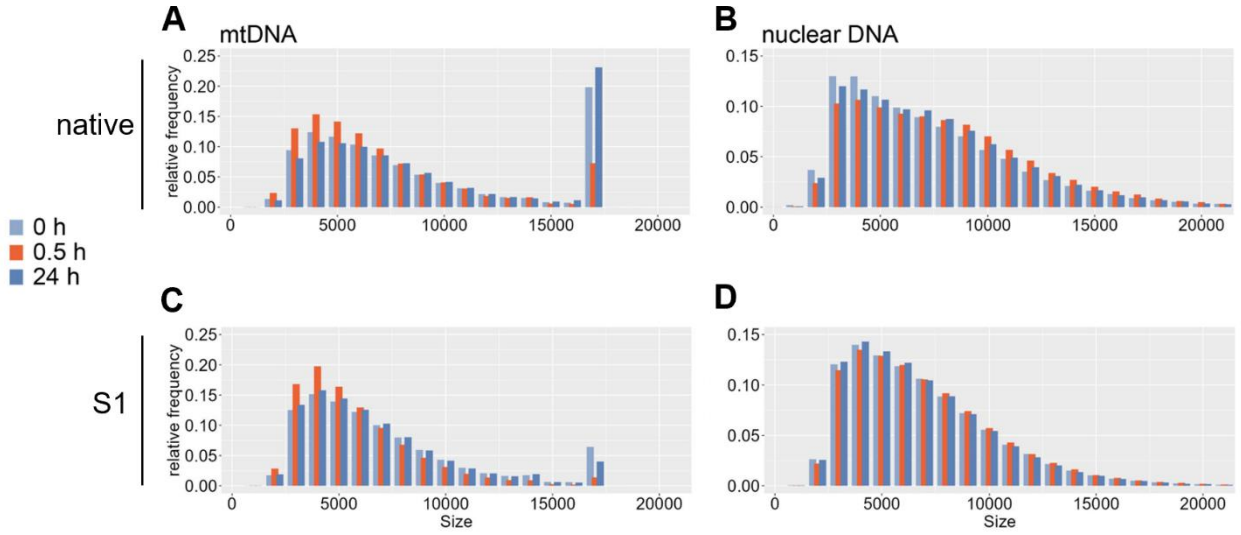

Fig. 11: PacBio sequencing mtDNA and nuclear DNA fragments by size. Top panels represent native DNA while bottom panels have been S1 nuclease digested. Left panels (A and C) show fragments aligned to mtDNA and right panels (B and D) show fragments aligned to nuclear DNA. The 0-hour or non-treated condition (light blue), 30 minutes after H_2O_2 treatment (orange), and 24 hours after H_2O_2 treatment (dark blue) are sequenced. The low frequency of fragments less than 3 kb is due to size exclusion during library preparation. 30 minutes after H_2O_2 oxidative stress, the frequency of short fragments increase in mtDNA but this increase is not found in the nuclear DNA fragments. Image generated by Dr. Gábor Zsurka and adapted from Trombly et al. (2023).

3.2.5.2 H_2O_2 generates DSBs and SSBs that are eliminated

In both short-read Illumina and long-read PacBio sequencing, aligning sequences to the mitochondrial genome allows for the determination of the quantity and location of DSBs, while the amount of SSBs is calculated by subtracting the number of DSBs from those breaks detected after S1-nuclease treatment. Before treatment, approximately 2-5 % of mtDNA molecules contain a DSB in the control cells (Trombly et al., 2023). In both ultra-deep sequencing techniques, DSBs increase significantly with H_2O_2 application and return to baseline after 24 hours (Figure 12), which confirms the results observed in the Southern blot. Likewise, SSBs increase after H_2O_2 and return to baseline after 24 hours, but this is not significant likely due to low sample number and the large variance observed at the 30-minute time point.

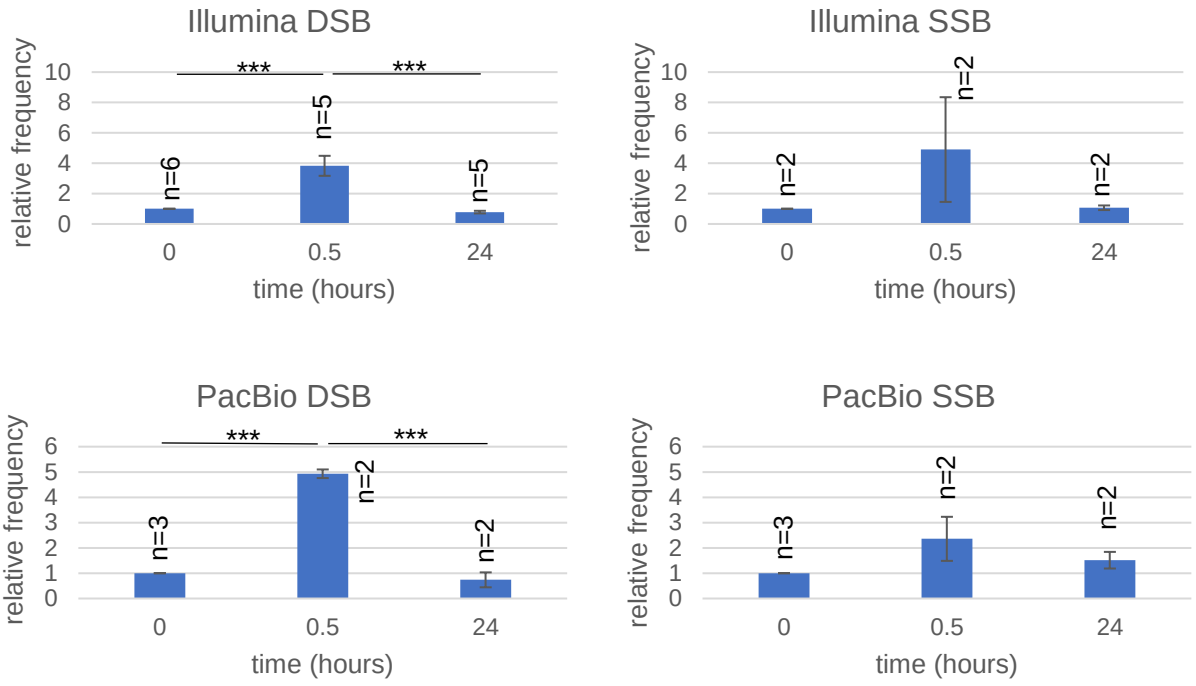

Fig. 12: Relative frequency of mtDNA breaks from deep sequencing. Quantification of DSBs from linker-mediated Illumina sequencing or long-read PacBio sequencing. SSBs were determined by subtracting the frequency of DSBs from S1 nuclease treated samples. Break frequencies are normalized to average coverage and the non-treated condition. error bars, ±SEM. ***, $p < 0.001$ by one-way ANOVA with Bonferroni post-hoc test. Both DSBs and SSBs increase 30 minutes after H_2O_2 but return to baseline after 24 hours. Data analyzed by Dr. Gábor Zsurka and adapted from Trombly et al. (2023).

3.3 Characterization of CRISPR/Cas9 generated knock-out HEK293 cell lines

To investigate the effect that specific proteins have on mtDNA integrity during oxidative stress, we generated knock-out cell lines using CRISPR/Cas9 genome editing technology in HEK293 cells. The genes of interest for our knock-out cell lines are those known to be involved in mtDNA maintenance, specifically in mtDNA degradation (Peeva et al., 2018) and those that are thought to be involved in BER (Alencar et al., 2019).

3.3.1 CRISPR/Cas9 modified HEK293 cell lines

The Sanger sequencing results of our successful CRISPR/Cas9 generated knock-out cell lines are outlined in Figure 13. Multiple knock-out cell lines for the same protein were generated for experimentation to confirm the validity of our results, and to rule out off-target CRISPR effects. When HDR oligonucleotides were utilized to introduce a specific mutation it was necessary to screen more clones due to a low likelihood of the desired point mutation resulting from homologous recombination compared to the generation of a

non-specific small indel knock-out mutation. APEX1$^{-/-}$ cell lines were generated that alter the positive residues in the C-terminus of the gene that allow APEX1 to be imported into mitochondria (Li et al. 2010): APEX1$^{-/-}{}_{b}$ is a truncated protein with a deletion of these positive residues, while APEX1$^{-/-}{}_{a}$ has specific changes in the two positive amino acids to neutral amino acids. LIG3$^{-/-}$ lines alter the third exon of the gene, eliminating the crucial catalytic core in exons 6–14 (Simsek and Jansin, 2011). The POLGexo$^{-/-}$ line contains the c.821A>C point mutation that eliminates the exonuclease function while keeping the polymerase activity intact (Peeva et al., 2018). All other knock-out cell lines contain loss of function mutations.

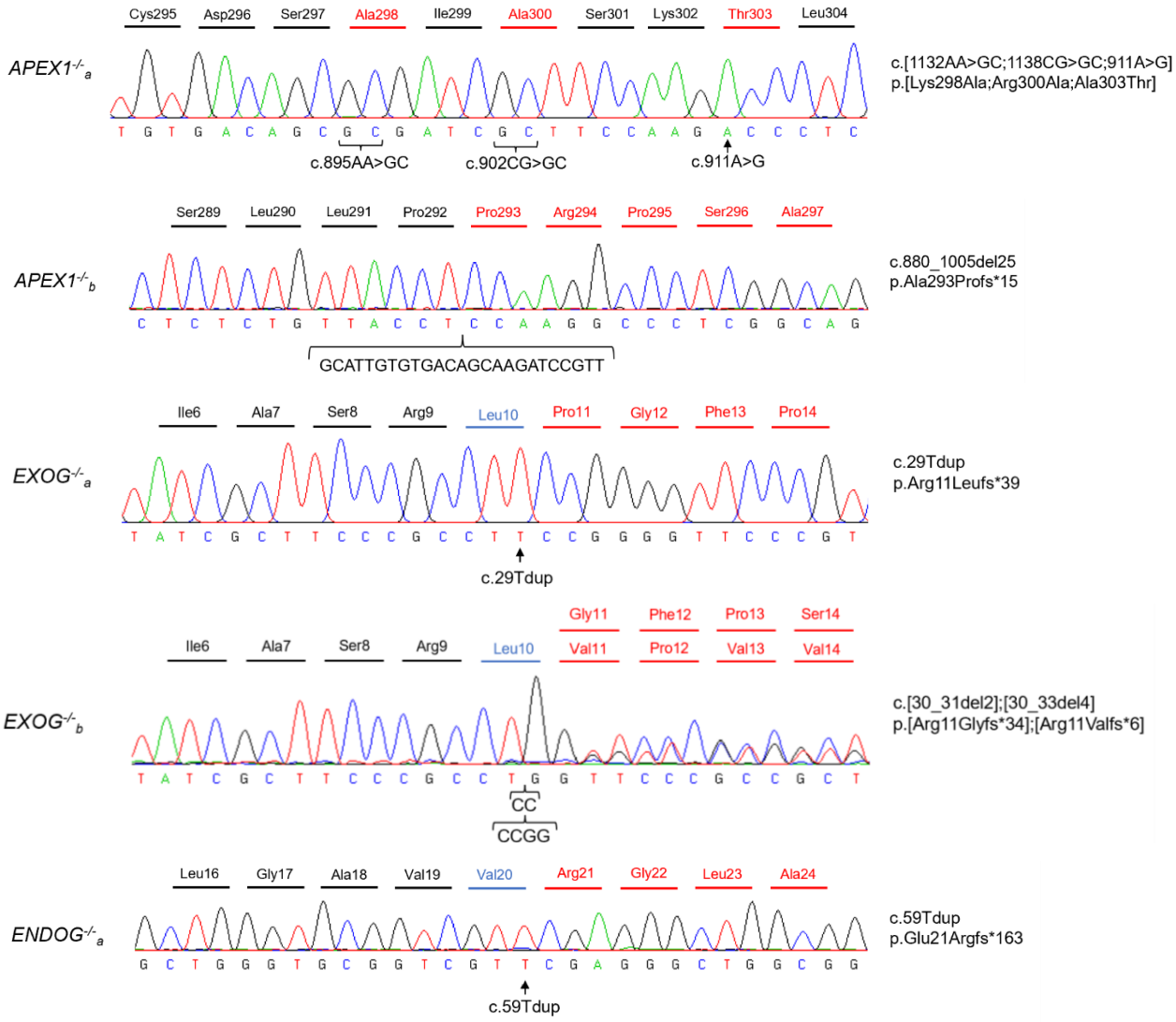

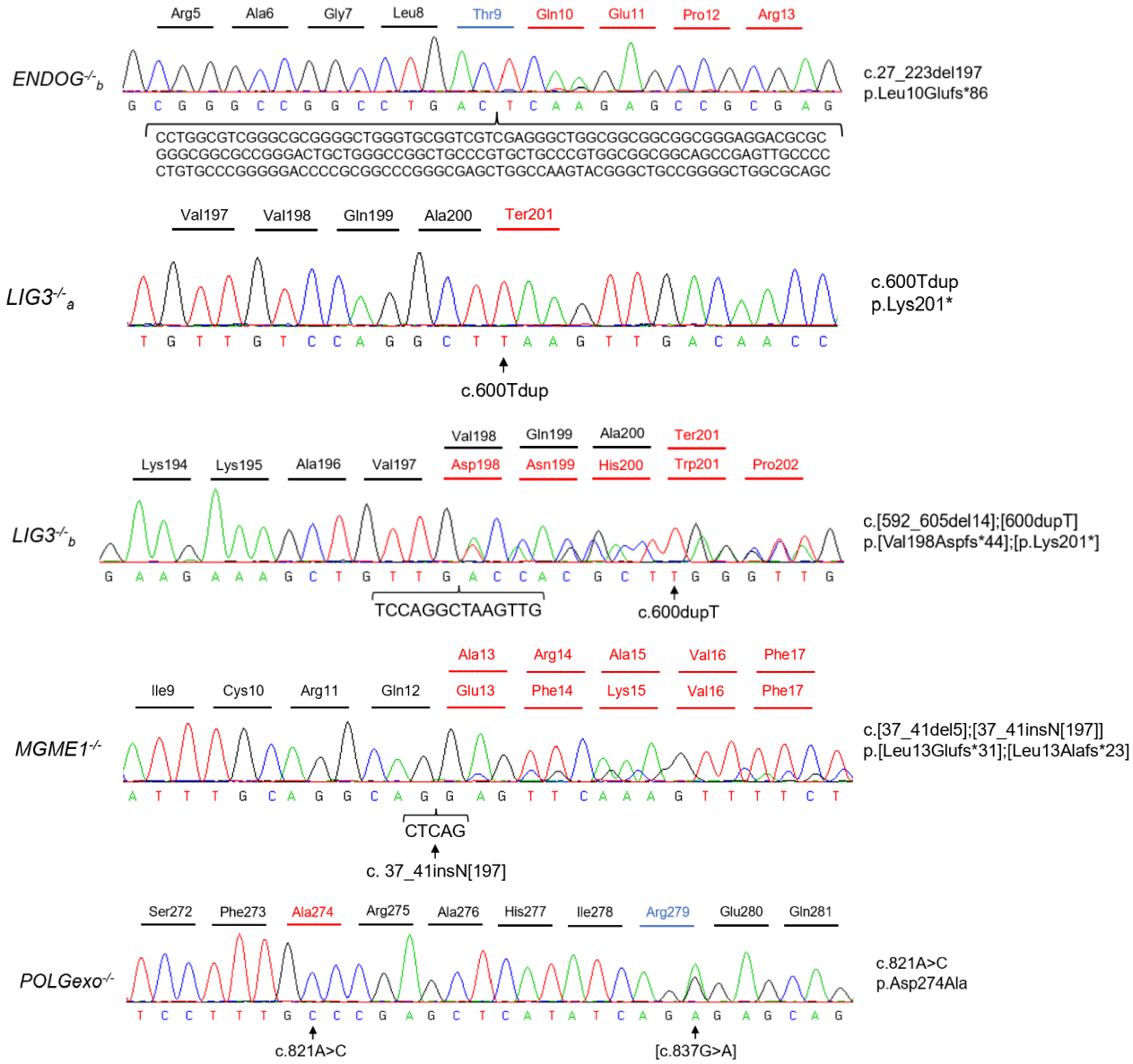

Fig. 13: Sequence chromatograms confirming the mutations in CRISPR/Cas9 modified cell lines. Sanger sequencing results were aligned to the known sequence for the gene of interest, and the resulting loss of function mutation was observed. Red amino acid codes indicate missense changes, blue amino acid code is a silent mutation.

Western blotting was additionally used to determine if our knock-out cell lines affected the expression of the genes at the protein level. No LIG3 protein was detected in either the LIG3$^{-/-}_{a}$ or LIG3$^{-/-}_{b}$ cell line (Figure 14), therefore the CRISPR/Cas9 generated mutations produced knock-out LIG3 cells with loss-of-function at the protein level.

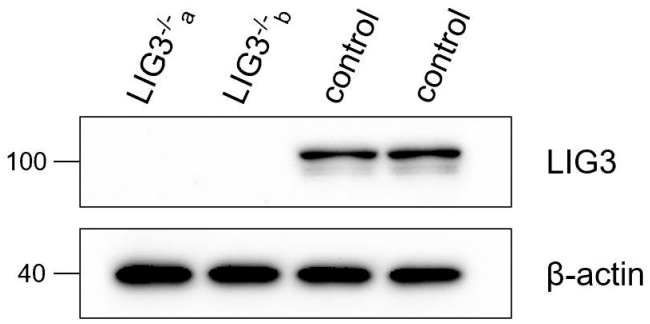

Fig. 14: Western blot analysis of protein content in LIG3$^{-/-}$ cells. The cell line tested is indicated on the top, protein molecular weight marker band sizes in kDa are on the left, and the gene tested is on the right. β-actin is measured as a loading control for protein amount. There is no LIG3 protein detected in either LIG3$^{-/-}$ line. Experiment performed by Dr. Alexei P. Kudin.

3.3.2 Knock-out cell lines survive applied oxidative stress

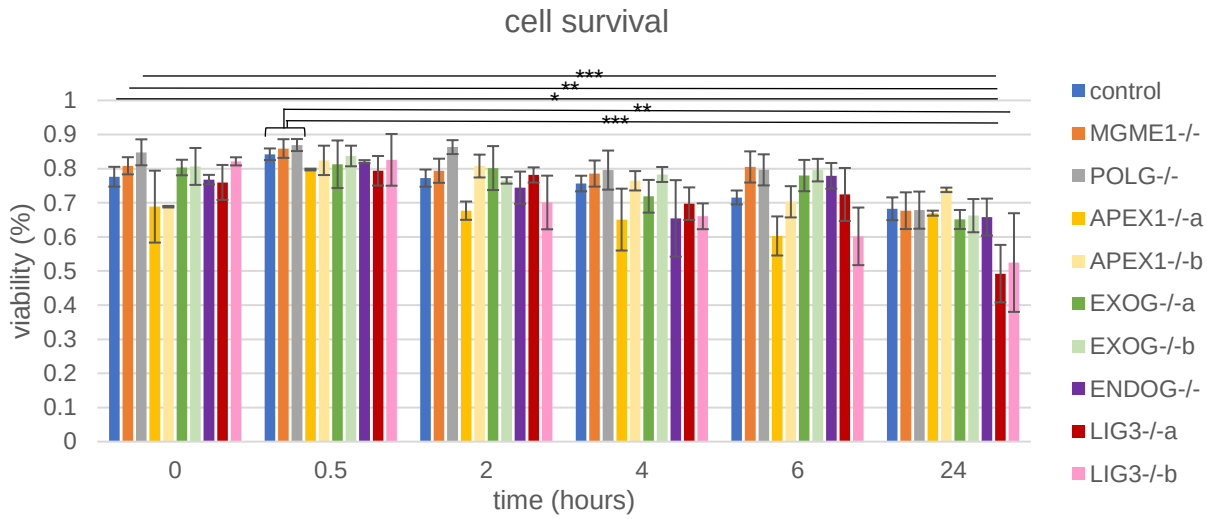

Fig. 15: Viability data for control and knock-out cells. At each time point (0 hour, 30 minute, 2, 4, 6, and 24 hours) viability is determined by calculating the percentage of alive cells out of the total number of cells. control n=15, MGME1$^{-/-}$ n=7, POLGexo$^{-/-}$ n=7, APEX1$^{-/-}{}_{a}$ n=2, APEX1$^{-/-}{}_{b}$ n=2, EXOG$^{-/-}{}_{a}$ n=3, EXOG$^{-/-}{}_{b}$ n=3, ENDOG$^{-/-}$ n=2, LIG3$^{-/-}{}_{a}$ n=2, LIG3$^{-/-}{}_{b}$ n=3. error bars, ±SEM. *, $p<0.05$, **, $p<0.01$, ***, $p<0.001$ by ANOVA with Bonferroni post-hoc. The viability of cells remains consistent throughout the experiment. Importantly, in most cell lines the survival remains above 60 % 24-hours after H_2O_2 application. Significantly less LIG3$^{-/-}$ cells survive after 24 hours.

There is no significant decrease in cell survival in the knock-out cell lines in the time course of 1 mM H_2O_2 at each time point when compared to the control (Figure 15). The average viability before H_2O_2 application is 78.2 %. Cell survival is consistent throughout the time course before decreasing to an average of 65 % viability 24-hours after H_2O_2. There is a significant decrease in the LIG3$^{-/-}$ cells where the viability decreases to approximately 50

% after 24-hours that is likely due to the importance of LIG3 in mtDNA maintenance, and cell death cannot be excluded and may a role in the effects observed 24-hours after H_2O_2 application in the LIG3$^{-/-}$ cells. Because the major fraction of cells survive the 1 mM H_2O_2 pulse, it was concluded that cell death would not be a major contributor in comparing the observed effects on mtDNA between the knock-out cell lines and control cells.

3.3.3 mtDNA copy number

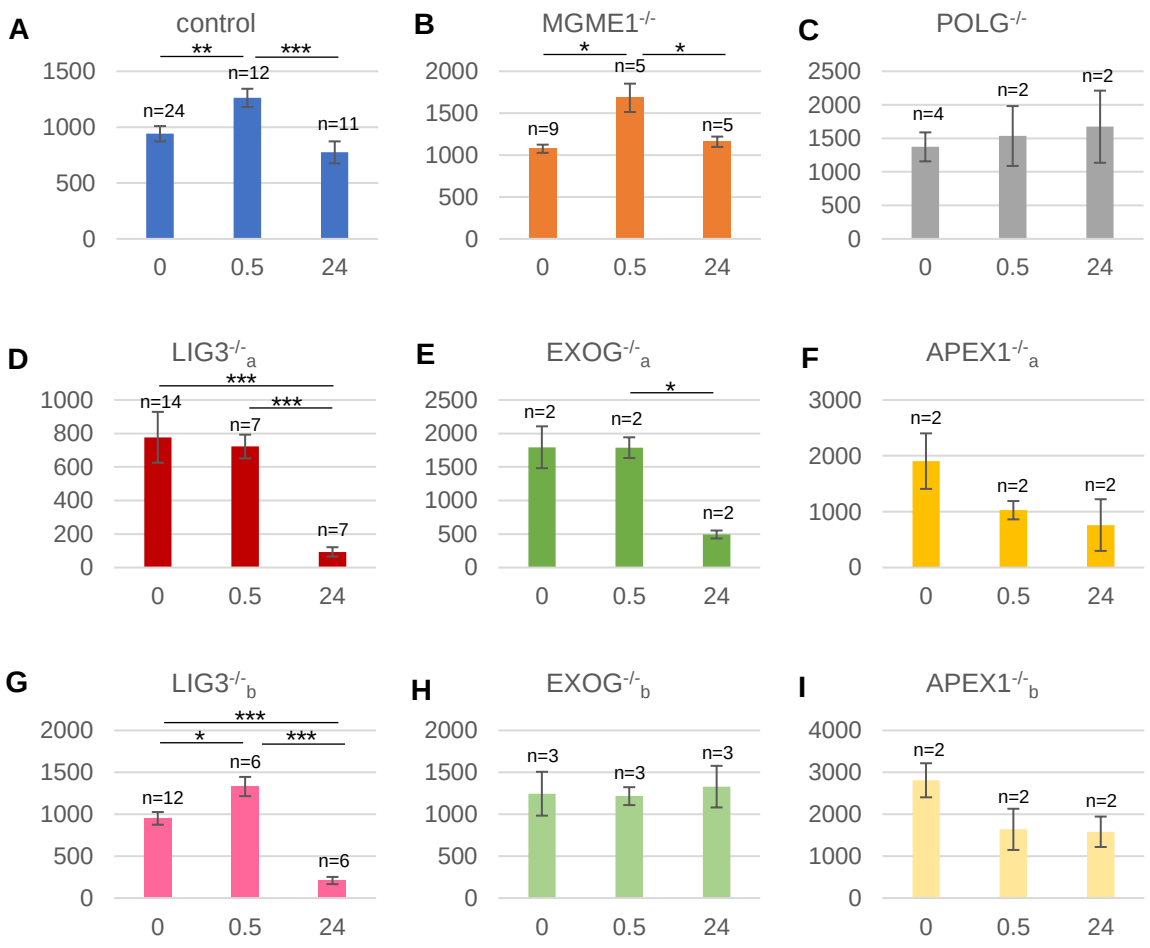

Fig. 16: qPCR mtDNA copy number in each cell line. Time after H_2O_2 exposure is on the x-axis and the copies of mtDNA per cell is on the y-axis. error bars, ±SEM. ***, $p < 0.001$; **, $p < 0.01$; *, $p < 0.05$ by Student's unpaired t-test. There is no significant difference between control cells and the knock-out cell lines at baseline. LIG3$^{-/-}$ cells and EXOG$^{-/-}{}_a$ cells show significant mtDNA depletion 24-hours after H_2O_2.

qPCR was used to determine the number of copies of mtDNA per cell by comparing the *MT-ND1* region of mtDNA to a single copy nuclear gene for *KCNJ10*. The control and knock-out HEK293 cell lines were evaluated in the native state as well as after acute H_2O_2 exposure and after 24 hours of recovery. No knock-out cell lines were found to have a sig-

nificant difference in mtDNA copy number from the control cells in baseline conditions, although in APEX1$^{-/-}$ lines the mtDNA copy number appears to be elevated. Interestingly, in control, MGME1$^{-/-}$, and LIG3$^{-/-}{}_{b}$ cell lines there is a significant increase in mtDNA copy number after the application of H_2O_2 (Figure 16A, B, and G) which is likely from the mtDNA becoming more available to the polymerase in the qPCR (Chen et al., 2007). The LIG3$^{-/-}$ lines as well as EXOG$^{-/-}{}_{a}$ show a significant depletion in mtDNA copy number 24 hours after H_2O_2 application (Figure 16D, E and G). This could explain the significant decrease in cell survival seen in the LIG3$^{-/-}$ cell lines (Figure 15), as mtDNA loss can be a significant stress. There are no real differences in copy number effects between the two LIG3$^{-/-}$ and two APEX1$^{-/-}$ lines, however the two EXOG clones show differences with EXOG$^{-/-}{}_{a}$ being much more effected by the application of H_2O_2 than EXOG$^{-/-}{}_{b}$. The difference between the two EXOG$^{-/-}$ clones could be due to the unstable nature of HEK293 cells or potentially an off target CRISPR effect.

3.4 Inhibited degradation after DSBs

In previous work done in our lab, we discovered that components of mtDNA replication machinery are also involved in linear mtDNA degradation (Peeva et al., 2018). From the previous study we know that in HEK293 cells a knock-out of MGME1 completely inhibits short-term degradation of mtDNA, while the knock-out of the POLG exonuclease function impairs mass degradation of linear mtDNA but this is not a complete block. In addition to the involvement of the exonuclease domain of POLG in the degradation of linear mtDNA, it is known that the polymerase and lyase domains are involved in the repair of mtDNA (Figure 4; Karlowicz et al., 2022). The inhibition of linear mtDNA degradation affords a unique opportunity to observe the effects of H_2O_2 in an environment where the clearance of linear mtDNA generated by DSBs is impaired.

3.4.1 Impaired supercoiled recovery in degradation impaired cell lines

Both MGME1$^{-/-}$ and POLGexo$^{-/-}$ have the open circle as the most prominent form of mtDNA before application of oxidative stress (Figure 17B). Like the control cells, 30 minutes after H_2O_2 is applied the open circle and both linear mtDNA species increase in the degradation impaired cell lines (Figure 17). This smear of DSB generated linear mtDNA fragments appears to persist in the MGME1$^{-/-}$ and POLGexo$^{-/-}$ cell lines but dissipate from the control cells as the dsDNA fragments are degraded. Most strikingly, the recovery of supercoiled mtDNA after H_2O_2 application is significantly diminished in MGME1$^{-/-}$ and POLGexo$^{-/-}$ cells

compared to the recovery observed in the control cells (Figure 17B). In addition to this inhibition of supercoiled mtDNA recovery, the MGME1 knock-out line shows persistence of the open circle mtDNA. Therefore, the inhibition of degradation results in persistence of linear mtDNA fragments and impairs the recovery of the native supercoiled mtDNA in the period of 24 hours after strong H_2O_2 exposure.

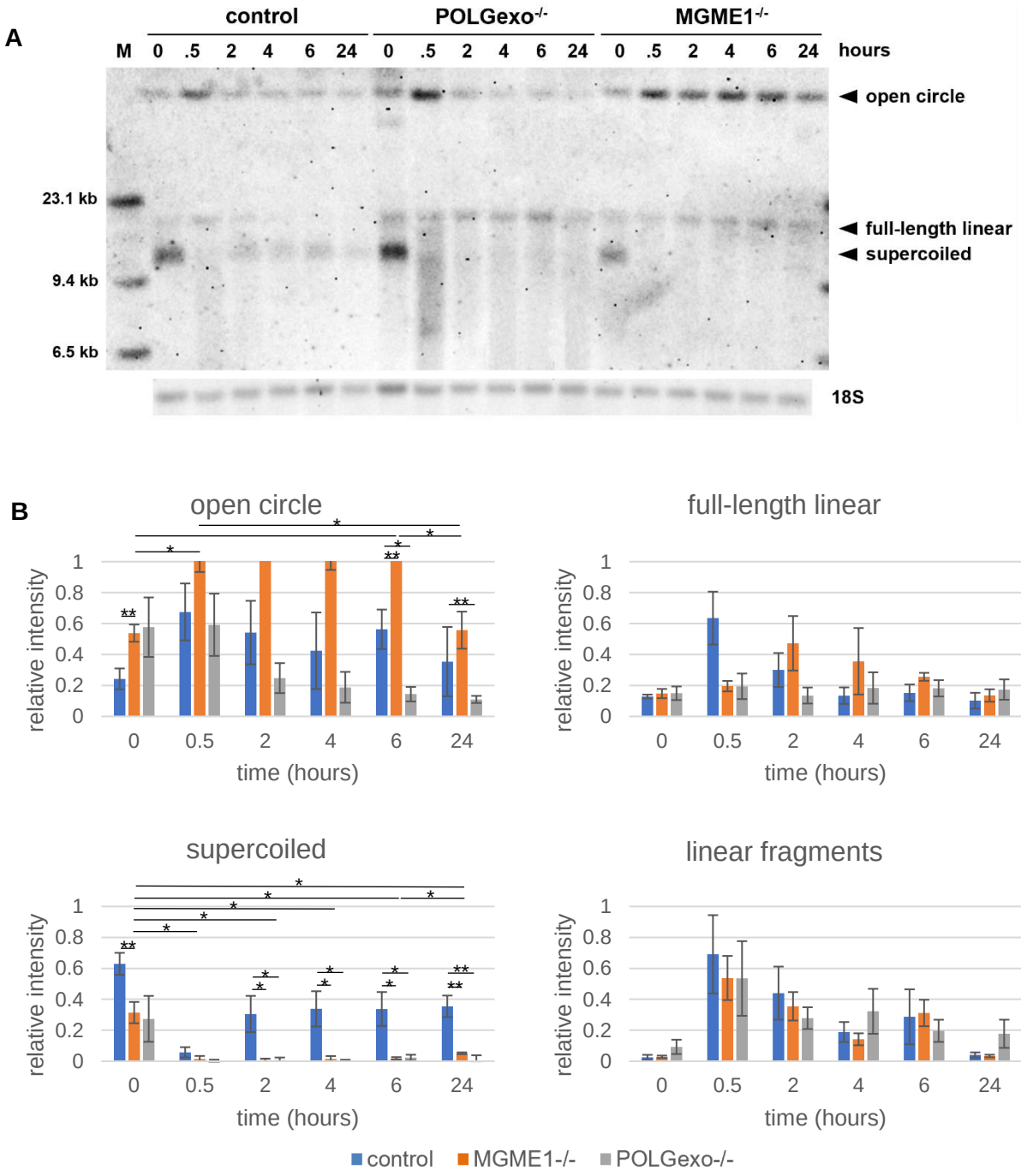

Fig. 17: Southern blot of 1 mM H_2O_2 on control, MGME1$^{-/-}$, and POLGexo$^{-/-}$. **A)** Southern blot depicting the time course of oxidative stress on control, MGME1$^{-/-}$, and POLGexo$^{-/-}$ cells. Top label is time after H_2O_2 application in hours with “M” molecular weight marker.

The blot has been labeled for the *MT-ND5* region of the mitochondrial genome. The 18S nuclear band is a loading control. Four main conformations of mtDNA can be seen: the open circle, the full-length double-stranded linear, the supercoiled circular genome, and a smear of linear mtDNA fragments of different sizes. **B)** Quantification of the intensity of the 3 major species of mtDNA. Control n=7, MGME1$^{-/-}$ n=3, POLGexo$^{-/-}$ n=3. error bars, ±SEM. *, p<0.05, **, p<0.01 by a Student's unpaired t-test between time points for the knock-out lines and between the knock-out lines and control at each time point. After H_2O_2 is applied, there is persistence of the linear mtDNA species and diminished recovery of supercoiled mtDNA in the MGME1 or POLGexo knock-out cell lines.

3.4.2 Oxidative damage DSBs persist in the absence of mtDNA degradation

qPCR used to determine the frequency of breaks in mtDNA revealed that before the applied oxidative stress MGME1$^{-/-}$ and POLGexo$^{-/-}$ cell-lines have an elevated number of breaks from the baseline level in the control cells ($p<0.001$), which results from decreased efficiency in the removal of intrinsic damage in these degradation impaired cell lines (Figure 18). Upon H_2O_2 application, the frequency of mtDNA damage increases in all samples, reaching a maximum after 30 minutes in the control but persisting for a longer period in the MGME1$^{-/-}$ and POLGexo$^{-/-}$ cells. 24 hours after H_2O_2, the frequency of mtDNA breaks in the control decreases to almost baseline level (0.359) but remains elevated in both the MGME1$^{-/-}$ and POLGexo$^{-/-}$ cell lines (5.03 and 5.78 respectively). This further emphasizes the physical damage that occurs with the H_2O_2 induced oxidative stress in all cell lines, and that this damage is eliminated through repair or degradation after 24 hours in the control cells, while persisting in the MGME1$^{-/-}$ and POLGexo$^{-/-}$ cell lines where degradation is inhibited.

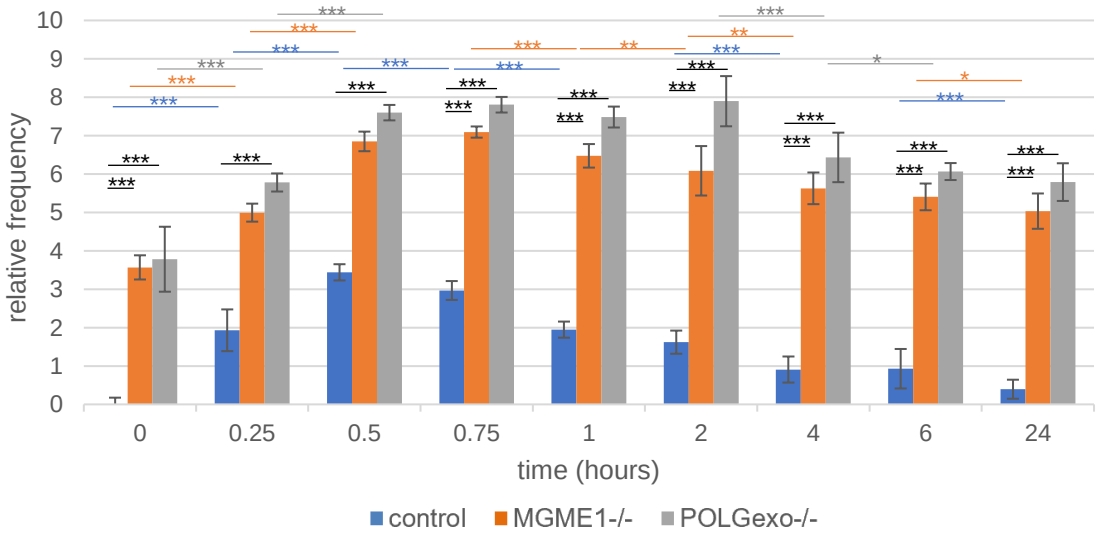

Fig. 18: The relative frequency of breaks in mtDNA for the H_2O_2 time course on control, MGME1$^{-/-}$, and POLGexo$^{-/-}$ cells. The relative frequency of breaks in the mtDNA minor arc

is calculated from the Ct difference between the short *MT-ND1* product and long mtDNA minor arc product. error bars, ±SD over n=18 technical replicates. ***, p<0.001 , **, p,0<01, *, p<0.05 by ANOVA with Tukey post-hoc test for changes between time point in each cell line (blue=control, orange=MGME1$^{-/-}$, grey=POLGexo$^{-/-}$) and between control cells and knock-out line at each time point (black). The Ct difference at the 0-hour time point for the control is baseline. The frequency of breaks is found to be elevated in the degradation impaired cell lines before transient H_2O_2. The relative frequency of breaks and therefore the mtDNA damage it represents increases with the addition of H_2O_2 in all cell lines. 24 hours after H_2O_2 the control returns to baseline levels, while the frequency of mtDNA breaks remains elevated and persists in the MGME1$^{-/-}$ and POLGexo$^{-/-}$ cells.

3.4.2.1 SSB repair is not impaired by loss of MGME1 or POLGexo

In both Illumina and PacBio deep-sequencing the POLGexo$^{-/-}$ cells contain a large amount of DSBs before the oxidative stress. DSBs increase in all cell types 30 minutes after H_2O_2 and remain elevated in both the MGME1$^{-/-}$ and POLGexo$^{-/-}$ cells (Figure 19A and C), which confirms the damage qPCR results. SSBs are elevated 30 minutes after H_2O_2 and return to baseline after 24 hours but this is not significant due to large variation and the small number of samples. Most interestingly, there is no significant difference in SSBs between the control and degradation impaired cell lines (Figure 19B and D), therefore repair of SSBs does not appear to be affected by the loss of MGME1 or POLGexo.

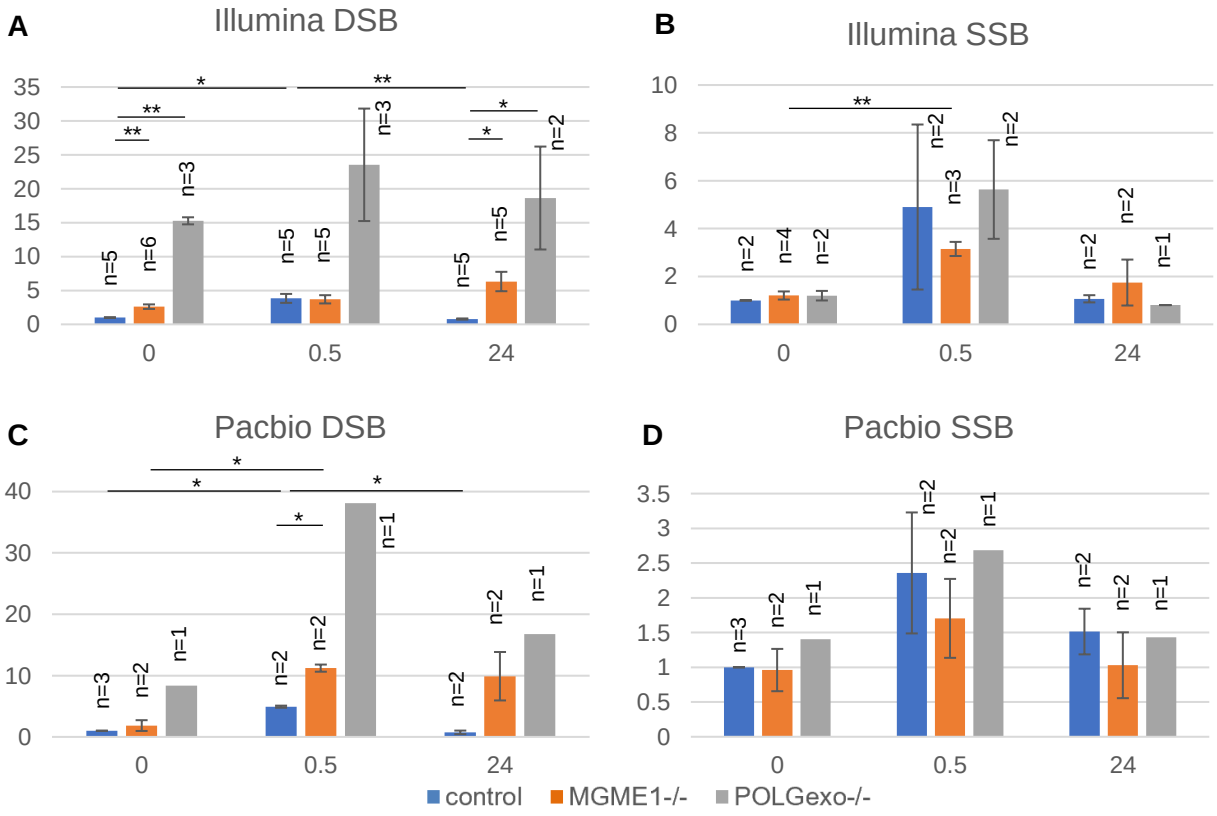

Fig. 19: Relative frequency of deep sequencing mtDNA breaks in control, MGME1$^{-/-}$, and POLGexo$^{-/-}$ cells. DSBs were quantified from linker-mediated Illumina sequencing or long-read PacBio sequencing. SSBs were determined by subtracting the frequency of DSBs from S1 nuclease treated samples. Break frequencies are normalized to average coverage and the non-treated control. error bars, ±SEM. *, p<0.05, **, p<0.01 by Student's unpaired t-test between each time point and between knock-out lines and control. Both DSBs and SSBs increase 30 minutes after H_2O_2 application in all cell lines. SSBs return to baseline after 24 hours while DSBs persist in the degradation impaired cell lines. POLGexo$^{-/-}$ contain a magnitude of order higher mtDNA breaks before the oxidative stress. Data analyzed by Dr. Gábor Zsurka and adapted from Trombly et al. (2023).

3.4.3 H_2O_2 impairs BrdU incorporation in the absence of degradation

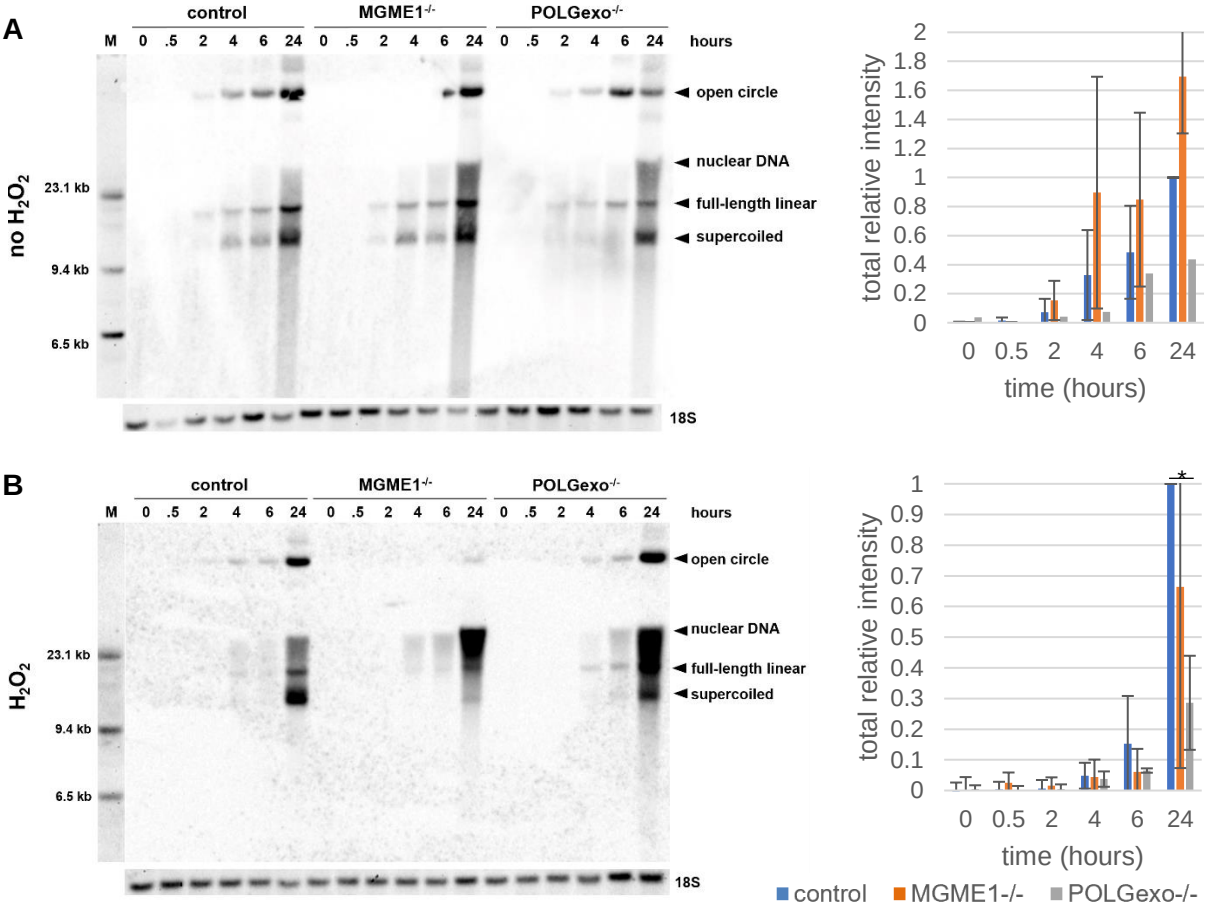

Fig. 20: BrdU incorporation in degradation impaired cell lines. In A and B: top label is "M" is the molecular weight marker and time in hours after BrdU is added to the medium. The blot has been labeled with a BrdU antibody to visualize the BrdU incorporated DNA. The 18S nuclear band is a loading control. The dark cloud smear at 25 kb that can be seen in most lanes is due to nuclear incorporation of BrdU. The quantification is the sum of the BrdU intensity of 3 major mtDNA species (open circle, full-length linear, and supercoiled), normalized to the 18S and to the 24-hour control sample. **A)** BrdU incorporation into control, MGME1$^{-/-}$, and POLGexo$^{-/-}$ cell lines. control n=4, MGME1$^{-/-}$ n=3, POLGexo$^{-/-}$ n=1. error bars, ±SEM. BrdU can be seen to be incorporated into the mtDNA starting at the 2 hour time point, with maximum intensity at 24 hours. There is no significant difference

between knock-out lines and control. **B)** BrdU incorporation in the presence of H_2O_2 oxidative stress in control, MGME1$^{-/-}$, and POLGexo$^{-/-}$ cell lines. control n=5, MGME1$^{-/-}$ n=4, POLGexo$^{-/-}$ n=2. error bars, ±SEM. *, p<0.01 by ANOVA with Bonferroni comparison of means between control and the degradation impaired cell lines at each time point. BrdU incorporation is delayed in all cell lines in the presence of oxidative stress. The MGME1$^{-/-}$ cells reach 66.4 % of the BrdU incorporated into the control, while the POLGexo$^{-/-}$ only reach 28.6 %.

In the absence of H_2O_2, there is no significant difference in the amount of BrdU that is incorporated into mtDNA between control and the MGME1$^{-/-}$ or POLGexo$^{-/-}$ cell lines (Figure 20A). With H_2O_2 application, the MGME1$^{-/-}$ cells only reach 66.4 % of the BrdU incorporated into the control, while POLGexo$^{-/-}$ cells incorporate significantly less and only reach 28.6 % of the control (Figure 20B). The fact that BrdU incorporation is not increased in the MGME1$^{-/-}$ and POLGexo$^{-/-}$ cell lines indicates that degradation is necessary for the repopulation of mtDNA after oxidative damage. The cloud of nuclear DNA starting at approximately 25 kb is particularly strong in the MGME1$^{-/-}$ and POLGexo$^{-/-}$ cells 24 hours after H_2O_2, likely because of the BrdU not being incorporated into mtDNA and therefore more is taken up by the nucleus despite nuclear inhibition.

3.4.4 OriH, OriL, and mTER frequent mtDNA ends appear after H_2O_2 application

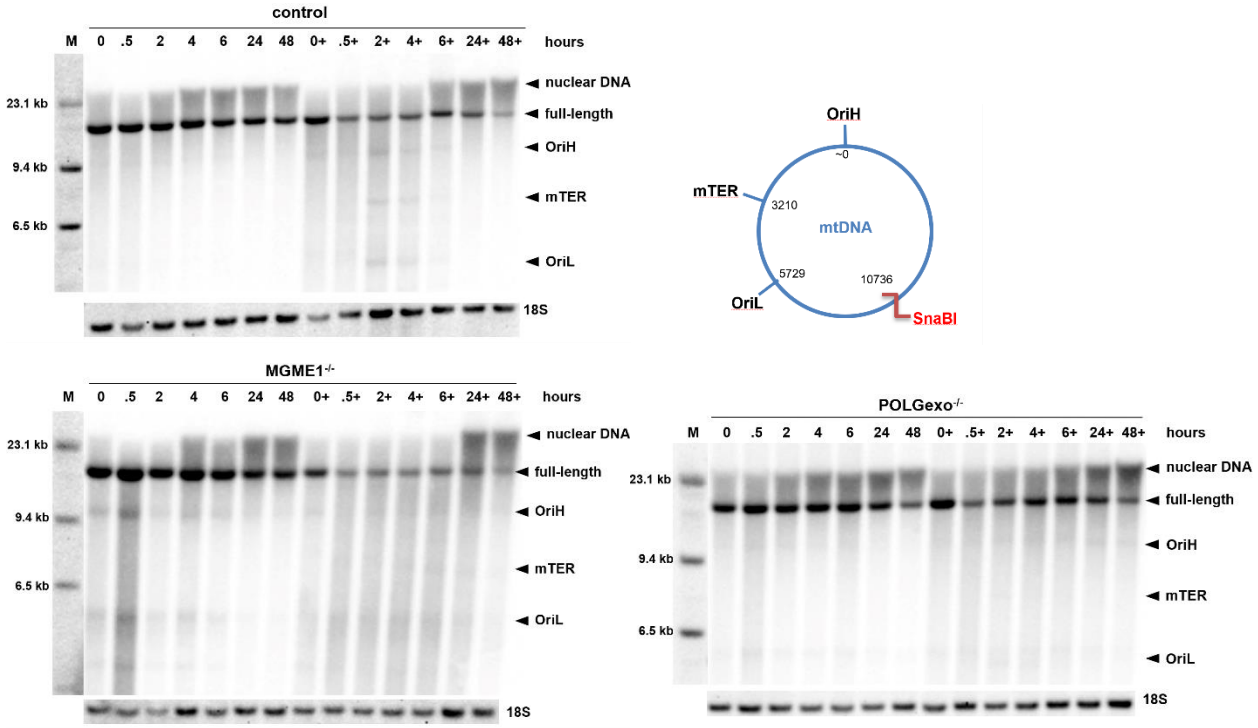

Fig. 21: BrdU pulse/chase in control, MGME1$^{-/-}$, and POLGexo$^{-/-}$ cells. The mtDNA in all samples has been linearized by digestion with *SnaB*I, and the scheme depicts the smaller mtDNA fragment ends that can be observed after this linearization of the mtDNA. Blots

are labeled for “M” the molecular marker and time in hours after BrdU has been removed from the medium, with the “+” indicating the addition of H_2O_2. When H_2O_2 is applied, a linear smear of mtDNA fragments appears in all samples. Prominent linear species with ends at the OriH, mTER, and OriL arise after 2 hours, which dissipate in the control after 24 hours. The OriH and OriL prominent ends are already present in the MGME1$^{-/-}$ and POLGexo$^{-/-}$ cell lines before oxidative stress, and the linear fragments persist.

In figure 21 the mtDNA has been linearized with *SnaB*I nuclease to investigate the total amount of BrdU incorporated mtDNA and to be able to detect prominent ends. The BrdU incorporated into the degradation inhibited cell lines appears comparable to the control but is unable to be directly quantified because the samples were run in different blots. In all cell lines, a smear of linear mtDNA fragments appears after H_2O_2 application. Frequent ends of linear fragments are visible at the OriH, mTER, and OriL areas of the mitochondrial genome that are intermediates of degradation (Peeva et al., 2018). In control cells, these ends appear at 30 minutes, are strongest 2 hours after H_2O_2, and dissipate over the time course of the experiment. Interestingly, in the MGME1$^{-/-}$ cells, and to a lesser extent in POLGexo$^{-/-}$, the frequent ends at OriH and OriL are visible without H_2O_2 and the linear fragments generated by H_2O_2 persist in the degradation impaired cell lines.

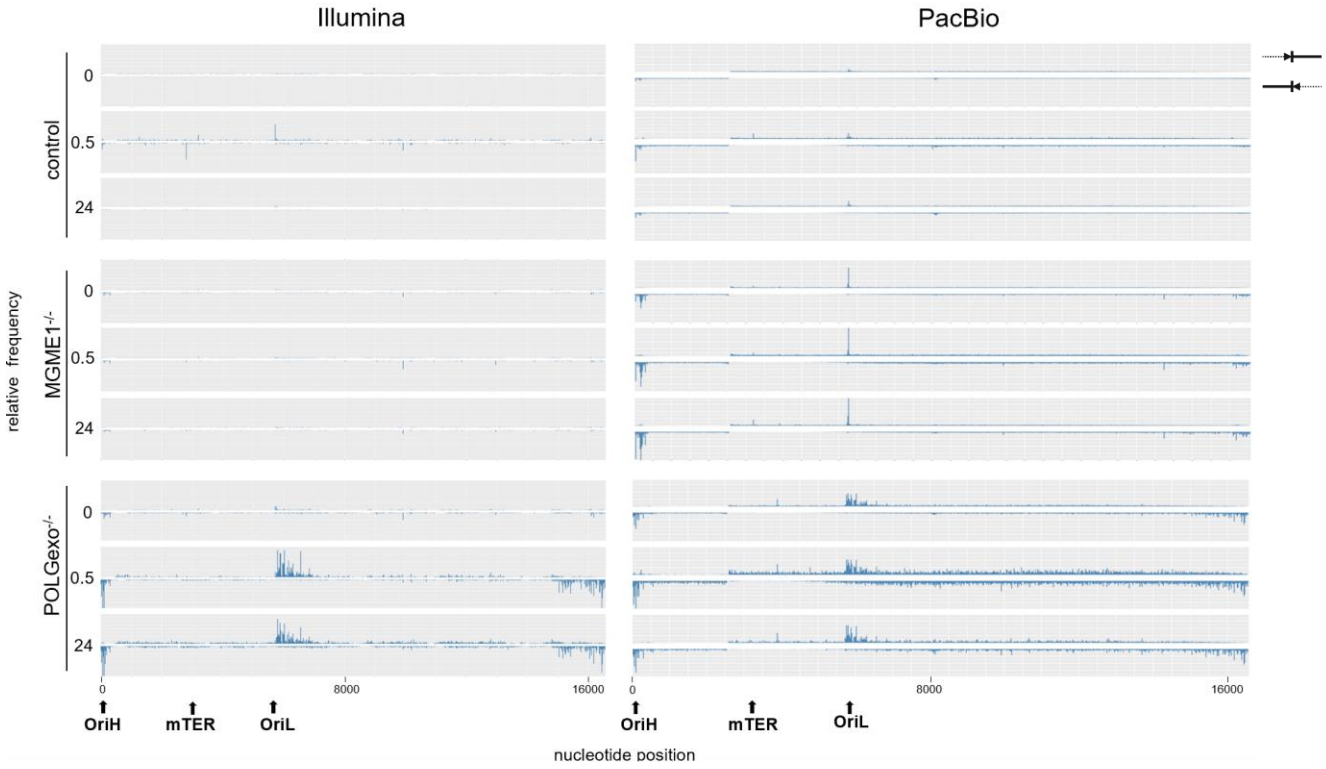

Fig. 22: The distribution of ends along the mitochondrial genome. Samples from control, MGME1$^{-/-}$, and POLGexo$^{-/-}$ were taken before treatment, 30-minutes after H_2O_2, and 24-hours after H_2O_2. Illumina deep sequencing is on the left and PacBio deep sequencing is

on the right. For each time point, the upper panel are ends in one direction and the lower panel is the opposite direction (see upper right scheme). Most strikingly, ends appear at the OriH, mTER, and OriL locations in the mitochondrial genome that do not exist before or 24-hours after H_2O_2 application in control. These ends are present in the MGME1$^{-/-}$ and POLGexo$^{-/-}$ cells regardless of treatment. POLGexo$^{-/-}$ contain orders of magnitude more breaks in mtDNA. Data analyzed and image generated by Dr. Gábor Zsurka.

As indicated in the previous BrdU experiment, Illumina and PacBio sequencing confirmed the location of frequent ends in mtDNA after oxidative damage as occurring in the OriH, OriL, and mTER sites (Figure 22). These frequent ends appear after 30 minutes of H_2O_2 in control cells and diminish after 24 hours. In MGME1$^{-/-}$ cells and POLGexo$^{-/-}$ these frequent ends are already present regardless of H_2O_2 oxidative stress and persist. Figure 22 also confirms the high magnitude of breaks in the POLGexo$^{-/-}$ cell line, which tend to cluster around these frequent end positions.

3.4.5 Nucleotide-sequence motifs relative to minor ends

Ultra-deep sequencing also allows for the determination of the nucleotide-base pattern present at the ends of the mtDNA fragments after H_2O_2 application. The relative frequency of nucleotides was determined in relation to the start or end of the sequenced fragments, excluding the top 100 major sites. In control cells, both Illumina and PacBio sequencing show a pattern of ends proximal to GC-stretches 30 minutes after H_2O_2 application, which was not present before treatment or after 24 hours of recovery (Figure 23A). This pattern of GC-stretches at the ends of control mtDNA fragments with transient oxidative damage is very similar to that of degrading mass linearized mtDNA by endonuclease-induced cleavage (Figure 4 in Peeva et al. 2018).

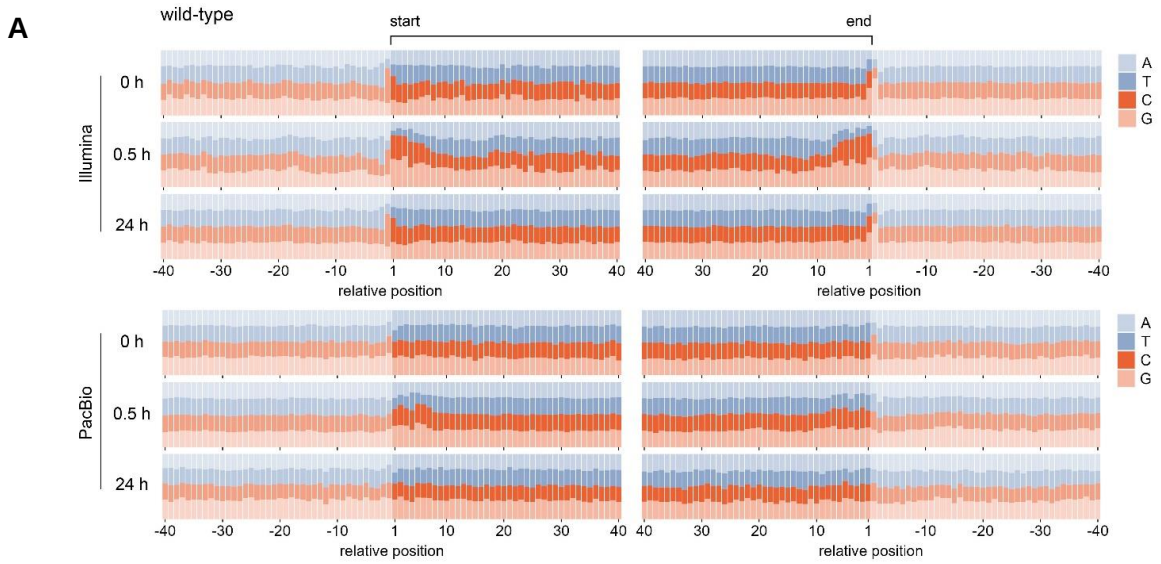

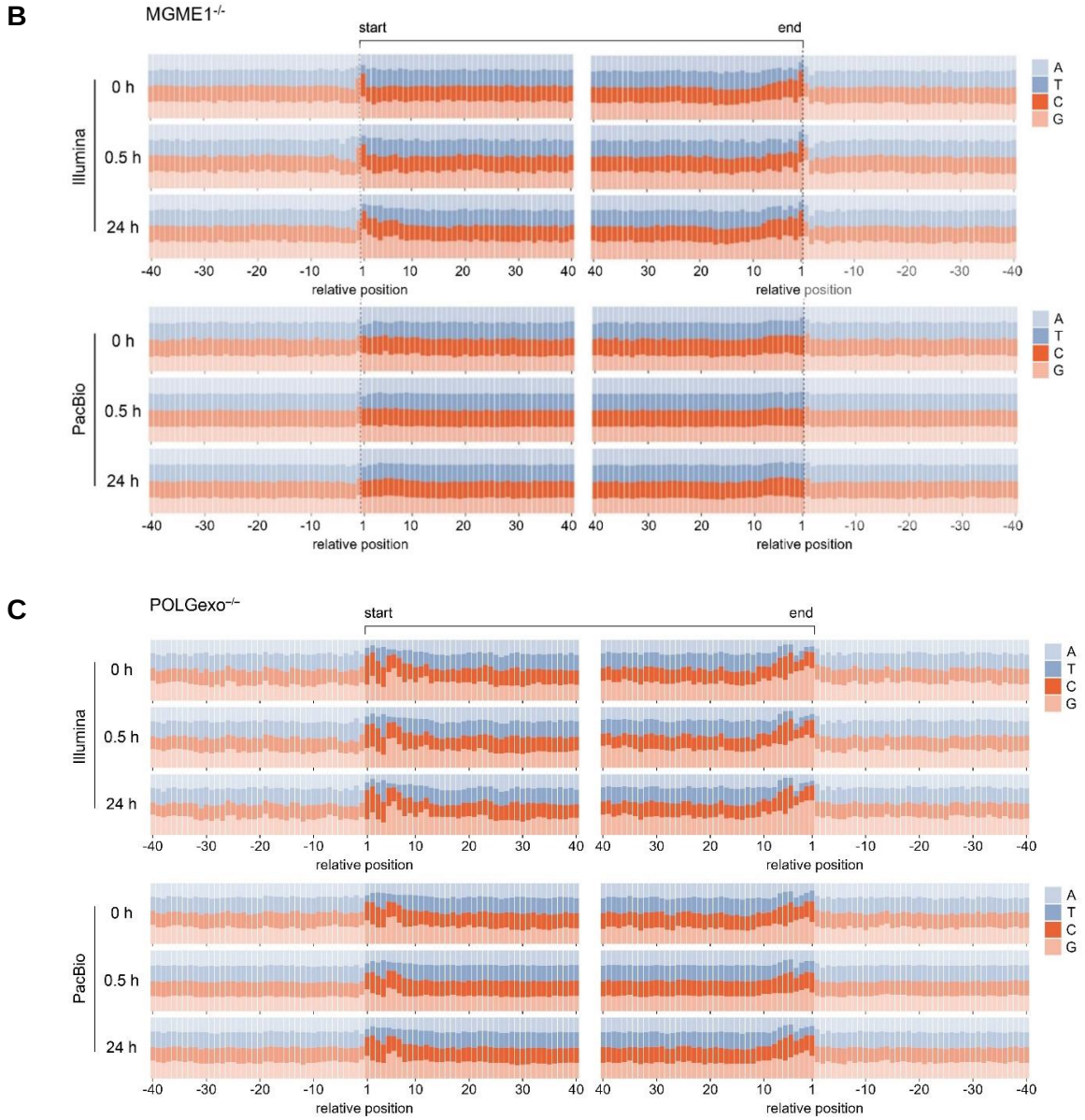

Fig. 23: Nucleotide-sequence motifs at ends detected via ultra-deep sequencing. Images generated by Dr. Gábor Zsurka and taken from Trombly et al. (2023). Nucleotides 40 base-pairs relative to detected ends were counted and position-specific frequencies were normalized to the overall nucleotide frequencies in mtDNA. **A**) wild-type/control, **B**) MGME1$^{-/-}$ and **C**) POLGexo$^{-/-}$ were analyzed. Results from Illumina sequencing of natively blunt linker-ligated ends is in the upper panels for each cell line, while PacBio sequencing of linear mtDNA is in the lower panels. Cell lines were analyzed before treatment, 30 minutes after H_2O_2, and 24 hours after H_2O_2. In wild-type, both sequencing techniques show ends proximal to GC-stretches 30 minutes after H_2O_2, that are not present before treatment or after 24 hours. The end pattern in MGME1$^{-/-}$ does not change with oxidative stress in either sequencing technique. POLGexo$^{-/-}$ show ends proximal to GC-stretches 30 minutes after H_2O_2, that are present before treatment and after 24 hours.

Unlike control cells, MGME1$^{-/-}$ cells have no change in nucleotide-base pattern at ends regardless of the application of H_2O_2 (Figure 23B). Additionally, it could be determined that the acute H_2O_2 exposure does not alter the pattern of blunt, ligatable ends. PacBio sequencing exhibits ends indicative of random breaks, while Illumina sequencing shows a tendency for G's and C's to be present at the ends which could be indicative of the base pattern at blunt ends. In the POLGexo$^{-/-}$ cells there is an association with ends at GC-stretches regardless of H_2O_2 application or sequencing technique (Figure 23C). Like the control cells 30-minutes after H_2O_2, these ends show a similar pattern to those found in mass linearized mtDNA (Peeva et al. 2018). Therefore, ends proximal to GC-stretches that appear upon oxidative damage in control cells and are always present in POLGexo$^{-/-}$ cells are indicative of ongoing residual degradation of linear mtDNA (Trombly et al., 2023). The difference between the two degradation impaired cell lines can be explained by the limited residual degradation activity present in POLGexo$^{-/-}$ cells, while the knock-out of MGME1 results in a complete block of linear mtDNA degradation, confirming the data from induced endonuclease-cleavage of mtDNA in Peeva et al. (2018).

3.4.6 Loss of ENDOG does not affect supercoiled mtDNA recovery after H_2O_2 damage

ENDOG is known to cleave DNA at GC-tracts and has been implicated in the elimination of mtDNA in spermatogenesis (DeLuca and O'Farrell, 2012). While Peeva et al. (2018) determined that ENDOG is not involved in the degradation of mass linearized mtDNA, it does not exclude the involvement of ENDOG in mtDNA maintenance in oxidative stress conditions. Evolutionarily, EXOG is a paralog for ENDOG (Cymerman et al., 2008) and both are known to be targeted to mitochondria which opens the possibility that ENDOG is involved in the repair of mtDNA after oxidative damage. There is no significant difference in the mtDNA after acute H_2O_2 in the ENDOG$^{-/-}$ cell lines compared to the control cells (Figure 24), other than there are less linear mtDNA generated in the ENDOG$^{-/-}$ cells. Therefore, ENDOG is not involved in mtDNA recovery after H_2O_2 oxidative damage.

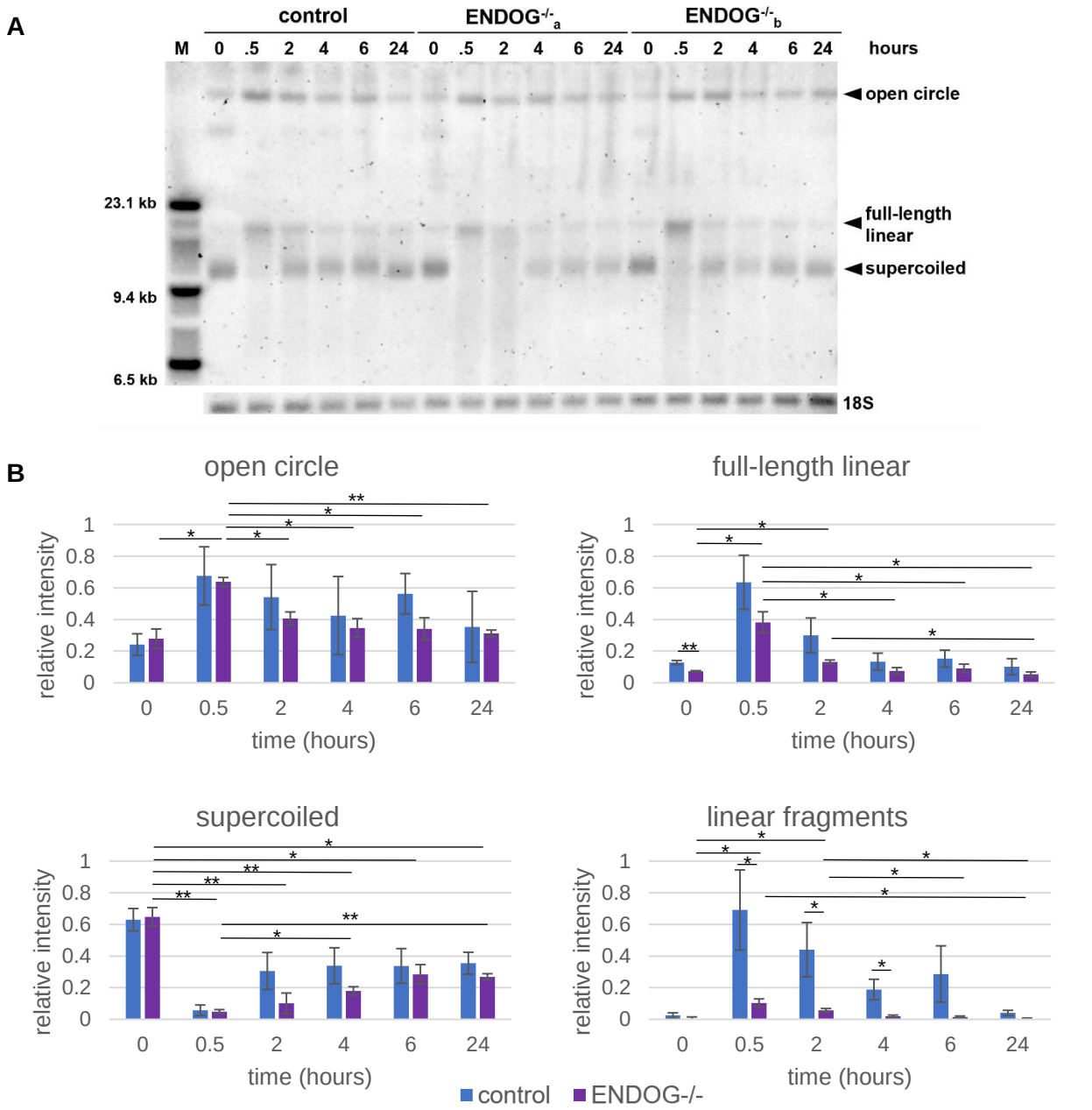

Fig. 24: Southern blot of 1mM H_2O_2 on control and ENDOG$^{-/-}$ cells. **A)** Southern blot depicting the time course of oxidative stress on control, ENDOG$^{-/-}$$_a$, and ENDOG$^{-/-}$$_b$. Top label is time after H_2O_2 application in hours with "M" molecular weight marker. The blot has been labeled for *MT-ND5*. The 18S nuclear band is a loading control. Four conformations of mtDNA can be seen: the open or relaxed circle, the full-length linear, the supercoiled circular genome, and a smear of linear mtDNA fragments of different sizes. **B)** Quantification of the intensity of the 4 major species of mtDNA from southern blots n=7 control and n=3 ENDOG$^{-/-}$. error bars, ±SEM. *, p<0.05, **, p<0.01 by a Student's unpaired t-test between control and ENDOG$^{-/-}$. After H_2O_2 is applied, the open circle and linear species significantly increase, while the supercoiled decreases significantly. During the rest of the time course of the experiment the supercoiled species is recovered, and the other species become less prominent. There is no significant difference between control and ENDOG$^{-/-}$ cells besides in the presence of linear mtDNA fragments.

3.5 Genes involved in repair of SSBs

BER, as outlined in figure 4, is the main repair mechanism for mtDNA damage. Knock-out cell lines for many of the proteins involved in each step of this pathway have been generated, and therefore it is possible to determine if these proteins are crucial for the repair of mtDNA damage after H_2O_2 oxidative stress.

3.5.1 APEX1 activity necessary for fast repair of mtDNA after H_2O_2 oxidative stress

APEX1 is involved in the initial steps of BER of mtDNA. After a DNA glycosylase removes the oxidatively damaged base, APEX1 cleaves the abasic site which generates a SSB. Alternatively, if a SSB is already present, APEX1 is involved in end processing before the SSB is then sealed by the remaining steps in BER. Before the oxidative stress application, the major mtDNA species in the APEX1$^{-/-}$ cell lines is the open circle form rather than the supercoiled (Figure 25). Unlike control cells that recover the supercoiled mtDNA after H_2O_2 oxidative damage, the APEX1$^{-/-}$ cells have delayed recovery of the supercoiled due to reduced BER activity, which is particularly evident in the APEX1$^{-/-}{}_a$ cell line that has significantly less supercoiled mtDNA through the 6-hour time point. Therefore, APEX1 mediated mtDNA repair is necessary for the recovery of intact supercoiled mtDNA after H_2O_2 oxidative damage seen in the control cells.

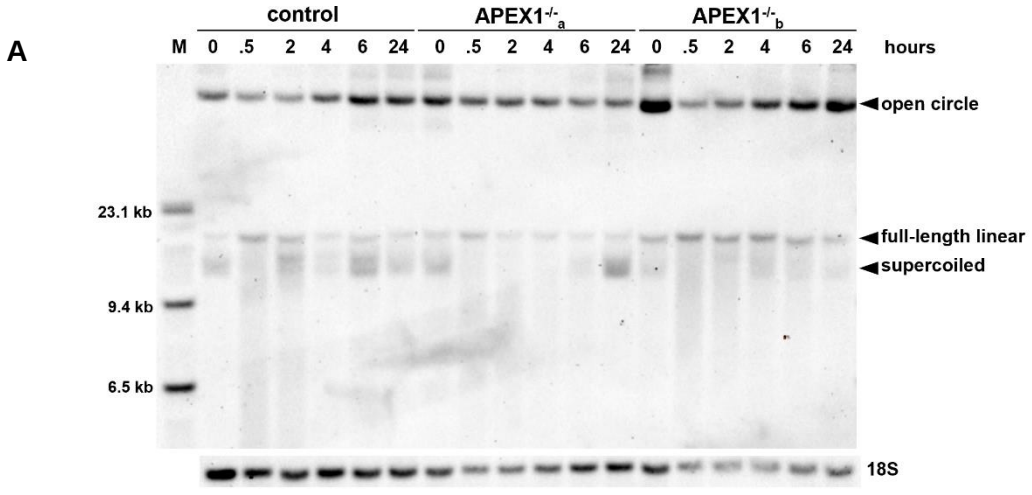

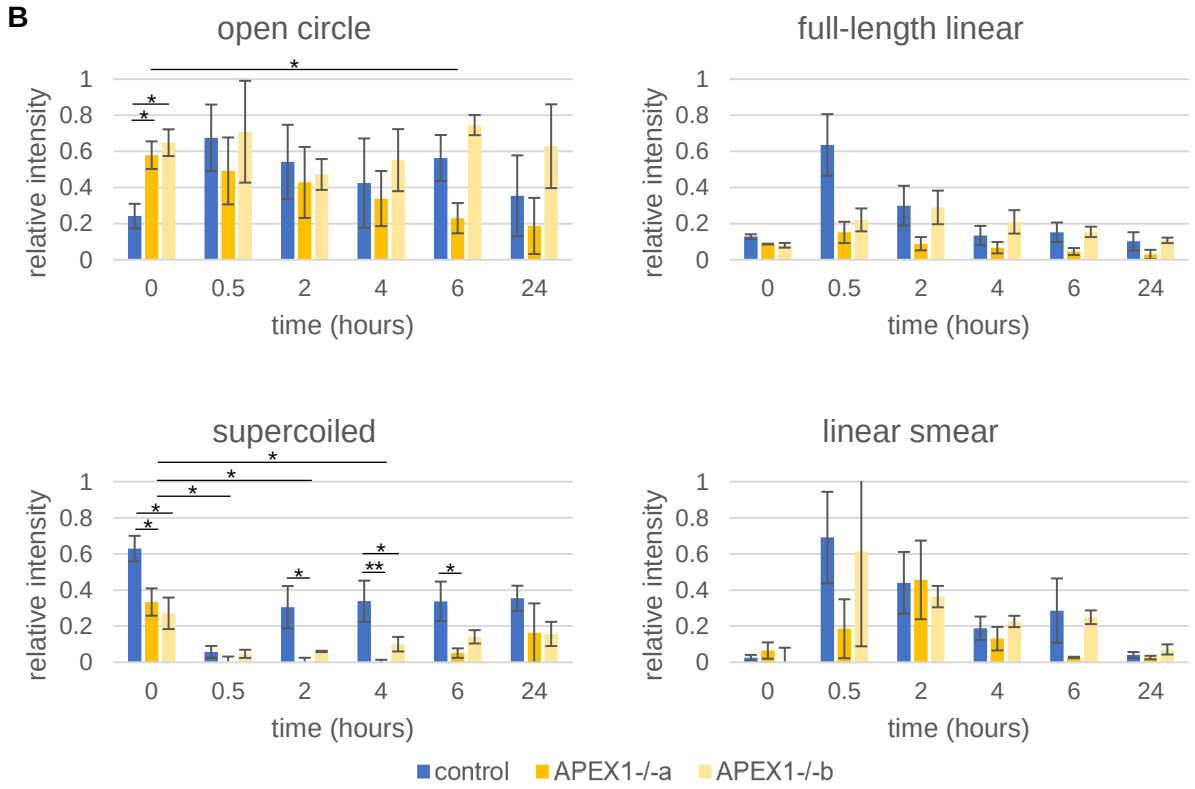

Fig. 25: Southern blot of 1 mM H_2O_2 on control and APEX1$^{-/-}$ cells. **A)** Southern blot depicting the time course of oxidative stress on control, APEX1$^{-/-}{}_a$, and APEX1$^{-/-}{}_b$ cells from a single experiment. Top label is time after H_2O_2 application in hours with "M" molecular weight marker. The blot has been labeled for *MT-ND5*. The 18S nuclear band is a loading control. Four main conformations of mtDNA can be seen: the open circle, the full-length linear, the supercoiled circular, and a smear of linear mtDNA fragments of different sizes. **B)** Quantification of the intensity of the 4 major species of mtDNA. Intensity averages for n=7 control and n=3 APEX1$^{-/-}{}_a$ and APEX1$^{-/-}{}_b$. error bars, ±SEM. *, $p<0.05$, **, $p<0.01$ by Student's unpaired t-test between time points for APEX1$^{-/-}$ and between control and APEX1$^{-/-}$. Before treatment, the major mtDNA species is the open circle in the APEX1$^{-/-}$. After H_2O_2 is applied, the mtDNA is damaged and the open circle and linear species become more prominent, with little to no supercoiled mtDNA remaining. After 24 hours the supercoiled species is recovered in the control cells, but this recovery of the supercoiled is impaired in the APEX1$^{-/-}$ lines.

3.5.2 EXOG LP-BER is unlikely to be involved in mtDNA repair after H_2O_2 oxidative stress

The 5'-3' exonuclease activity of EXOG is believed to be involved flap removal in long-patch BER of mtDNA by removing the overhangs generated when POLG fills in missing bases (Alencar et al., 2019). Like control cells, the major mtDNA species in EXOG$^{-/-}$ cells before treatment is the supercoiled species, which is damaged after H_2O_2 is applied resulting in the open circle and linear species becoming more prominent, and the supercoiled mtDNA is recovered during the time course of the experiment (Figure 26).

The mtDNA in two EXOG clones can be seen to react differently to the applied oxidative stress. EXOG$^{-/-}_{b}$ does not significantly differ from control cells, while EXOG$^{-/-}_{a}$ appears to have more fragmented mtDNA after the applied oxidative stress, and as a result is not as able recover the supercoiled mtDNA. This could also be correlated with the decrease in mtDNA copy number 24 hours after oxidative stress (Figure 16E) seen in this cell line that is absent in the other EXOG knock-out.

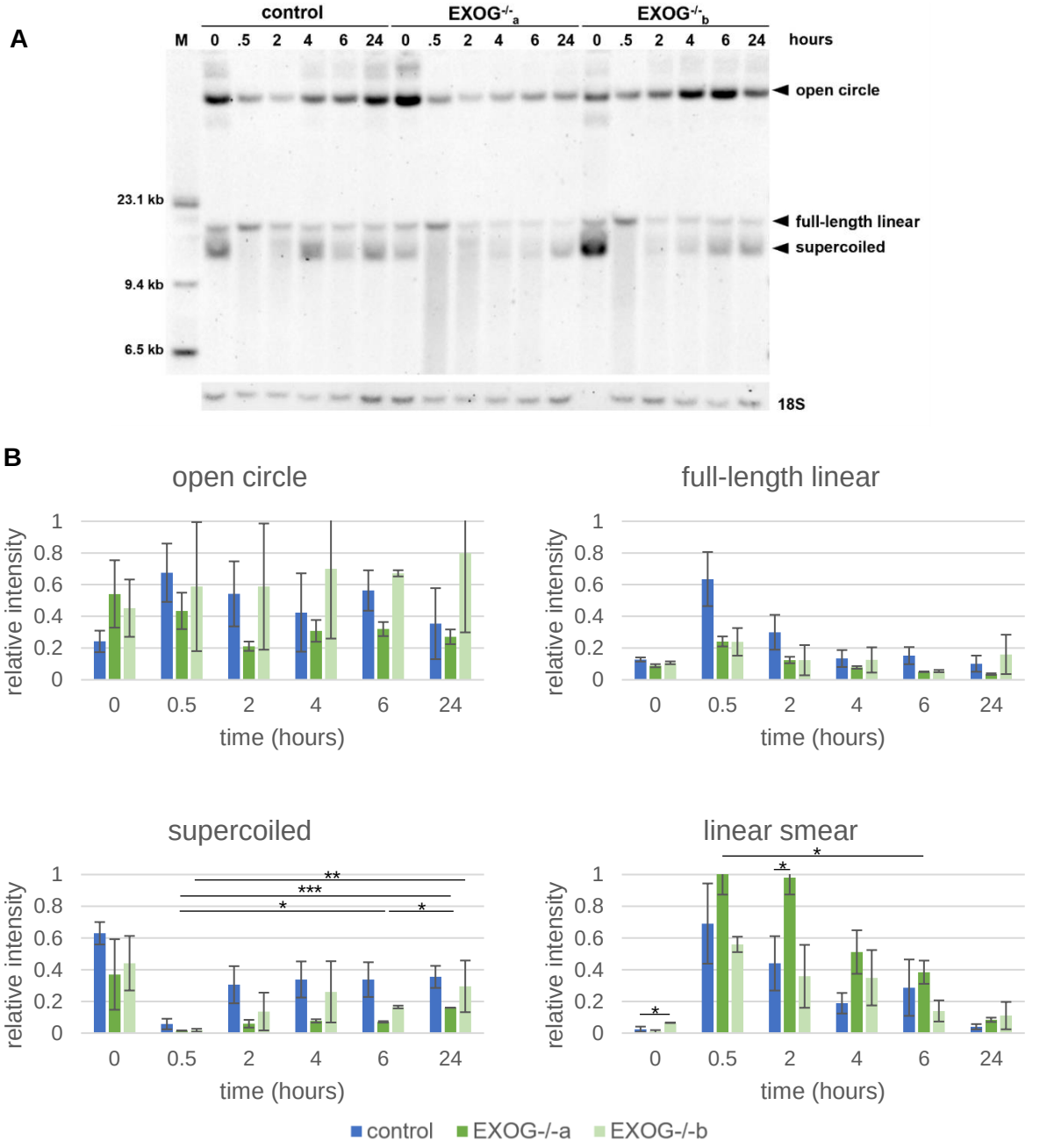

Fig. 26: Southern blot of 1 mM H_2O_2 on control and EXOG$^{-/-}$ cells. **A)** Southern blot depicting the time course of oxidative stress on control, EXOG$^{-/-}_{a}$, and EXOG$^{-/-}_{b}$ cells. Top label is time after H_2O_2 application in hours with "M" molecular weight marker. The blot

has been labeled for *MT-ND5*. The 18S nuclear band is a loading control. Four main conformations of mtDNA can be seen: the open circle, the full-length linear, and the supercoiled circular genome, and a smear of linear mtDNA fragments of different sizes. **B)** Quantification of the intensity of the 3 major species of mtDNA. Intensity averages n=7 control and n=2 $EXOG^{-/-}{}_a$ and $EXOG^{-/-}{}_b$. error bars, ±SEM. *, $p<0.05$, **, $p<0.01$, ***, $p<0.001$ by Student's unpaired t-test between time points for $EXOG^{-/-}$ lines and between control and $EXOG^{-/-}$. Before treatment the major species is in the native supercoiled, after H_2O_2 is applied the mtDNA is damaged and the open circle and linear species become the most prominent, and the supercoiled is recovered after 24 hours. The smear of fragmented mtDNA species is more prominent in the $EXOG^{-/-}{}_a$ cell lines after applied H_2O_2.

3.5.3 LIG3 activity is vital for cells after H_2O_2 oxidative stress

A major step in both replication and repair of mtDNA is the ligation of ends, for which LIG3 is the sole mitochondrially targeted DNA ligase (Simsek et al., 2011). Interestingly, in both $LIG3^{-/-}$ lines there is supercoiled mtDNA still present, therefore the LIG3 sealing activity is not necessary for supercoiling to occur or some other ligase is acting within mitochondria (Figure 27B). The open circle mtDNA is the major species present in the $LIG3^{-/-}$ cells in basal conditions, rather than the supercoiled. After the pulse of H_2O_2, the $LIG3^{-/-}$ cell lines have depletion of all mtDNA species (Figure 27), which correlates to the copy number change in Figure 16. This depletion and lack of recovery of mtDNA in these cell lines is likely a result of the mass damage that occurs with the H_2O_2 pulse and the generation of linear fragments that are degraded, as well as the persistence of SSBs that are unable to be ligated with the open circle conformation being the most prevalent mtDNA species 24-hours after H_2O_2. Therefore, LIG3 is crucial for the recovery of mtDNA after H_2O_2 oxidative damage, and its absence is likely inhibiting both repair as well as *de novo* replication to replenish numbers after degradation.

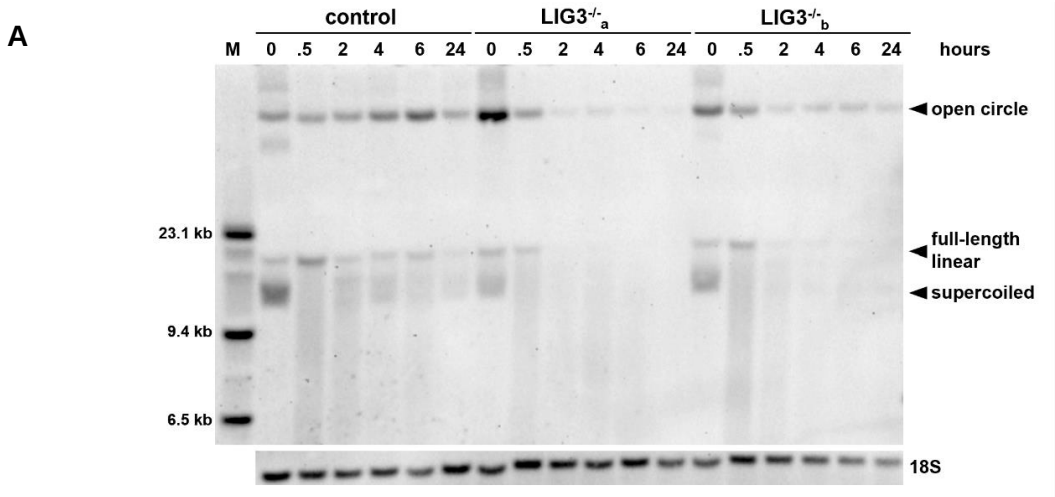

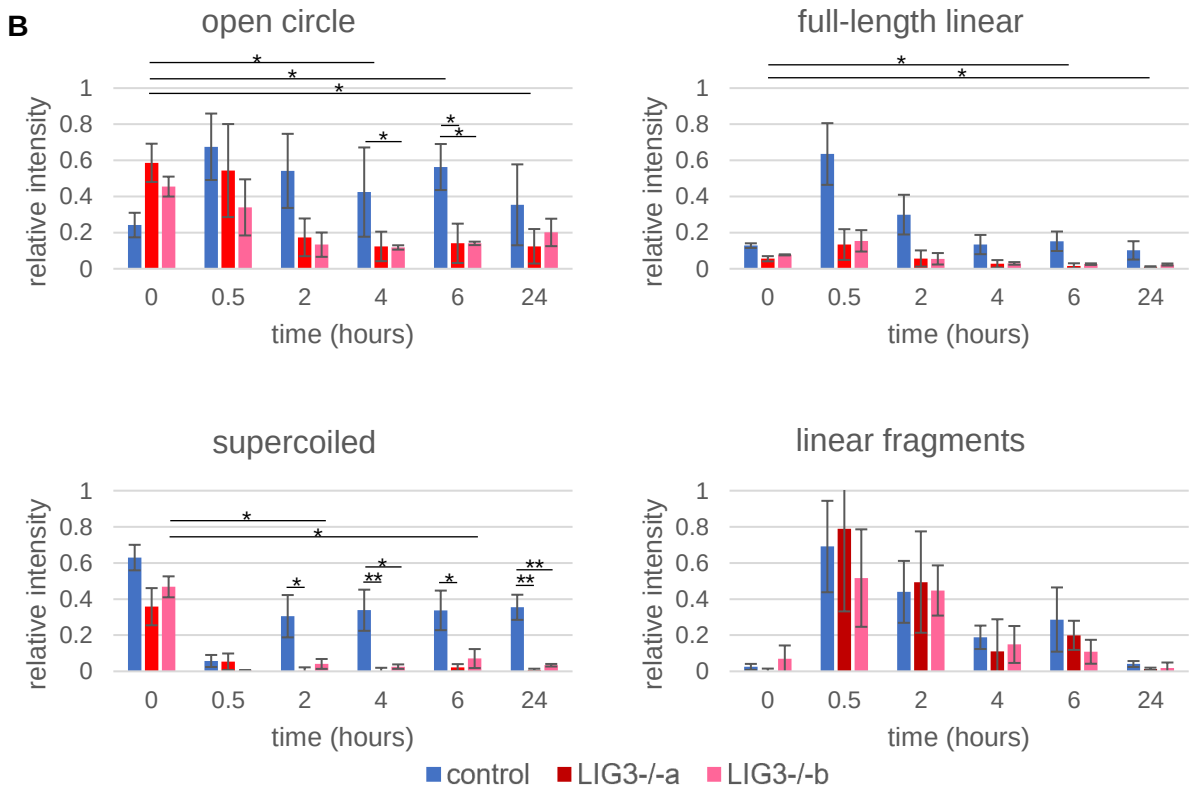

Fig. 27: Southern blot of 1 mM H_2O_2 on control and LIG3$^{-/-}$ cells. **A)** Southern blot of the H_2O_2 time course on control, LIG3$^{-/-}{}_a$, and LIG3$^{-/-}{}_b$ cells. Top label is time after H_2O_2 in hours with "M" molecular weight marker. The blot has been labeled for *MT-ND5*. The 18S nuclear band is a loading control. Four main conformations of mtDNA can be seen: the open circle, the full-length linear, the supercoiled circular genome, and a smear of linear mtDNA fragments of different sizes. **B)** Quantification of the intensity of the 4 species of mtDNA from southern blots averaged over n=7 control, n=3 LIG3$^{-/-}{}_a$, and n=2 LIG3$^{-/-}{}_b$. error bars, ±SEM. *, $p<0.05$, **, $p<0.01$ by Student's unpaired t-test between time points for LIG3$^{-/-}{}_a$ and LIG3$^{-/-}{}_b$ and between control and LIG3$^{-/-}$. The major species in LIG3$^{-/-}$ cells before treatment is the open circle. After H_2O_2 is applied, the mtDNA is damaged and the open circle and linear species become the most prominent, with little to no supercoiled mtDNA remaining. All mtDNA species deplete in the LIG3$^{-/-}$ cells 24-hours after H_2O_2.

BrdU incorporation into mtDNA in LIG3$^{-/-}$ cells without H_2O_2 is comparable to control cells (Figure 28A). However, when H_2O_2 is applied in parallel with the BrdU, no BrdU is visibly incorporated into LIG3$^{-/-}$ cells after 24 hours, which confirms the high degree of mtDNA depletion observed in the LIG3$^{-/-}$ lines under oxidative stress (Figure 28B). Likewise, BrdU pulse/chase confirms the rapid rate of BrdU elimination from the LIG3$^{-/-}$ cells after the H_2O_2 pulse, with very little BrdU mtDNA remaining after only two hours (Figure 29). Compared to control cells (Figure 10), the depletion of BrdU mtDNA occurs at a faster rate in LIG3$^{-/-}$ cells with H_2O_2 treatment, but this difference is only significant after 6 hours. This depletion of mtDNA seen in the LIG3$^{-/-}$ cell lines with H_2O_2 is correlated with the decrease in mtDNA

copy number as mentioned previously, and it is possible that cell death is a contributing factor (Figure 15).

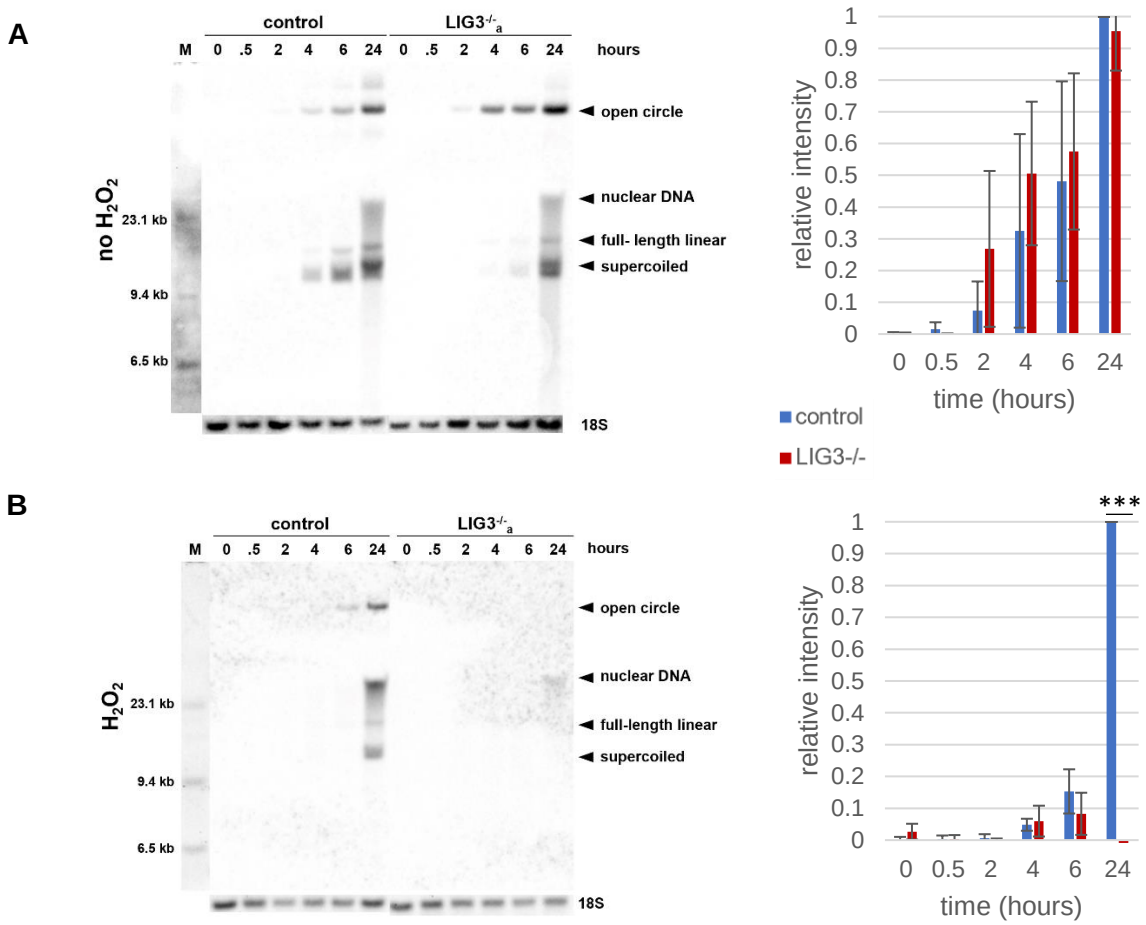

Fig. 28: BrdU incorporation assays in LIG3$^{-/-}_{a}$ cells. In A and B: BrdU blots and the quantification of the sum of the BrdU intensity of 3 major mtDNA species (open circle, full-length linear, and supercoiled). Top label "M" molecular weight marker and time in hours. The blot has been labeled with a BrdU antibody to visualize the BrdU incorporated DNA. The 18S nuclear band is a loading control. The dark cloud smear at approximately 25 kb is due to nuclear BrdU incorporation. Quantification is normalized to the 18S and to the 24-hour control sample. **A)** BrdU incorporation into control and LIG3$^{-/-}_{a}$ cells. n=4 control, n=2 LIG3$^{-/-}$. error bars, ±SEM. BrdU can be seen to be incorporated into the mtDNA starting at the 2-hour time point, with maximal intensity at 24 hours. There is no significant difference between control and LIG$^{-/-}$. **B)** BrdU incorporation in the presence of H_2O_2 in control and LIG3$^{-/-}_{a}$ cells. n=5 control, n=2 LIG3$^{-/-}$. error bars, ±SEM. ***, $p<0.001$ by a Student's unpaired t-test. BrdU incorporation is reduced in all cell lines in the presence of H_2O_2. No visible BrdU is incorporated into LIG3$^{-/-}$ cells due to the depletion of mtDNA that occurs in the knock-out line after the H_2O_2 pulse.

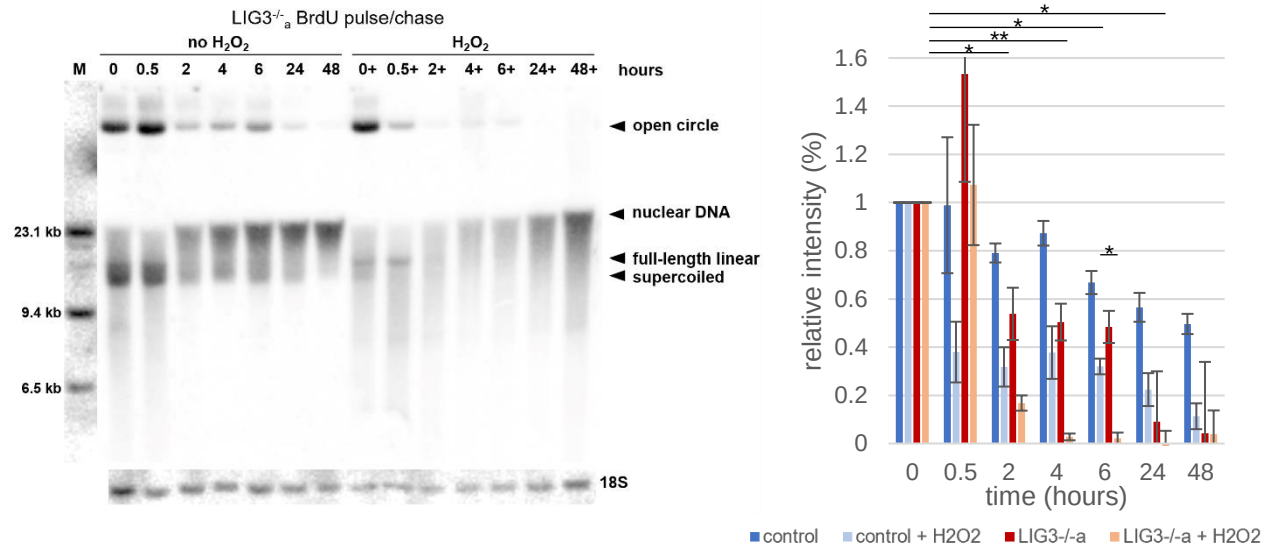

Fig. 29: BrdU pulse/chase experiments on LIG3$^{-/-}$$_a$ cells. Southern blot: The label at the top shows the "M" is the molecular weight marker and time in hours. The blot has been labeled with a BrdU antibody to visualize the BrdU incorporated DNA. The 18S nuclear band is a loading control. The dark cloud smear approximately 25 kb is due to nuclear incorporation of BrdU. Quantification of the sum of the BrdU intensity of 3 major mtDNA species (open circle, linear, and supercoiled). Samples normalized to the non-treated time point for each cell line and corresponding treatment (no H_2O_2 and +H_2O_2). n=2 control (Figure 10) and LIG3$^{-/-}$$_a$. error bars, ±SEM. *, p<0.01, **, p<0.001 by a Student's unpaired t-test. BrdU depletes significantly in LIG3$^{-/-}$ cells where H_2O_2 has been applied. There is a significant depletion observed at the 6-hour time point in LIG3$^{-/-}$ cells compared to the control cells with H_2O_2.

In Illumina and PacBio deep sequencing there is an increase in both DSBs and SSBs in LIG3$^{-/-}$ cells upon H_2O_2 treatment (Figure 30). Due low sample number and the depletion of mtDNA in the LIG3$^{-/-}$ lines after H_2O_2 oxidative stress, the 24-hour results can only be limitedly interpreted because only a small amount of mtDNA remains and cell death is likely a factor.

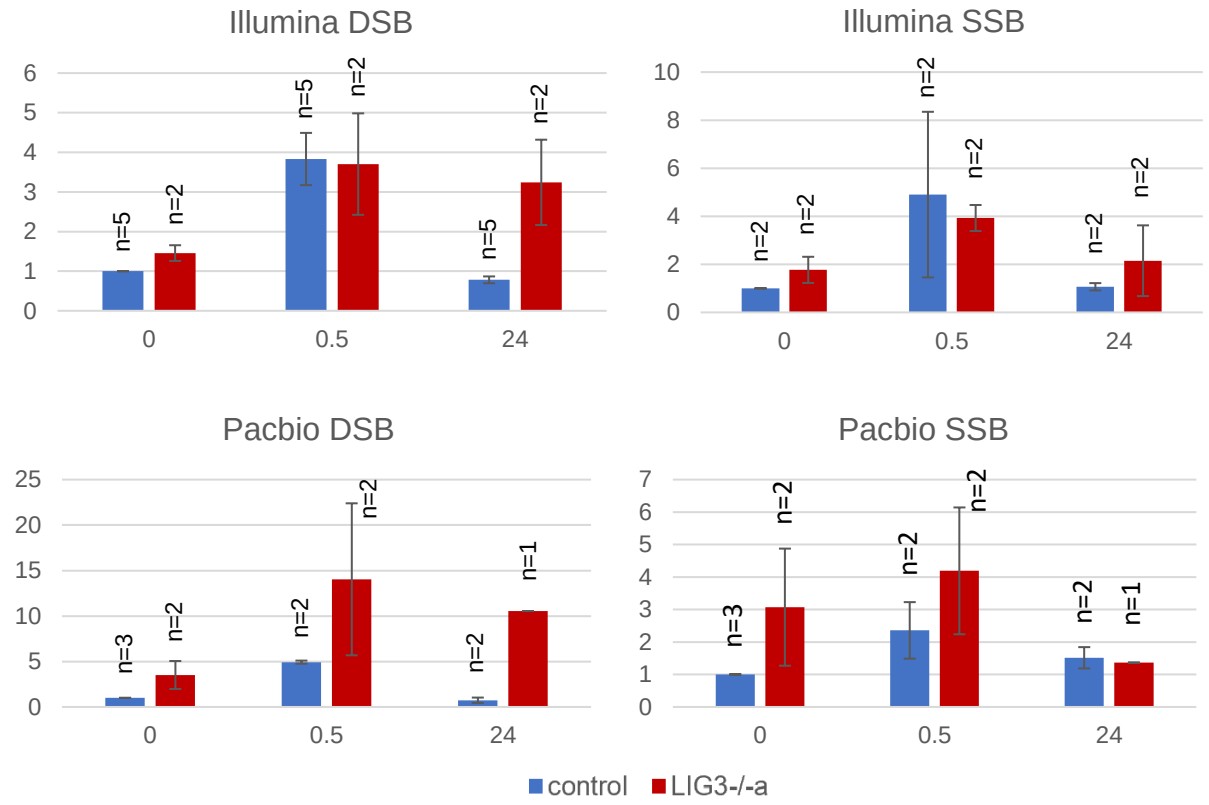

Fig. 30: Relative frequency of deep sequencing mtDNA breaks in control and LIG3$^{-/-}$$_a$ cells. Relative frequency is on the y-axis and time after H_2O_2 application is on the x-axis. Quantification of DSBs from linker-mediated Illumina sequencing or long-read PacBio sequencing. SSBs were determined by subtracting the frequency of DSBs from S1 nuclease treated samples. Break frequencies have been normalized to average coverage and to the non-treated control sample. error bars, ±SEM. Both DSBs and SSBs increase 30 minutes after H_2O_2 in LIG3$^{-/-}$ cells. Data analyzed by Dr. Gábor Zsurka.

3.6 Deferiprone mitigates mtDNA oxidative damage

Deferiprone is an iron chelator that is known to lower the amount of free iron present in mitochondria and thus can decrease the generation of the damaging hydroxyl radical. Kakhlon et al. (2008) found that deferiprone application decreased the available iron pool within mitochondria and mitigated the effects of H_2O_2 oxidative stress. Cells were treated with 50 µM deferiprone for 24 hours before the application of H_2O_2 and throughout the time course. Deferiprone treatment did not have any effect on cell viability (Figure 31A). Treatment with deferiprone before H_2O_2 application resulted in less mtDNA damage as evident by the remaining supercoiled signal in control cells after 30 minutes (Figure 31B). Interestingly, LIG3$^{-/-}$ cells treated with deferiprone do not suffer from the mass depletion of mtDNA after H_2O_2 application (Figure 31B and C). There is also a strong presence of

the open circle mtDNA, possibly from less damage occurring to the mtDNA, and therefore reduced formation of linear species. With deferiprone treatment mtDNA copy number remains stable in all cell lines, regardless of the application of H_2O_2 (Figure 32A). The relative frequency of mtDNA breaks increases upon the application of H_2O_2 in all cell lines, and after 24 hours the break frequency decreases in the control but persist in LIG3$^{-/-}$ cells. Most strikingly, with deferiprone treatment there is significantly less damage to mtDNA 30 minutes after H_2O_2 (Figure 32B). Therefore, deferiprone mitigates the damage that occurs after our applied H_2O_2 pulse by reducing the amount of mtDNA strand breaks that appear.

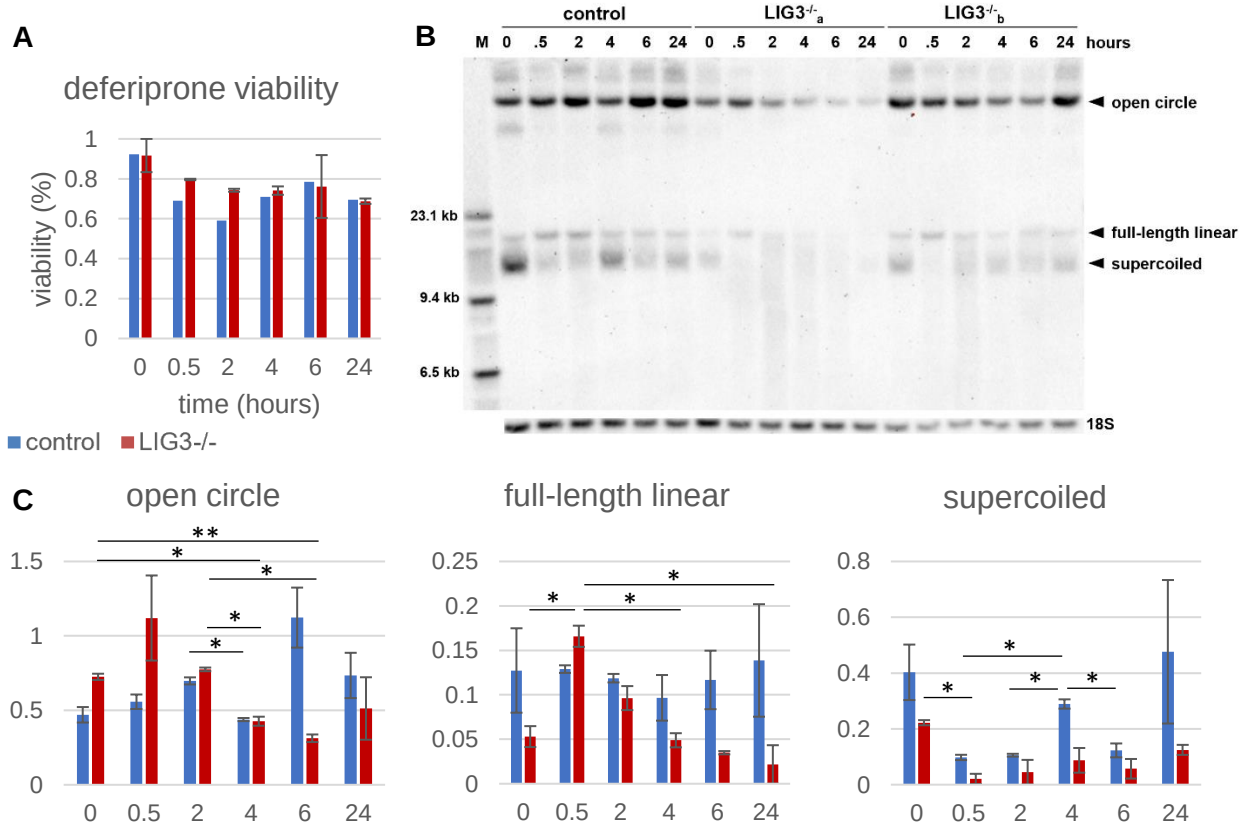

Fig. 31: Viability and Southern blot of deferiprone treated control and LIG3$^{-/-}$ cells. **A**) Cell survival in a H_2O_2 time course with deferiprone added for control and LIG3$^{-/-}$. There is no significant difference in survival with the addition of deferiprone into the medium. **B**) Southern blot of a deferiprone and H_2O_2 time course on control and LIG3$^{-/-}$ cell lines. The blot has been labeled with "M" molecular marker and time in hours after H_2O_2 application and probed for *MT-ND5*. The 18S nuclear band is a loading control. Three main mtDNA conformations can be seen: the open circle, the full-length linear, and the supercoiled. **C**) The intensity of the 3 major species of mtDNA was quantified and averaged n=2 for control (blue) and LIG3$^{-/-}$(red). error bars, ±SEM. *, $p<0.05$, **, $p<0.01$ by a Student's unpaired t-test. Deferiprone treatment before H_2O_2 application appears to increase the recovery of supercoiled mtDNA in all cell lines. Most strikingly, there does not seem to be mass

depletion of mtDNA in the LIG3$^{-/-}$ cells after H_2O_2, and no significant differences between LIG3$^{-/-}$ and control.

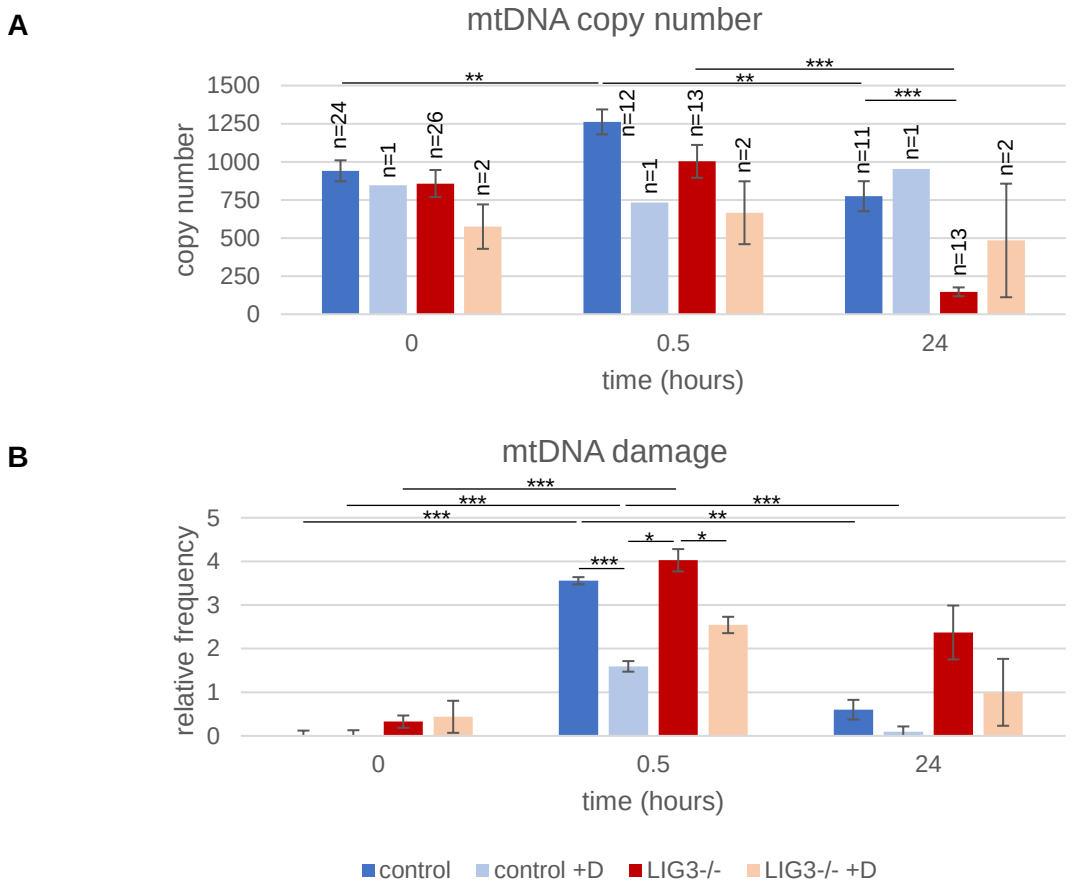

Fig. 32: mtDNA copy number and damage quantification of deferiprone treated control and LIG3$^{-/-}$ cells. For control (blue) and LIG3 $^{-/-}$ cells (red) in normal H_2O_2 experiments and with deferiprone treatment (light blue and peach, respectively). error bars, ±SEM. *, p<0.05, **, p<0.01, ***, p<0.001 by Student's unpaired t-test. Samples are taken in the basal conditions, 30 minutes after acute H_2O_2 application, and after 24 hours of recovery. **A**) mtDNA copy numbers. With deferiprone treatment mtDNA copy number is more stable in all cell lines and there is no significant change in copy number, most strikingly there is no strong depletion in LIG3$^{-/-}$ cells with deferiprone. **B**) The relative frequency of breaks in mtDNA minor arc as determined by qPCR Ct value differences. n=3 for both control treatments and LIG3$^{-/-}$ in normal medium, n=2 for LIG3$^{-/-}$ with deferiprone. Replicates for control cells with deferiprone are technical rather than experimental. The Ct difference for the 0-hour control sample is considered baseline. The frequency of breaks increases with H_2O_2 treatment in all cell lines and persist in the LIG$^{-/-}$ in normal medium. With deferiprone, there is less mtDNA damage as measured by the frequency of breaks 30-minutes after H_2O_2.

4. Discussion

4.1 H_2O_2 paradigm of oxidative damage

4.1.1 H_2O_2 degrades rapidly and results in a pulse of oxidative damage

Hydrogen peroxide is a relatively unreactive ROS that is able travel long distances and to enter the cell and into the mitochondria freely via aquaporins (Henzler and Steudle, 2000). H_2O_2 has long been used as an experimental source of oxidative stress (Kaneko and Inoue, 1998), and previous work has found that H_2O_2 is rapidly degraded under cell culture conditions (Houot et al., 2001*).* This was confirmed by our results where the Amplex™ red measured H_2O_2 decayed quickly in cell culture medium, and this decay was exacerbated in medium containing cells (Figure 5; Trombly et al., 2023). The rapid decay of H_2O_2 in the cell culture medium is intensified by the pyruvate added to the medium as a metabolic support for the HEK293 cells (Guarino et al., 2019). In addition, the presence of catalase within cells results in the generation of O_2 and H_2O from H_2O_2 in a manner proportional to the number of cells (Ransy et al., 2020). Five minutes after addition to the medium with cells the concentration of H_2O_2 was negligible. The rapid H_2O_2 decay in our experimental conditions allows us to characterize the applied oxidative stress as a transient pulse; therefore, the oxidative insult acts acutely and its damage to mtDNA and the subsequent recovery of mtDNA can be followed.

4.1.2 Mitochondrial specific action due to the Fenton reaction

Further confirming the validity of our cell model of oxidative stress is the fact that there was no measurable effect on the fragmentation of nuclear DNA measured by PacBio long-read sequencing. There was no transient increase in small fragments 30-minutes after H_2O_2 application in nuclear DNA for both native DNA and S1-nuclease digested samples (Figure 11), unlike with mtDNA where the frequency of small fragments increased due to oxidative damage after H_2O_2 application. Thus, our measured changes can be attributed to mitochondria related effects and not to nuclear. These measurements are limited by the fact that the size range detectable by PacBio sequencing has a range of up to 20 kb, therefore larger nuclear DNA fragments are not detected. This does not exclude the fact that proteins, lipids, and RNA can also be damaged by ROS (Cadenas, 1989), but this was not investigated in the scope of this thesis. Previous studies have similarly confirmed that applied H_2O_2 did not affect nuclear DNA, while other tested applications of oxidative stress such as menadione did affect nuclear DNA (Goffart et al., 2021). A potential

explanation for the damage to mtDNA is that the H_2O_2 pulse generates oxidative damage by the formation of the hydroxyl radical in the mitochondria matrix via the Fenton reaction due to the presence of relatively high amounts of free iron (Petrat et al., 2002). This higher level of iron within mitochondria explains why mtDNA mutates at a much faster rate than nuclear DNA (Alencar et al., 2019), and while the cause of these different mutation rates has yet to be solidified, ROS likely play a strong role in this process. Diseases have been associated with an overload of iron within mitochondria (Levi and Rovida, 2009) due to the damaging effect that ROS can have, particularly on iron-sulfur clusters. Deferiprone, which has been found to lower the available free iron pool in mitochondria and mitigate the effects of the H_2O_2 generated oxidative stress (Kaklon et al., 2008), was used to confirm the Fenton reaction theory. LIG3$^{-/-}$ cells were shown to be particularly vulnerable to the H_2O_2 treatment, and therefore were selected to be treated with deferiprone because they would show the most dramatic effects. With deferiprone the LIG3$^{-/-}$ cell lines have significantly better viability 24-hours after the H_2O_2 pulse as well as do not have the strong mtDNA depletion visible in the Southern blot or in mtDNA copy number measurements (Figure 31A and C, Figure 32A), which are otherwise present without the application of the iron chelator. mtDNA damage 30-minutes after H_2O_2 application was significantly less with deferiprone treatment (Figure 32B). Treatment with deferiprone was able to mitigate the mtDNA damage generated by the H_2O_2 pulse, further supporting that our observed damage was likely a result of the hydroxyl radical produced via the Fenton reaction within mitochondria (Dizdaroglu and Jaruga, 2012).

4.1.3 HEK293 cells survive 1 mM H_2O_2 oxidative stress

H_2O_2 as a method of ROS application has come into question recently, and alternative methods have been investigated (Goffart et al., 2021). This is due to the low stability and relatively short half-life of H_2O_2 and the fact that enzymatic and chemical elimination within cells remains difficult to quantify (Ransy et al., 2020), making reproducibility a challenge. Previous studies have asserted that H_2O_2 concentrations above 200 µM were enough to result in cell death (Goffart et al., 2021), however the medium in these experiments was not supplemented with uridine and pyruvate. Without pyruvate in the medium there is likely to be more persistent action of the applied hydrogen peroxide (Guarino et al., 2019), and in our experimental conditions cells were able to survive concentrations of 1 mM H_2O_2. There was no significant change in viability and cell survival remained above 60 % through

the time course of the experiment, therefore cell death is not a significant factor in the differences in mtDNA seen in the control and the majority of the knock-out cell lines (Figure 15). However, LIG3$^{-/-}$ cell lines do show a significant decrease to 50 % viability 24-hours after H_2O_2 exposure, therefore at this time point cell death cannot be completely excluded as a contributing factor and the results should be interpreted with caution. It is possible that this significant viability decrease in LIG3$^{-/-}$ cells is attributed to the dramatic mtDNA depletion that is also observed at this time point (Figure 16) because the loss of mtDNA is known to contribute to cell death (Shokolenko et al., 2013), but the of the presence of uridine and pyruvate in the cell culture medium should allow our cells to survive a ρ^0 status (Spadafora et al, 2016). Uridine and pyruvate have been previously shown to help cells survive mtDNA loss and oxidative stress (Walker et al., 2003; Miwa et al., 2000) via the supplementation of nucleotides and energy production support, which helps to rescue cells in the case of mitochondria dysfunction and OXPHOS deficiency (Adant et al., 2022). The fact that the LIG3$^{-/-}$ cell lines have increased cell death from the pulse of H_2O_2 even in this supported medium opens the possibility that some other action from the addition of H_2O_2 is leading to increased apoptosis.

It has not yet been completely elucidated how the nucleus senses mtDNA damage and is able to employ the repair and degradation machinery to mitochondria (Nadalutti et al., 2022). Recently, it has been determined that mitochondrial RNA in the cytoplasm is associated with nuclear sensing of DSBs in mtDNA and responsible for triggering an immune response (Tigano et al., 2021) which can be associated with inflammation. Most of the nuclear-encoded proteins for mtDNA maintenance are found in complexes: the replication proteins responsible for degradation (Peeva et al., 2018) and SSB repair (Tann et al., 2011). As these proteins are already assembled within mitochondria, the nuclear sensing of mtDNA damage for their recruitment likely does not play a major role. It has been found that cells that have previously been exposed to ROS gain resistance to future damage and a greater capacity to repair oxidative DNA damage (Grishko et al., 2005), so the mtDNA maintenance proteins may simply be upregulated when necessary. H_2O_2 is not only a source of damaging ROS, but also serves as a signaling molecule within cells that helps to regulate the cell cycle, metabolism, redox balance, and the response to inflammatory stress (Kowaltowski et al., 2009) even at low µM concentrations (Dröge, 2002), therefore H_2O_2 in the cytosol could help recruit repair and degradation proteins to

mitochondria. The use of high concentrations of H_2O_2 is closer to inflammatory states, and 1 mM was shown to result in a mild increase in mitochondrial respiration (Ransy et al., 2020), which could also aid in nuclear sensing of mtDNA damage. ROS within cells can have positive effects in preventing cancer progression by triggering apoptosis, but within these same immune cells if ROS inflammation is chronic, it can actually contribute to the development of cancer (Degtyareva et al., 2019). Apoptosis has also been triggered by persistent oxidative damage to mtDNA due to the loss of the mitochondria membrane potential (Nadalutti et al., 2022), and mitophagy is another important quality control mechanism to remove deficient mitochondria. We did not address mitophagy in this thesis, however because our H_2O_2 pulse was transient and not chronic it is possible that the signaling cascades that lead to autophagy and mitophagy were not activated. Additionally, we only followed the short-term effects after H_2O_2 application, and over a longer time scale these processes likely play a larger role.

4.1.4 mtDNA copy number changes

mtDNA copy number per cell is a biomarker of mitochondrial function, varies per tissue type, and is known to decrease with age (Castellani et al., 2020). Lower copy numbers naturally lead to less translation of OXPHOS proteins encoded by mtDNA and less cellular energy production. There was no significant difference between the CRISPR/Cas9 edited cell lines and the control cells, therefore none of the genes had a major influence on mtDNA copy number under basal conditions (Figure 16). APEX1$^{-/-}$ cells do appear to have elevated copy number, which could be a compensatory mechanism to deal with persistent mtDNA damage due to the vital role APEX1 plays in BER. The fact that baseline mtDNA copy number in LIG3$^{-/-}$ cells is not significantly different than the control cells is particularly interesting because of the crucial role that the LIG3 plays in both replication and repair and therefore the knock-out should result in depletion of mtDNA. There was a significant increase in mtDNA copy number 30 minutes after H_2O_2 application in control, MGME1$^{-/-}$, and LIG3$^{-/-}{}_b$ cells. In the short time scale of 30-minutes it is highly unlikely that this increase would be due to replication as mtDNA requires over 1 hour to complete replication in ideal conditions (Clayton, 1982). This increase is also found in the MGME1$^{-/-}$ cells, even though loss of MGME1 has been shown to impede stress-induced initiation of mtDNA replication (Torregosa-Muñumer et al., 2019). In addition, previous studies have found that there was no change in mtDNA copy number associated with low levels of oxidative damage, and

specifically that H_2O_2 treatment did not increase replication intermediates like other damaging agents such as UV or $KBrO_3$ (Torregosa-Muñumer et al., 2015). There is also no evidence of a compensatory increase in mtDNA replication in the BrdU experiments, where incorporation in the presence of H_2O_2 is significantly less (Figure 9). qPCR copy number can be affected by supercoiling of mtDNA (Chen et al., 2007), and a 15-minute initial denaturing step was implemented to convert the supercoiled into the relaxed forms that are better amplifiable (Zsurka et al., 2023). We cannot exclude the fact that when H_2O_2 is applied the mtDNA is damaged and becomes more accessible to primers and the polymerase in the qPCR. Due to these factors, it is most likely that the increase in copy number seen 30 minutes after H_2O_2 is a result of qPCR experimental conditions and not related to an increased amount of mtDNA molecules. mtDNA copy number can potentially be used as a biomarker for disease. Alterations in mtDNA copy number are associated with chronic inflammation and immune disfunction, and oxidative stress is a known source of this chronic inflammation (Castellani et al., 2020). However, there is still considerable variability in mtDNA copy number and more work needs to be done to have a reliable baseline from which changes in copy number can be a reliable diagnostic tool for disease.

4.1.5 H_2O_2 application results in mtDNA SSBs and DSBs

It has long been known that oxidative damage is particularly relevant in mitochondria, Yakes and Van Houten (1997) found that oxidative lesions within mtDNA persist longer than in nuclear DNA. 1 mM H_2O_2 may be outside the range of physiological conditions, as Hyslop et al. (1995) measured in vivo brain concentrations of ~150 µM H_2O_2 from respiratory chain generated superoxide produced in ischemia-reperfusion. However, under conditions such as when plasma membrane NADPH oxidases in microglia or invading immune cells are activated, considerably higher local concentrations of H_2O_2 can be expected in vivo (Claude et al., 2013; Simpson and Oliver, 2020), therefore the 1 mM used in this study is physiologically relevant. Some experiments were also performed at 0.5 mM (Trombly et al., 2023), but 1 mM was selected to observe a strong effect of the applied oxidative stress. Ransy et al. (2020) asserts that the use of high concentrations of H_2O_2 may be justified to increase the frequency of oxidative damage while not altering the molecular mechanism of their generation. H_2O_2 can induce damage to mtDNA that includes strand breaks and abasic sites, and to a lesser extent mutagenic base modifications (Shokolenko et al., 2009). H_2O_2 has been confirmed to generate DSBs and SSBs and has

been proposed as a mutagen in thyroid cells (Driessens et al., 2009). When observing control cells, mtDNA in its native conformation is in the supercoiled form (Menger et al., 2021). After the acute application of 1 mM H_2O_2 there is an increase in both SSBs and DSBs as the mtDNA is oxidatively damaged (Figure 8, Figure 12), which can be seen in the significant decrease in the intact supercoiled species with a corresponding increase in the open circle and linear including smaller linear fragments of different sizes (Figure 7). The initial hydroxyl radical attack damages the sugar backbone of mtDNA (Dizdaroglu and Jaruga, 2012) generating a SSB, but prolonged presence of the hydroxyl radical causes SSBs to be further damaged into DSBs which leads to degradation (Trombly et al., 2023). Due to the 1 mM concentration used in this study, there is a higher incidence of lesions to the sugar-phosphate backbone of mtDNA which resulted in DSBs. This confirms previous assertions that the oxidative damage from H_2O_2 is more often a result of direct damage to the DNA backbone, rather than nucleotide base mutagenesis or DNA polymerase incurporation errors (Degtyareva et al., 2019), although base modifications cannot be excluded.

4.2 mtDNA recovery after oxidative damage

Beginning 2 hours after H_2O_2 is applied, the relative amount of damaged mtDNA species decreases and the supercoiled species starts to recover, reaching maximum recovery in the time course after 24-hours. The recovery of the supercoiled mtDNA is considerable and approaches but does not reach the level of supercoiled mtDNA before the applied H_2O_2 (Figure 7), presumably due to degradation of linear mtDNA species that result from DSBs (Peeva et al., 2018). mtDNA is recovered via the repair of SSBs in the short term (2 to 6 hours), and the compensatory replication of new mtDNA molecules from intact mtDNA over a longer time frame (24 hours).

4.2.1 *De novo* mtDNA synthesis is not responsible for the fast supercoiled recovery

BrdU incorporation was utilized to provide insight into the recovery kinetics after the applied H_2O_2. Under normal conditions, BrdU is gradually incorporated into the mitochondrial genome via replication to produce new mtDNA molecules corresponding with cell division with a sustained mtDNA copy number as well as with normal mtDNA turnover. Significantly less BrdU incorporates into mtDNA after H_2O_2 application due to the oxidative damage that results (Figure 9). The presence of SSBs and oxidative base modifications interfere with mtDNA replication (Stojkovič et al., 2016) and these must be repaired before replication can occur. Concurrently, when DSBs are generated the mtDNA is degraded

which leads to less available template DNA. It is also possible that the insult of H_2O_2 results in a transient arrest of cell division, which would lead to a reduction in mtDNA replication. Likewise, in the pulse/chase experiments the removal of BrdU labelled mtDNA in the presence of H_2O_2 is higher than in its absence, confirming that mtDNA degradation results from the applied H_2O_2 (Figure 10). The BrdU data suggest that the fast recovery of supercoiled mtDNA seen in the Southern blotting after 2–6 hours is not from *de novo* mtDNA replication, but rather from the repair of SSBs. This fast recovery cannot be explained by *de novo* replication because BrdU incorporation is not significantly increased in the presence of H_2O_2, and mtDNA replication after H_2O_2 is likely delayed due to lower amounts of available intact template mtDNA that must undergo repair before being available for replication (Trombly et al., 2023). With the applied H_2O_2, BrdU is preferentially incorporated in the open circle mtDNA confirmation (Figure 9A), with the supercoiled fraction not appearing until 24 hours after oxidative stress, further confirming that the fast recovery of supercoiled mtDNA seen in normal Southern blots is from repair. Over a longer time period, *de novo* replication likely plays a larger role in the recovery of mtDNA, and it has been proposed that mtDNA replication is upregulated as a compensatory mechanism to cope with oxidative damage (Wiehe et al., 2018). Interestingly, in many Southern blots across many different experiments there can be seen an apparent decrease in the supercoiled fraction and a relative increase in the open circle form of mtDNA 6 hours after H_2O_2 application. The change in conformation could be the from mtDNA being opened to undergo replication to repopulate mtDNA numbers. This would support the idea of repair being a relatively fast process and the main mechanism for the fast recovery seen in control cells, as SSBs must be repaired before replication can occur.

4.2.2 BER of SSBs

It can be seen from the BrdU incorporation data that the fast recovery of supercoiled mtDNA seen in the control cells 2–6 hours after our H_2O_2 pulse is not from *de novo* mtDNA replication, and therefore can be attributed to the repair of SSBs. BER is the main repair pathway of mtDNA after oxidative damage (Alencar et al., 2019), particularly of oxidized bases and SSBs. This pathway in mitochondria involves certain glycosylases, APEX1, POLG, LIG3, and in LP-BER EXOG. The generation of CRISPR/Cas9 knock-out cell lines allow for the investigation of the function of these proteins in the recovery of mtDNA after a pulse of H_2O_2. The impaired recovery of the supercoiled mtDNA species in APEX1$^{-/-}$ and

LIG3$^{-/-}$ cell lines demonstrates the importance of SSB repair and replication to repopulate intact mtDNA after H_2O_2 application.

4.2.2.1 APEX1 is a crucial for the fast repair of oxidative lesions

Izumi et al. (2005) discussed the difficulties of generating a APEX1 knock-out, however we were able to successfully produce APEX1$^{-/-}$ HEK293 cell lines by using pyruvate and uridine in the cell culture medium and by knocking out the lys299 and arg301 residues in the C-terminus crucial for mitochondrial targeting (Li et al., 2010), potentially preserving the AP-endodeoxyribonuclease activity and only altering mitochondrial import. APEX1 is a vital step in BER and in the APEX1$^{-/-}$ cells the open circle mtDNA is the most abundant species before H_2O_2 treatment due to the persistence of SSBs and abasic sites. The open circle species increase and persist after the applied oxidative stress, as well as the recovery of the supercoiled mtDNA is delayed (Figure 25). APEX1 mediated SSB repair is necessary for the supercoiled mtDNA recovery that is observed in the control cells, and there is also evidence that abasic sites and other oxidative lesions impair mtDNA replication (Stojkovič et al., 2016) which would also inhibit supercoiled recovery. APEX1$^{-/-}$ cells have a slightly elevated mtDNA copy number than control at the 0-hour, this increase in copy number could a compensatory mechanism for persistent abasic sites that impede normal replication, but this difference can potentially be attributed to the strong presence of the open circle conformation which is better able to be amplified by qPCR. The mtDNA copy number in APEX1$^{-/-}$ lines also has a tendency to decrease 24-hours after H_2O_2, which could be a result of the degradation of DSBs and the inability to repair SSBs that impedes mtDNA repopulation. SSB repair involving APEX1 is therefore necessary for the recovery of supercoiled mtDNA after oxidative damage from a H_2O_2 pulse.

4.2.2.2 POLG exonuclease function is not involved in SSB repair

The POLGexo$^{-/-}$ cell line inhibits degradation of mtDNA (Peeva et al., 2018) but does not appear to inhibit repair of SSB generated by H_2O_2 oxidative damage as evidence by the deep sequencing data (Figure 19), but this needs to be further investigated. Detection of SSBs is difficult in POLGexo$^{-/-}$ cells due to the large amount of persistent linear species that exist in this cell line. There is likely no effect in the repair of SSBs because only the exonuclease function has been eliminated, while the polymerase and lyase activities remain intact. The loss of the exonuclease function of POLG is known to result in replication errors that leads to nicks, DSBs, and linear mtDNA (Nissanka et al., 2018). It is

possible that another polymerase such as POLβ supports short patch BER within mitochondria due to its similar polymerase and dRP-lyase activities (Alencar et al., 2019), and could compensate for our mutant POLG in this cell line.

4.2.2.3 EXOG LP-BER is not involved in mtDNA recovery

mtDNA in EXOG$^{-/-}$ cells behaved similar to the control cells with the application of H_2O_2, but with an increase in linear fragments of different sizes in the EXOG$^{-/-}{}_a$ cell line (Figure 26). Previous studies have asserted that a diminished presence of EXOG results increased persistent SSBs in mtDNA (Tann et al., 2011; Nadalutti et al., 2022), therefore making DSBs that produce the smear of linear species more likely to form. These linear species are rapidly degraded, and the less severe forms of mtDNA oxidative damage can be repaired by short-patch BER where EXOG is not involved (Figure 4). Interestingly, EXOG$^{-/-}{}_a$ shows a significant decrease in mtDNA copy number 24 hours after H_2O_2, which is not observed in EXOG$^{-/-}{}_b$ (Figure 16). This could be from more persistent SSBs being present in the EXOG$^{-/-}{}_a$ line, which results in more DSBs from the H_2O_2 application with a greater proportion of mtDNA being degraded as linear mtDNA and therefore the recovery is diminished relative to the control cells. The lack of involvement of EXOG$^{-/-}$ raises the possibility that only short-patch BER is involved in the repair of oxidative damage after H_2O_2 (Alencar et al., 2019), or the involvement of another exonuclease in long-patch BER (Tann et al., 2011). EXOG$^{-/-}$ cells not being significantly affected by oxidative damage as well as in the basal condition also seems to contradict previous work that asserted EXOG is important for mtDNA integrity (Szymanski et al., 2017), however more work needs to be done in order to support this assertion and elucidate the reason behind the differences between the two EXOG$^{-/-}$ lines.

4.2.2.4 LIG3 is necessary to maintain mtDNA after oxidative damage

Shokolenko et al. (2013) generated LIG3 knock-out in mice embryonic fibroblasts and found the cells to be depleted of mtDNA and auxotrophic for uridine and pyruvate, which could explain why previous attempts at LIG3 knock-outs were lethal (Simsek and Jansin, 2011). LIG3$^{-/-}$ lines were successfully generated in our high glucose medium that is supplemented for uridine and pyruvate. Interestingly, our LIG3$^{-/-}$ cell lines do not result in a ρ^0 mtDNA status during basal growth (Figure 16), despite the vital role that LIG3 plays in the final steps of both replication and repair. This leaves open the possibility of another DNA ligase facilitating ligation in mitochondria in the absence of LIG3, such as LIG1 (Simsek

et al., 2011), or this could be a characteristic specific to HEK293 cells. Comparable to what Shokolenko et al. (2013) found in cells with a knock-down of LIG3, our LIG3$^{-/-}$ cells maintained their mtDNA copy number before oxidative stress (Figure 16D and G) and have increased mtDNA degradation and slow recovery from mtDNA depletion. After H_2O_2 is applied, all mtDNA species deplete in the LIG3$^{-/-}$ cell lines with very limited supercoiled mtDNA recovery and the open circle remaining as the most prominent species after 24 hours (Figure 27). It is interesting to note that LIG3$^{-/-}{}_a$ appears to undergo more damage with the application of H_2O_2 compared to LIG3$^{-/-}{}_b$. The heterogenous and unstable karyotype of HEK293 cells can potentially explain the differences between the two LIG3$^{-/-}$ clones, similar to the differences seen in the EXOG$^{-/-}$ clones (Stepanenko and Dmitrenko, 2015), with LIG3$^{-/-}{}_b$ possibly having the upregulation of a pathway that causes this cell line more resistant to the applied H_2O_2. In the LIG3$^{-/-}$ cells, linear mtDNA generated by DSBs is degraded while SSBs cannot be ligated therefore the open circle species remains and the persistent damage impairs replication. The SSBs that are unable to be repaired due to the lack of LIG3 are transformed to DSBs by a second hit or replication errors which leads to degradation and drastic depletion in these cell lines. Pre-existing SSBs cause LIG3$^{-/-}$ cells to be more vulnerable to oxidative damage and which leads to a severe lack of template mtDNA for replication to repopulate mtDNA numbers. The H_2O_2-induced depletion of mtDNA in LIG3$^{-/-}$ cells supports the idea that the amount of LIG3 within mitochondria is indicative of and critical for cell survival after prolonged oxidative stress (Akbari et al., 2016), as the loss of mtDNA integrity when repair or replication are unable to be ligated to intact mtDNA molecules drives diminished mitochondrial function (Nadalutti et al., 2022). Therefore, LIG3 is crucial for the recovery of mtDNA after H_2O_2 oxidative damage, and its absence is likely inhibiting both repair as well as *de novo* replication to replenish numbers after degradation.

4.3 Linear mtDNA degradation after DSB

Degradation of linear mtDNA after DSBs has been implicated as a protective mechanism to reduce mutagenesis, rather than investing in the energy cost of repair (Zhao, 2019) which can be error prone and result in deletions in mtDNA. mtDNA has been shown to be rapidly degraded after direct strand damage from oxidative stress, as well as when there is an overwhelming amount of oxidative lesions or BER is inhibited (Shokolenko et al., 2009; Shokolenko et al., 2013; Furda et al., 2012). Furda et al. (2012) observed mtDNA

loss and persistent mtDNA lesions in mouse embryonic fibroblasts upon H_2O_2 treatment, however we do not see this mtDNA loss or ρ^0 status in our cells with 1 mM H_2O_2. We likely do not have mtDNA loss because (i) our treatment is at transient pulse, (ii) our cells are grown in supported medium, and (iii) the different properties of HEK293 cells compared to fibroblasts.

4.3.1 ENDOG is not necessary for degradation after oxidative damage

The mtDNA in ENDOG$^{-/-}$ cells does not significantly differ from the control cells with the application of H_2O_2, however there is a calculated significant decrease in linear fragments that appear in the short term (Figure 24). Wiehe et al. (2018) found that ENDOG levels increased upon oxidative damage as a compensatory mechanism because ENDOG cleaves mtDNA after oxidative damage and is involved in replication stimulation. This would help generate linear mtDNA for degradation and removal after oxidative damage and supports the observation that less linear fragments of different sizes are produced in the ENDOG$^{-/-}$ cells. It is possible that the strong 1 mM H_2O_2 pulse produced a large amount of DSBs that rendered cutting by ENDOG unnecessary. Because the recovery of mtDNA was not diminished because of the decrease in linear fragments after H_2O_2 oxidative stress, it was determined that ENDOG does not play a major role in the degradation of mtDNA after H_2O_2 induced oxidative damage.

4.3.2 Impaired degradation in MGME1$^{-/-}$ and POLGexo$^{-/-}$ inhibits recovery of supercoiled mtDNA

When observing oxidative damage, the MGME1$^{-/-}$ and the POLGexo$^{-/-}$ cell lines provide the unique opportunity to detect what happens to mtDNA after H_2O_2 when degradation is impaired (Peeva et al., 2018). In MGME1$^{-/-}$ and POLGexo$^{-/-}$ cell lines the open circle is the most prominent species before any oxidative stress is applied. Both of these proteins are involved in mtDNA replication which when unable to be completed could result in more open circle species, or the prevalence of open circle could imply involvement in some form of SSB repair. After H_2O_2, the supercoiled diminishes and full-length linear as well as a smear of linear fragments of different sizes increase, which persist throughout the time course (Figure 17). Most strikingly, there is impaired recovery of the supercoiled species in these cell lines (Figure 17B) that results from the persistence of oxidative damaged mtDNA molecules that normally would be degraded (Figure 18). Without degradation, the linear mtDNA is a nucleotide trap within mitochondria resulting in less available nucleo-

tides for replication, which can also negatively impact nuclear DNA (Hämäläinen et al., 2019). The MGME1$^{-/-}$ cells show persistence of the open circle form of mtDNA, potentially due to the involvement the protein is known to have in the maintenance of the D-loop, as well as the regulation of mtDNA replication and transcription termination (Urrutia et al., 2022) due to its end processing activities (Uhler et al., 2016), the absence of which would lead to the accumulation of non-ligatable breaks or flaps in mtDNA and not allow for super-coiling.

In the BrdU incorporation experiments, POLGexo$^{-/-}$ incorporates less BrdU than control cells likely because of the decrease in cell division that was observed in this knock-out line. The lack of POLG proof-reading activity in this cell line leads to an increase in mtDNA mutations that could impair replication and contribute to less energy production and slower cell divisions. Significantly less BrdU is incorporated into the POLGexo$^{-/-}$ cells in the presence of H_2O_2 compared to the control, and there is also a trend of decreased incorporation in MGME1$^{-/-}$ (Figure 20). This decreased incorporation likely results from persistent damaged template mtDNA and a lack of nucleotides which remain sequestered into linear molecules. Interestingly, there is also a strong nuclear DNA smear of BrdU incorporation after 24 hours in the presence of H_2O_2 in the degradation impaired cell lines, indicating that there is more free BrdU available within the cell that is able to be incorporated into the nuclear DNA.

Ultra-deep sequencing confirms the increase of DSBs upon the application of H_2O_2 which persist in the degradation impaired cell lines (Figure 19). The POLGexo$^{-/-}$ cell line has orders of magnitude more DSBs before H_2O_2 treatment, which has also been found by Trifunovic et al. (2004) and Hämäläinen et al. (2019), and leads to technical problems to detect comparable changes in this cell line. There is no significant difference in the SSB pattern between control and the degradation impaired cell lines, therefore the loss of MGME1 and POLGexo function does not appear to affect the repair of SSBs that are generated by H_2O_2. A limitation of SSB determination by ultra-deep sequencing is the nature of the S1 nuclease treatment. Because of this some involvement of POLGexo in SSB repair cannot be completely excluded, and MGME1 could also play some in repair due to the persistent open-circle mtDNA observed in the MGME1$^{-/-}$ cells.

4.3.3 Pattern of degradation stalling locations at detected ends

4.3.3.1 Frequent ends correspond to the OriH, OriL, and mTER

A small drawback to the Southern blot visualization of mtDNA damage is that the linear 11 kb fragment, spanning the major arc of mtDNA from the OriH to the OriL, is likely to run to the same point in the blot as the supercoiled mtDNA. However, in vitro digested mtDNA allows for better elucidation of these fragments. In the *SnaB*I digested BrdU pulse/ chase experiments we can visualize increased degradation via linear fragments that occurs with the application of H_2O_2 in control cells, with frequent ends being located at the OriH, OriL, and mTER locations in mtDNA as degradation intermediates (Figure 21; Peeva et al., 2018). Because the antibody labels all mtDNA that has incorporated BrdU, the end locations are estimated based on size relative to the digestion site but can occur in either direction. These frequent degradation-typical ends appear in the control cells 30 minutes after H_2O_2 and disappear after 24 hours, while they are always present in the degradation impaired cell lines, and the same pattern was found by deep sequencing (Figure 22). Deep sequencing was also able to confirm the locations of the ends in mtDNA as the OriH, OriL, and mTER. The ends around the OriH can partially be explained by the fact that the NCR and D-loop region are known hot spots of oxidative damage accumulation within mtDNA (Rothfuss et al., 2010). The fact that the ends at these locations are always present regardless of oxidative stress treatment in the MGME1$^{-/-}$ cells supports the knowledge that this line contains persistent 11 kb fragments (Nicholls et al., 2014).

4.3.3.2 Minor sites of oxidative damage show a pattern of GC-stretches

When looking at the nucleotide bases present at minor ends, a pattern of GC-stretches at the ends of the sequenced mtDNA fragments appears in control cells 30-minutes after H_2O_2 that is not present before treatment or 24 hours after the applied H_2O_2 (Figure 23A). The GC-pattern at ends of control mtDNA fragments with transient oxidative damage as well as the location of prominent ends is very similar to that of degrading mass mito*Eag*I-linearized mtDNA previously discovered by our lab (Peeva et al., 2018). The fact that the pattern is no longer present 24-hours after H_2O_2 indicates completed degradation of linear mtDNA generated by the applied H_2O_2. In the MGME1$^{-/-}$ cells where degradation is absent there is a less prominent degradation specific base pattern present, which is indicative of a second line of slow degradation with similar stalling sites in Illumina sequencing (Figure 23B). POLGexo$^{-/-}$ cells have ends at GC-stretches regardless of H_2O_2 application (Figure

23C). In all cell lines, ends associated with GC-stretches are likely the result of degradation stalling due to the formation of G-quadruplexes. These G-quadruplexes structures are known to stall the mitochondrial replisome (Doimo et al., 2023), and these components of the replication machinery are also involved in mtDNA degradation (Peeva et al., 2018). This would explain why the same pattern is found in the control cells after acute H_2O_2 and persistently in the POLGexo$^{-/-}$ line that has limited rapid mtDNA degradation over short distances. In the POLGexo$^{-/-}$ line, degradation proceeds minimally and is stalled by these GC-stretches, while the control with fully functional degradation machinery briefly stalls at these locations but can bypass them and complete degradation (Trombly et al., 2023). Nissanka et al. (2018) also found some limited degradation in their POLG-exonuclease deficient yeast cells when observing deletion breakpoints, although they suggest that another nuclease would be responsible for this activity.

4.3.4 Impact of DSBs on mtDNA

Because the recovery of supercoiled mtDNA is impaired in the degradation impaired cell lines, it can be determined that degradation of linear mtDNA species is a necessary step for the recovery of intact mtDNA after H_2O_2 oxidative damage. The persistence of linear species likely prevents the replication of mtDNA that restores intact molecules in control cells, and the presence of linear mtDNA increases the likelihood of deletion generation and recombinant forms of mtDNA that are harmful (Fragkoulis et al., 2024). DSBs are not only produced via direct H_2O_2 oxidative damage; replication stalling at areas of template damage or natural replication stalling sites leads to replication fork regression and DSBs within mtDNA (Torregosa-Muñumer et al., 2019; Doimo et al., 2023). These are most often found in the major arc of the H-strand, due to the presence of repeats within mtDNA and the formation of G-quadruplex structures (Fontana and Gahlon, 2020). Damaging mtDNA rearrangements and deletions can occur if degradation is not able to cope with the number of linear fragments produced via this double insult of DSBs via H_2O_2 damage and replication stalling. As asserted in Trombly et al. (2023), this could explain the formation of mtDNA deletions in pathological brain tissue with chronic inflammation (Volmering et al., 2016), because invading immune cells or microglia have been shown to be a strong source of H_2O_2 (Simpson and Oliver, 2020). An abundance of DSBs contributing to a large amount of mtDNA degradation can also lead to mtDNA depletion syndromes and can also lead to activation innate immune response triggered by fragmented mtDNA (Zhao, 2019).

4.5 The fate of mtDNA after H_2O_2 oxidative stress

When mtDNA is exposed to H_2O_2, oxidative stress is induced through the production of the hydroxyl radical via the Fenton reaction in the mitochondrial matrix (Henle et al., 1999), regardless of the H_2O_2 is produced from intrinsic processes or is from an external source. Figure 35 depicts a proposed scheme of what occurs to the mtDNA after this attack from the hydroxyl radical, as elucidated from the research in this thesis. The hydroxyl radical causes not only base modifications in mtDNA, but more often physical damage resulting in single-strand and later double-strand breaks. Control HEK293 cells survive the H_2O_2 pulse and recover their mtDNA in a period of hours. When SSBs occur, these are rapidly repaired by a BER pathway that utilizes POLG, APEX1, and LIG3 (Alencar et al., 2019). SSB repair is responsible for the fast recovery of mtDNA seen in the control; increased replication is not responsible for this recovery because BrdU incorporation indicating *de novo* mtDNA was not increased in the presence of H_2O_2 (Trombly et al., 2023). Impaired recovery of the supercoiled mtDNA species in APEX1$^{-/-}$ and LIG3$^{-/-}$ cell lines demonstrates the importance of BER of SSBs and subsequent replication to repopulate intact mtDNA. When DSBs occur, the linear mtDNA is rapidly degraded via the MGME1 and POLG degradation pathway to prevent the formation of harmful mtDNA deletion rearrangements (Peeva et al., 2018; Nissanka et al., 2018). mtDNA degradation of linear mtDNA is a fast process, in Nissanka et al. (2019) linear intermediates were only seen for 2 hours after DSB induction, which is similar to the presence of the major ends observed in control cells that appear after the H_2O_2 pulse. Efficient degradation and the clearance of damaged mtDNA is necessary for the recovery of mtDNA after oxidative damage (Trombly et al., 2023), as damage in the MGME1$^{-/-}$ and POLGexo$^{-/-}$ cells persists and impairs supercoiled mtDNA recovery. Persistent linear mtDNA can lead to a depleted nucleotide pool which inhibits both mtDNA and nuclear replication (Hämäläinen et al., 2019), as well as linear mtDNA released into the cytosol of the cell can trigger an inflammatory response (Tigano et al., 2021). This confirms previous claims by Shokolenko et al. (2009) that moderate oxidative damage is repaired by BER and more pronounced damage intermediates are degraded. APEX1 and MGME1 were both found to be upregulated in conditions of oxidative stress (Goffart et al., 2021), indicating the important role that both repair and removal of damaged mtDNA have after oxidative damage. Taken together, the results of this thesis have helped to elucidate the type of mtDNA damage that results from H_2O_2,

and the interplay of repair, degradation, and *de novo* synthesis of mtDNA in the recovery of intact mtDNA species.

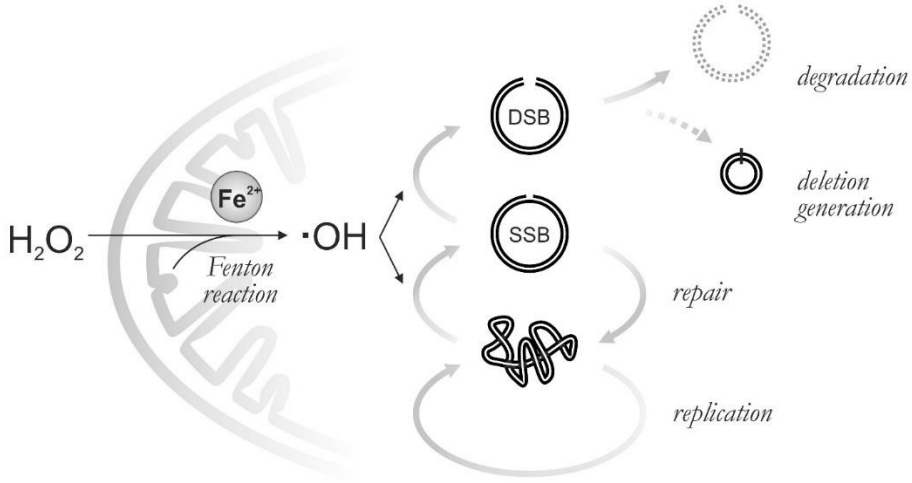

Fig. 33: Scheme of what occurs to mtDNA after exposure to H_2O_2. Taken from Trombly et al. (2023). H_2O_2 from both external and internal sources reacts with free iron within mitochondria to form the harmful hydroxyl radical (•OH) via the Fenton reaction. This hydroxyl radical attacks intact supercoiled mtDNA which forms SSBs. The SSBs are then either repaired or receive another attack from the hydroxyl radical forming DSBs, which can also be formed due to replication stalling at the SSB location. Once a DSB is formed, linear mtDNA is rapidly degraded to prevent the formation of harmful mtDNA depletions and to reutilize nucleotides.

5. Abstract

Mitochondria are vital within eukaryotic cells and the maintenance of mitochondrial DNA (mtDNA) is therefore crucial to maintain mitochondria function. mtDNA has been shown to be particularly vulnerable to oxidative damage due to its proximity to reactive oxygen species (ROS) generated by oxidative phosphorylation (OXPHOS) and the electron transport chain in generating energy for cells in the form in ATP (Alencar et al., 2019). The hydroxyl radical produced via the Fenton reaction with free iron in the mitochondrial matrix has been shown to generate oxidative damage in mtDNA (Petrat et al., 2002). Utilizing Southern blotting and ultra-deep sequencing, this thesis aims to determine a paradigm for the damage that occurs to mtDNA after a transient H_2O_2 pulse, and then to elucidate when this damage is repaired versus when these damaged molecules are degraded and mtDNA is repopulated by replication with intact species, and what proteins are involved in this process. CRISPR/Cas9 technology was employed to generate knock-out HEK293 cell lines of genes known to be involved in the maintenance of mtDNA: MGME1 and POLGexo known to degrade linear mtDNA (Peeva et al., 2018), and APEX1, POLG, EXOG, and LIG3 known to be involved in base excision repair (BER) (Alencar et al., 2019). The strong 1 mM H_2O_2 pulse results in sugar-backbone damage in the form of single-strand breaks (SSBs) and double-strand breaks (DSBs) in mtDNA, which are eliminated in the control cells that have recovery of the native supercoiled mtDNA species within a period of hours. SSB repair is responsible for the fast recovery of mtDNA seen in the control; increased replication is not responsible for this recovery because BrdU incorporation indicating *de novo* mtDNA was not increased in the presence of H_2O_2 (Trombly et al., 2023). Impaired recovery of supercoiled mtDNA in APEX1$^{-/-}$ and LIG3$^{-/-}$ demonstrates the importance of SSB repair and subsequent replication to repopulate intact mtDNA. Additionally, efficient degradation and the clearance of damaged templates is also necessary for the recovery of mtDNA after H_2O_2 oxidative damage (Trombly et al., 2023), as damage in MGME1$^{-/-}$ and POLGexo$^{-/-}$ cells persists and impairs supercoiled mtDNA recovery. Taken together, the results of this thesis have helped to elucidate the type of mtDNA damage that results from H_2O_2, with repair responsible for mtDNA recovery in the short time scale and degradation with *de novo* synthesis of mtDNA also playing an important role for the recovery of intact mtDNA species.

6. List of figures

7. List of tables

8. References

Aaij C, Borst P. The gel electrophoresis of DNA. Biochem Biophys Acta 1972; 269: 192-200.

Adant I, Bird M, Decru B, Windmolders P, Wallays M, de Witte P, Rymen D, Witters P, Vermeersch P, Cassiman D, Ghesquière B. Pyruvate and uridine rescue the metabolic profile of OXPHOS dysfunction. Mol Metab 2022; 63: 101537.

Akbari M, Keijzers G, Maynard S, Scheibye-Knudsen M, Desler C, Hickson ID, Vilhelm AB. Overexpression of DNA ligase III in mitochondria protects cells against oxidative stress and improves mtDNA base excision repair. DNA Repair 2014; 16: 44-53.

Alencar RR, Batalha CMPF, Freire TS, de Souza-Pinto NC. Chapter Eight – Enzymology of mitochondrial DNA repair. The Enzymes 2019; 45: 257-287.

Allkanjari K, Baldock RA. Beyond base excision repair: an evolving picture of mitochondrial DNA repair. Bioscience Reports 2021; 41: 10.

Alexeyev MF. Is there more to aging than mitochondrial DNA and reactive oxygen species? FEBS Journal 2009; 276: 5768-5787.

Anderson S, Bankier AT, Barrell BG, de Bruijn MHL, Coulson AR, Drouin J, Eperon IC, Nierlich DP, Roe BA, Sanger F, Schreier PH, Smith AJH, Staden R, Young IG. Sequence and organization of the human mitochondrial genome. Nature 1981; 290: 457–465.

Ballista-Hernández J, Martínez-Ferrer M, Velez R, Climent C, Sanchez-Vazquez M, Torres C, Rodríguez-Muñoz A, Ayala-Peña S, Torres-Ramos CA. Mitochondrial DNA integrity is maintained by APE1 in carcinogen-induced colorectal cancer. Mol Cancer Res 2017; 15: 831-841.

Baumstark-Khan C. Effects of aphidicolin on cell recovery and repair of DNA damage in irradiated human fibroblasts. Strahlenther Onkol 1991; 167: 726-732.

Bender A, Krishnan KJ, Morris CM, Taylor GA, Reeve AK, Perry RH, Jaros E, Hersheson JS, Betts J, Klopstock T, et al. High levels of mitochondrial DNA deletions in substantia nigra neurons in aging and Parkinson disease. Nat Genet 2006; 38: 515–517.

Bohr VA. Repair of oxidative DNA damage in nuclear and mitochondrial DNA, and some changes with aging in mammalian cells. Free Radic Biol Med 2002; 32:804–812.

Brown TA, Cecconi C, Tkachuk AN, Bustamante C, Clayton DA. Replication of mitochondrial DNA occurs by strand displacement with alternative light-strand origins, not via a strand-coupled mechanism. Genes and Development 2005; 19: 2466-2476.

Cadenas E. Biochemistry of oxygen toxicity. Annual Review of Biochem 1989; 58: 79-110.

Castellani CA, Longchamps RJ, Sun J, Guallar E, Arking DE. Thinking outside the nucleus: Mitochondrial DNA copy number in health and disease. Mitochondrion 2020; 53: 214-223.

Chaudhry MA, Weinfeld M. Induction of double-strand breaks by S1 nuclease, mung bean nuclease, and nuclease P1 in DNA containing abasic sites and nicks. Nucleic Acids Research 1995; 23: 3805-3809.

Chen J, Kadlubar FF, Chen JZ. DNA supercoiled suppresses real-time PCR: a new approach to the quantification of mitochondrial DNA damage and repair. Nucleic Acids Research 2007; 35: 1377-1388.

Claude J, Linnartz-Gerlach B, Kudin AP, Kunz WS, Neumann H. Microglial CD33-related Siglec-E inhibits neurotoxicity by preventing the phagocytosis-associated oxidative burst. J Neurosci 2013; 33: 18270-18276.

Clayton DA. Replication of animal mitochondrial DNA. Cell 1982; 28: 693-705.

Copeland WC, Kasiviswanathan R, Longley MG. Analysis of translesion DNA synthesis by the mitochondrial DNA polymerase γ. Methods Molecular Biology 2016; 1351: 19-26.

Cymerman IA, Chung I, Beckmann BM, Bujnicki JM, Meiss G. EXOG, a novel paralog of Endonuclease G in higher eukaryotes. Nucleic Acids Research 2008; 26: 1369-1379.

Davis AF, Clayton DA. In Situ Localization of Mitochondrial DNA Replication in Intact Mammalian Cells. J Cell Biol 1996; 135: 883-893.

Degtyareva NP, Saini N, Sterling JF, Placentra VC, Klimczak LJ, Gordenin DA, Doetsch PW. Mutational signatures of redox stress in yeast single-strand DNA and of aging in human mitochondrial DNA share a common feature. PLoS Biol 2019; 17: e3000263.

DeLuca SZ, O'Farrell PH. Barriers to male transmission of mitochondrial DNA in sperm development. Dev Cell 2012; 22: 660-668.

Dizdaroglu M, Jaruga P. Mechanisms of free radical-induced damage to DNA. Free Radical Research 2012; 46: 382-419.

Doimo M, Chaudhari N, Abrahamsson S, L'Hôte V, Nguyen TVH, Berner A, Ndi M, Abrahamsson A, Nath Das R, Aasumets K, Goffart S, Pohjoismäki JLO, López MD, Chorell E, Wanrooij S. Enhanced mitochondrial G-quadruplex formation impedes replication fork progression leading to mtDNA loss in human cells. Nucleic Acids Research 2023; 51: 7392-7408.

Driessens N, Versteyhe S, Ghaddhab C, Burniat A, De Deken X, Van Sande J, Dumont J, Miot F, Corvilain B. Hydrogen peroxide induces DNA single- and double-strand breaks in thyroid cells and is therefore a potential mutagen for this organ. Endocrine-Related Cancer 2009; 16: 845-856.

Dröge W. Free radicals in the physiological control of cell function. Physiol Rev 2002; 82:47-95.

Ellenberger T, Tomkinson AE. Eukaryotic DNA ligases: structural and functional insights. Annu Rev Biochem 2008; 77: 313-338.

Falkenberg M, Gustafsson CM. Mammalian mitochondrial DNA replication and mechanisms of deletion formation. Crit Rev Biochem Mol Biol 2020; 55: 509-524.

Fontana GA, Gahlon HL. Mechanisms of replication and repair in mitochondrial DNA deletion formation. Nucleic Acids Research 2020; 48: 11244-11258.

Fragkoulis G, Hangas A, Fekete Z, Michell C, Moraes CT, Willcox S, Griffith JD, Goffart S, Pohjoismäki JLO. Linear DNA-driven recombination in mammalian mitochondria. Nucleic Acids Research 2024; gkae040.

Fransen M, Nordgren N, Wang B, Apanasets O. Role of peroxisomes in ROS/RNS-metabolism: Implications for human disease. Biochimica et Biophysica Acta 2012; 1822: 1363-1373.

Freudenthal BD, Beard WA, Perera L, Shock DD, Kim T, Schlick T, Wilson SH. Uncovering the polymerase induced cytotoxicity of an oxidized nucleotide. Nature 2015; 517: 635-639.

Fu Y, Tigano M, Sfier A. Safeguarding mitochondrial genomes in higher eukaryotes. Nature Structural and Molecular Biology 2020; 27: 687-695.

Furda AM, Marrangoni AM, Lokshin A, Van Houten B. Oxidants and not alkylating agents induce rapid mtDNA loss and mitochondrial dysfunction. DNA Repair 2012; 11: 684-692.

Genoud S, Roberts BR, Gunn AP, Halliday GM, Lewis SJG, Ball HJ, Hare DJ, Double KL. Subcellular compartmentalization of copper, iron, manganese, and zinc in the Parkinson's disease brain. Metallomics 2017; 9: 1447–1455.

Goffart S, Tikkanen P, Michell C, Wilson T, Pohjoismäki J. The Type and Source of Reactive Oxygen Species Influences the Outcome of Oxidative Stress in Cultured Cells. Cells 2021: 10, 1075.

Gorman GS, Schaefer AM, Ng Y, Gomez N, Blakely EL, Alston CL, Feeney C, Horvath R, Yu-Wai-Man P, Chinnery PF, Taylor RW, Turnbull DM, McFarland R. Prevalence of nuclear and mitochondrial DNA mutations related to adult mitochondrial disease. Ann Neurol 2015; 77: 753-759.

Graziewicz MA, Longley MJ, Copeland WC. DNA polymerase gamma in mitochondrial DNA replication and repair. Chem Rev 2006; 106: 383-405.

Grishko VI, Rachek LI, Spitz DR, Wilson GL, LeDoux SP. Contribution of Mitochondrial DNA Repair to Cell Resistance from Oxidative Stress. J Biol Chem 2005; 280: 8901-8905.

Guarino VA, Oldham WM, Loscalzo J, Zhang Y. Reaction rate of pyruvate and hydrogen peroxide: assessing antioxidant capacity of pyruvate under biological conditions. Nature Scientific Reports 2019; 9:19568.

Hämäläinen RH, Landoni JC, Ahlqvist KJ, Goffart S, Ryytty S, Rahman MO, Brilhante V, Icay K, Hautaniemi S, Wang L, Laiho M, Suomalainen A. Defects in mtDNA replication challenge nuclear genome stability through nucleotide depletion and provide a unifying mechanism for mouse progerias. Nat Metab. 2019; 1: 958-965.

Hanes JW, Thal DM, Johnson KA. Incorporation and replication of 8-Oxo-deoxyguanosine by the human mitochondrial DNA polymerase. J Biol Chem 2006; 281: 36241–36248.

Henle ES, Han Z, Tang N, Rai P, Luo Y, Linn S. Sequence-specific DNA cleavage by Fe^{2+}-mediated Fenton reactions has possible biological implications. J Biol Chem 1999; 274: 962–971.

Henzler T, Steudle E. Transport and metabolic degradation of hydrogen peroxide in *Chara carallina*: Model calculations and measurements with the pressure probe suggest transport of H_2O_2 across water channels. J Exp Bot 2000; 51: 2053-2066.

Holt IJ, Lorimer HE, Jacobs HT. Coupled leading and lagging-strand synthesis of mammalian mitochondrial DNA. Cell 2000; 100: 515–524.

Houot V, Etienne P, Petitot AS, Barbier S, Blein JP, Suty L. Hydrogen peroxide induces programmed cell death features in cultured tobacco BY-2 cells, in a dose-dependent manner. Journal of Experimental Botany 2001; 52: 1721-1730.

Hussain M, Mohammed A, Saifi S, Khan A, Kaur E, Priya S, Agarwal H, Sengupta S. MITOL-dependent ubiquitylation negatively regulates the entry of PolγA into mitochondria. PLoS Biol 2021; 19: e3001139.

Hyslop PA, Zhang Z, Pearson DV, Phebus LA. Measurement of striatal H_2O_2 by microdialysis following global forebrain ischemia and reperfusion in the rat: correlation with the cytotoxic potential of H_2O_2 in vitro. Brain Res 1995; 671: 181-186.

Itsara LS, Kennedy SR, Fox EJ, Yu S, Hewitt JJ, Sanchez-Contreras M, Cardozo-Pelaez F, Pallanck LJ. Oxidative stress is not a major contributor to somatic mitochondrial DNA mutations. PLoS Genet 2014; 10: e1003974.

Izumi T, Brown DB, Naidu CV, Bhakat KK, Macinnes MA, Saito H, Chen DJ, Mitra S, Setlow RB. Two Essential but Distinct Functions of the Mammalian Abasic Endonuclease. PNAS 2005; 102: 5739-5743.

Kai Y, Takamatsu C, Tokuda K, Okamoto M, Irita K, Takahashi S. Rapid and random turnover of mitochondrial DNA in rat hepatocytes of primary culture. Mitochondrion 2006; 6: 299-304.

Kakhlon O, Manning H, Breuer W, Melamed-Book N, Lu C, Cortopassi G, Munnich A, Cabantchik Z. Cell functions impaired by frataxin deficiency are restored by drug-mediated iron relocation. Blood 2008; 112: 5219-5227.

Kaneko M, Inoue F. The sensitivity to DNA single strand breakage in mitochondria, but not in nuclei, of Chinese hamster V79 and variant cells correlates with their cellular sensitivity to hydrogen peroxide. Toxicol Lett 1998; 99: 15-22.

Karlowicz A, Dubiel AB, Czerwinska J, Bledea A, Purzycki P, Grzelewska M, McAuley RJ, Szczesny RJ, Brzuska G, Krol E, Szczesny B, Szymanski MR. *In vitro* reconstitution reveals a key role of human mitochondrial EXOG in RNA primer processing. Nucleic Acids Research 2022; 50: 7991-8007.

Kennedy SR, Salk JJ, Schmitt MW, Loeb LA. Ultra-sensitive sequencing reveals an age-related increase in somatic mitochondrial mutations that are inconsistent with oxidative damage. PloS Genetics 2013; 9: e1003794.

Kasahara A, Scorrano L. Mitochondria: from cell death executioners to regulators of cell differentiation. Trends Cell Biol 2014; 24: 761-770.

Kolesar JE, Wang CY, Taguchi YV, Chou SH, Kaufman BA. Two-dimensional intact mitochondrial DNA agarose electrophoresis reveals the structural complexity of the mammalian mitochondrial genome. Nucleic Acids Research 2013; 41: e58.

Kornblum C, Nicholls TJ, Haack TB, Schöler S, Peeva V, Danhauser K, Hallmann K, Zsurka G, Rorbach J, Iuso A, Wieland T, Sciacco M, Ronchi D, Comi GP, Moggio M, Quinzii CM, DiMauro S, Calvo SE, Mootha VK, Klopstock T, Strom TM, Meitinger T, Minczuk M, Kunz WS, Prokisch H. Loss-of-function mutations in MGME1 impair mtDNA replication and cause multisystemic mitochondrial disease. Nature Genetics 2013; 45: 214-219.

Kowaltowski AJ, de Souza-Pinto NC, Castilho RF, Vercesi AE. Mitochondria and reactive oxygen species. Free Radic Biol Med 2009; 47: 333-343.

Kudin AP, Bimpong-Buta NY, Vielhaber S, Elger CE, Kunz WS. Characterization of superoxide-producing sites in isolated brain mitochondria. J Biol Chem 2004; 279: 4127-4135.

Kudin AP, Malinska D, Kunz WS. Sites of generation of reactive oxygen species in homogenates of brain tissue determined with the use of respiratory substrates and inhibitors. Biochim Biophys Acta 2008; 1777: 689-695.

Kudin AP, Augustynek B, Lehmann AK, Kovács R, Kunz WS. The contribution of thioredoxin-2 reductase and gluta-thione peroxidase to H(2)O(2) detoxification of rat brain mitochondria. Biochim Biophys Acta 2012; 1817: 1901-1906.

Lakshmipathy U, Campbell C. Antisense-mediated decrease in DNA ligase III expression results in reduced mitochondrial DNA integrity. Nucleic Acids Res 2001; 29: 668-678.

Lakshmipathy U, Campbell C. The human DNA ligase III gene encodes nuclear and mitochondrial proteins. Mol Cell Biol 1999; 19: 3869-3876.

Levi S, Arosio P. Mitochondrial ferritin. Int J Biochem Cell Biol 2004; 36: 1887-1889.

Levi S, Rovida E. The role of iron in mitochondrial function. Biochim Biophys Acta 2009; 1790: 629–636.

Li M, Zhong Z, Zhu J, Xiang D, Dai N, Cao X, Qing Y, Yang Z, Xie J, Li Z, Baugh L, Wang G, Wang D. Identification and characterization of mitochondrial targeting sequence of human apurinic/apyrimidic exonuclease 1. J Biol Chem 2010; 285: 14871-14881.

Li X, Fang P, Mai J, Choi ET, Wang H, Yang X. Targeting mitochondrial ROS as novel therapy for inflammatory diseases and cancers. J Hematol Oncol 2013; 6: 19.

Macao B, Uhler J, Siibak T, Zhu X, Shi Y, Sheng W, Olson M, Stewart JB, Gustafsson CM, Falkenberg M. The exonuclease activity of DNA polymerase γ is required for ligation during mitochondrial DNA replication. Nat Commun 2015; 6: 7303.

Magnusson J, Orth M, Lestienne P, Taanman JW. Replication of mtDNA occurs throughout the mitochondria of cultured human cells. Exp Cell Res 2003; 289: 133-142.

Malinska D, Kudin AP, Bejtka M, Kunz WS. Changes in mitochondrial ROS synthesis during differentiation of skeletal muscle cells. Mitochondrion 2012; 12: 144-148.

Malik AN, Czajka A. Is mitochondrial DNA content a potential biomarker of mitochondrial dysfunction? Mitochondrion 2013; 13: 481-492.

Menger KE, Rodríguez-Luis A, Chapman J, Nicholls TJ. Controlling the topology of mammalian mitochondrial DNA. Open Biol 2021; 11: 210168.

Mills EL, Kelly B, O'Neill LAJ. Mitochondria are the powerhouses of immunity. Nat Immunol 2017; 18: 488-498.

Miralles Fusté J, Shi Y, Wanrooij S, Zhu X, Jemt E, Persson Ö, Sabouri N, Gustafsson CM, Falkenberg M. In vivo occupancy of mitochondrial single-stranded DNA binding protein supports the strand displacement mode of DNA replication. PLoS Genet 2014; 10: e1004832.

Miwa H, Fujii J, Kanno H, Taniguchi N, Aozasa K. Pyruvate secreted by human lymphoid cell lines protects cells from hydrogen peroxide mediated cell death. Free Radical Research 2000; 33: 45-56.

Nadalutti CA, Ayala-Peña S, Santos JH. Mitochondrial DNA damage as a driver of cellular outcomes. Am J Physiol Cell Physiol 2022; 322: C136-C150.

National Institute of Health, 2023: Mitochondria. http://genome.gov/genetics-glossary/Mitochondria (04.11.2023)

Nicholls DG, Ferguson SJ. Bioenergetics 4. London – Waltham – San Diego: Elsevier Academic Press, 2013.

Nicholls TJ, Minczuk M. In D-loop: 40 years of mitochondrial 7S DNA. Exp Gerontol 2014; 56:175-81.

Nicholls TJ, Zsurka G, Peeva V, Schöler S, Szczesny RJ, Cysewski D, Reyes A, Kornblum C, Sciacco M, Moggio M, Dziembowski A, Kunz WS, Minczuk M, Linear mtDNA fragments and unusual mtDNA rearrangements associated with pathological deficiency of MGME1 exonuclease. Human Molecular Genetics 2014; 23: 6147-6162.

Nissanka N, Bacman SR, Plastini MJ, Moraes CT. The mitochondrial DNA polymerase gamma degrades linear DNA fragments precluding the formation of deletions. Nature Communications 2018; 9: 2491.

Nissanka N, Minczuk M, Moraes CT. Mechanisms of Mitochondrial DNA deletion formation. Trends in Genetics 2019; 35: 235-244.

Papa S, Martino PL, Capitanio G, Gaballo A, De Rasmo D, Signorile A, Petruzzella V. The Oxidative Phosphorylation System in Mammalian Mitochondria. Adv Exp Med Biol 2012; 942: 3-37.

Pigeolet E, Corbisier P, Houbion A, Lambert D, Michiels C, Raes M, Zachary MD, Remacle J. Glutathione peroxidase, superoxide dismutase, and catalase inactivation by peroxides and oxygen derived free radicals. Mech Ageing Dev 1990; 51: 283-297.

Puebla-Osorio N, Lacey DB, Alt FW, Zhu C. Early embryonic lethality due to targeted inactivation of DNA ligase III. Mol Cell Biol 2006; 26: 3935-3941.

Petrat F, Weisheit D, Lensen M, de Groot H, Sustmann R, Rauen U. Selective determination of mitochondrial chelatable iron in viable cells with a new fluorescent sensor. J Biochem 2002; 362: 137-147.

Ransy C, Vas C, Lombes A, Bouilland F. Use of H_2O_2 to cause oxidative stress, the catalase issue. Int J Mol Sci 2020*;* 21: 9149.

Rath S, Sharma R, Gupta R, Ast T, Chan C, Durham TJ, Goodman RP, Grabarek Z, Haas ME, Hung WHW, Joshi PR, Jourdain AA, Kim SH, Kotrys AV, Lam SS, McCoy JG, Meisel JD, Miranda M, Panda A, Patgiri A, Rogers R, Sadre S, Shah H, Skinner OS, To TL, Walker MA, Wang H, Ward PS, Wengrod J, Yuan CC, Calvo SE, Mootha VK. MitoCarta3.0: an updated mitochondrial proteome now with sub-organelle localization and pathway annotations. Nucleic Acids Res 2021; 49: D1541-D1547.

Rothfuss O, Gasser T, Patenge N. Analysis of differential DNA damage in the mitochondrial genome employing a semi-long run real-time PCR approach. Nucleic Acids Res 2010; 38: e24.

Scheibye-Knudsen M, Fang EF, Croteau DL, Wilson DM, Bohr VA. Protecting the mitochondrial powerhouse. Trends Cell Biol 2015; 25: 158-170.

Schmidt T, Schmid-Burgk JL, Hornung V, Synthesis of an arrayed sgRNA library targeting the human genome. Nature Scientific Reports 2015; 5: 14987.

Shishido K, Ando T. Action of single-strand-specific S1 endonuclease on locally altered structures in double-stranded DNA. Agr Biol Chem 1975; 39: 673-681.

Shokolenko I, Alexeyev M. Mitochondrial DNA: Consensuses and Controversies. DNA 2022; 2: 131-148.

Shokolenko I, Venediktova N, Bochkareva A, Wilson GL, Alexeyev MF. Oxidative stress induces degradation of mitochondrial DNA. Nucleic Acis Research 2009; 37: 2539-2548.
Simsek D, Jasin M. DNA ligase III: a spotty presence in eukaryotes, but an essential function where tested. Cell Cycle 2011; 10: 3636-3644.

Shokolenko IN, Alexeyev MF. Mitochondrial DNA: a disposable genome? Biochim Biophys Acta 2015; 1852: 1805-1509.

Shokolenko IN, Fayzulin RZ, Katyal S, McKinnon PJ, Wilson GL, Alexeyev MF. Mitochondrial DNA ligase is dispensable for the viability of cultured cells but essential for mtDNA maintenance. J Biol Chem 2013; 288: 26594-26605.

Shokolenko IN, Wilson GL, Alexeyev MF. The "fast" and the "slow" modes of mitochondrial DNA degradation. Mitochondrial DNA A DNA Mapp Seq Anal 2016; 27: 490-498.

Simsek D, Furda A, Gao Y, Artus J, Brunet E, Hadjantonakis AK, Van Houten B, Shuman S, Mckinnon PJ, Jansin M. Crucial role of DNA ligase III in mitochondria but not in Xrcc1-dependent repair. Nature 2011; 471: 245-248.

Simpson DSA, Oliver PL. ROS Generation in Microglia: Understanding Oxidative Stress and Inflammation in Neuro-degenerative Disease. Antioxidants 2020; 9: 743.

Spadafora D, Kozhukhar N, Chouljenko VN, Kousoulas KG, Alexeyev MF. Methods for Efficient Elimination of Mitochondrial DNA from Cultured Cells. PLoS One 2016; 11: e0154684.

Stepanenko AA, Dmitrenko VV. HEK293 in cell biology and cancer research: phenotype, karyotope, tumorigenicity, and stress-induced genome-phenotype evolution. Genes 2015; 569: 182-190.

Stewart JB, Chinnery PF. Extreme heterogeneity of human mitochondrial DNA from organelles to populations. Nat Rev Genet 2021; 22: 106-118.

Stewart JB, Chinnery PF. The dynamics of mitochondrial DNA heteroplasmy: implications for human health and disease. Nat Rev Genet 2015; 16: 530-542.

Stojkovič G, Makarova AV, Wanrooij PH, Forslund J, Burgers PM, Wanrooij S. Oxidative DNA damage stalls the human mitochondrial replisome. Sci Rep 2016; 6: 28942.

Stuart JA, Mayard S, Hashiguchi K, Souza-Pinto NC, Bohr VA, Localization of mitochondrial DNA base excision repair to an inner membrane-associated particulate fraction. Nucleic Acids Research 2005; 33: 3722–3732.

Svec D, Tichopad A,Novosadova V, Pfaffl MW, Kubista M. How good is a PCR efficiency estimate: Recommendations for precise and robust qPCR efficiency assessments. Biomolecular Detection and Quantification 2015; 3: 9-16.

Szczepanowska K, Trifunovic A. Origins of mtDNA mutations in ageing. Essays Biochem 2017; 61: 325-337.

Szczesny B, Tann AW, Longley MJ, Copeland WC, Mitra S. Long Patch Base Excision Repair in Mammalian Mitochondrial Genomes. J Biol Chem 2008; 283:26349-26356.

Szymanski MR, Yu W, Gmyrek AM, White MA, Molineux IJ, Lee JC, Yin YW. A domain in human EXOG converts apoptotic endonuclease to DNA-repair exonuclease. Nature communications 2017; 8: 14959.

Tann AW, Boldogh I, Meiss G, Qian W, Van Houten B, Mitra S, Szczesny B. Apoptosis induced by persistent single-strand breaks in mitochondrial genome: critical role of exog (5’-exo/endonuclease) in their repair. J Biol Chem 2011; 286: 31975-31983.

Tell G, Quadrifoglio F, Tiribelli C, Kelley MR. The many functions of APE1/Ref-1: not only a DNA repair enzyme. Antioxid Redox Signal 2009; 11: 601-620.

Tigano M, Vargas DC, Tremblay-Belzile S, Fu Y, Sfeir A. Nuclear sensing of breaks in mitochondrial DNA enhances immune surveillance. Nature 2021; 591:477-481.

Torregrosa-Muñumer R, Goffart S, Haikonen JA, Pohjoismäki JL. Low doses of ultraviolet radiation and oxidative damage induce dramatic accumulation of mitochondrial DNA replication intermediates, fork regression, and replication initiation shift. Mol Biol Cell 2015; 26: 4197-4208.

Torregosa-Muñumer R, Hangas A, Goffart S, Blei D, Zsurka G, Griffith J, Kunz WS, Pohjoismäki JLO. Replication fork rescue in mammalian mitochondria. Scientific Reports 2019; 9: 8785.

Trifunovic A, Wredenberg A, Falkenberg M, Spelbrink JN, Rovio AT, Bruder CE, Bohlooly-Y M, Gidlöf S, Oldfors A, Wibom R, Törnell J, Jacobs HT, Larsson NG. Premature ageing in mice expressing defective mitochondrial DNA polymerase. Nature 2004; 429: 417-423.

Trombly G, Said AM, Kudin AP, Peeva V, Altmüller J, Becker K, Köhrer KE, Zsurka G Kunz WS. The fate of oxidative strand breaks in mitochondrial DNA. Antioxidants 2023; 12: 1087.

Trounce IA, Kim YL, Jun AS, Wallace DC. Assessment of mitochondrial oxidative phosphorylation in patient muscle biopsies, lymphoblasts, and transmitochondrial cell lines. Methods Enzymol 1996; 264: 484-509.

Tullman J, Guntas G, Dumont M, Ostermeier M. Protein switches identified from diverse insertion libraries created using S1 nuclease digestion of supercoiled-form plasmid DNA. Biotechnol Bioeng 2011; 108: 2535-2543.

Turrens JF. Mitochondrial formation of reactive oxygen species. J Physiol 2003; 552: 335-344.

Uhler JP, Falkenberg M. Primer removal during mammalian mitochondrial DNA replication. DNA Repair 2015; 34: 28-38.

Uhler JP, Thörn C, Nicholls TJ, Matic S, Milenkovic D, Gustaffson CM, Falkenberg M. MGME1 processes flaps into ligatable nicks in concert with DNA polymerase γ during mtDNA replication. Nucleic Acids Res 2016; 44: 5861-5871.

Urrutia KM, Xu W, Zhao L. The 5’-phosphate enhances the DNA-binding and exonuclease activities of human mitochondrial genome maintenance exonuclease 1 (MGME1). J Biol Chem 2022; 298: 102306.

Volmering E, Niehusmann P, Peeva V, Grote A, Zsurka G, Altmüller J, Nürnberg P, Becker AJ, Schoch S, Elger CE, Kunz WS. Neuropathological signs of inflammation correlate with mtDNA deletions in mesial temporal lobe epilepsy. Acta Neuropathol 2016; 132: 277-288.

Wallace DC. Diseases of the mitochondrial DNA. Annu Rev Biochem 1992; 61: 1175-1212.

Wang D, Kreutzer DA, Essigmann JM. Mutagenicity and repair of oxidative DNA damage: Insights from studies using defined lesions. Mutat Res 1998; 400:99–115.

Wiehe RS, Gole B, Chatre L, Walther P, Calzia E, Ricchetti M, Wiesmüller L. Endonuclease G promotes mitochondrial genome cleavage and replication. Oncotarget 2018; 9:18309-18326.

Wu CC, Lin JLJ, Yang-Yen HS, Yuan HS. A unique exonuclease ExoG cleaves between RNA and DNA in mitochondrial DNA replication. Nucleic Acids Res 2019; 47: 5405-5419.

Xu W, Barrientos T, Andrews NC. Iron and copper in mitochondrial diseases. Cell Metab 2013; 17: 319-328.

Yakes FM, Van Houten B. Mitochondrial DNA damage is more extensive and persists longer than nuclear DNA damage in human cells following oxidative stress. Cell Biology 1997; 94: 514-519.

Yasukawa T, Reyes A, Cluett TJ, Yang MY, Bowmaker M, Jacobs HT, Holt IJ. Replication of vertebrate mitochondrial DNA entails transient ribonucleotide incorporation throughout the lagging strand. EMBO J 2006; 25: 5358-5371.

Yu Z, O'Farrell PH, Yakubovich N, DeLuca SZ. The Mitochondrial DNA Polymerase Promotes Elimination of Paternal Mitochondrial Genomes. Current Biology 2017; 27: 1033-1039.

Zhao L. Mitochondrial DNA degradation: a quality control measure for mitochondrial genome maintenance and stress response. The Enzymes 2019; 45: 311-341.

Zsurka G, Peeva V, Kotlyar A, Kunz WS. Is There Still Any Role for Oxidative Stress in Mitochondrial DNA-Dependent Aging? Genes 2018; 9: 175.

Zsurka G, Trombly G, Schöler S, Blei D, Kunz WS. Functional Assessment of Mitochondrial DNA Maintenance by Depletion and Repopulation Using 2',3'-Dideoxycytidine in Cultured Cells. Methods Mol Biol 2023; 2615:229-240.

9. Acknowledgements

While this thesis is the sum of years of dedicated research on my part, it would not have been possible without the generous support of the people in my life. I would like to thank the members of my lab. First, I would like to thank my supervisor, Prof. Dr. Wolfram S. Kunz, for providing me with the opportunity to work on this project, for his guidance and advice, and for always being approachable and understanding. I would also like to thank Dr. Gabor Zsurka for his scientific expertise and direction, and his generous help with data analysis. Dr. Viktoriya Peeva for inspiring me to be a woman in science and for being a ray of sunshine. Afaf M. Said for her moral support and a listening ear. Dr. Alexey Kudin for his experimental help. Susanne Beyer and Kerstin Hallmann for their technical support. I would also like to thank the members of my PhD thesis committee: Prof. Dr. Rudolf J. Wiesner, Prof. Dr. Wolfgang Voos, and Prof. Dr. med. Cornelia Kornblum.

I would like to thank my neuroscience master's friends, many of which have stayed in Bonn and we have embarked on this PhD journey together, who have always helped to build me up, commiserate, and share advice along the way. I would also like to thank my friends back in Michigan, who are there for me regardless of how much time and how many miles have separated us. I want to thank my in-laws for their unwavering support and curiosity. A huge thank you goes out to my parents, without whom I would not be who I am today. They have supported me mentally, emotionally, financially, and in so many more ways and there is no way to articulate how much they have contributed to my journey. And finally I need to thank my husband, Benjamin King, who has followed me chasing my dreams across the world and without him this truly would have never happened.

Thank you all.